UNIVERSIDAD NACIONAL AUTÓNOMA DE MÉXICO

PROGRAMA DE POSGRADO EN CIENCIAS DE LA TIERRA
INSTITUTO DE GEOLOGÍA

MECANISMOS GEOQUÍMICO-AMBIENTALES QUE DICTAN LA MOVILIDAD Y EL DESTINO DEL As(V) EN SISTEMAS ACUOSOS CONTAMINADOS: ADSORCIÓN vs. PRECIPITACIÓN

TESIS

QUE PARA OPTAR POR EL GRADO DE:
DOCTOR EN CIENCIAS DE LA TIERRA

PRESENTA:
KATHERINE ROCÍO VACA ESCOBAR

TUTOR Dr. MARIO VILLALOBOS PEÑALOSA
Instituto de Geología

MIEMBROS DEL COMITÉ TUTOR
Dra. Silvia Castillo Blum Facultad de Química
Dra. Margarita Gutiérrez Ruíz Facultad de Química

MÉXICO, D. F. SEPTIEMBRE 2015

JURADO

Presidente

Dra. Silvia Elena Castillo Blum
Facultad de Química, UNAM

Vocal

Dra. Anne Hansen Hansen
Instituto Mexicano de Tecnología del Agua

Secretario

Dr. Mario Villalobos Peñalosa
Instituto de Geología, UNAM

Suplente

Dra. Nadia Villegas Martínez
Instituto Potosino de Ciencia y Tecnología

Suplente

Dr. Javier Aguilar Carrillo de Albornoz
Universidad Autónoma de San Luis Potosí

Sustentante	Tutor
M. en C. Katherine Rocío Vaca Escobar	Dr. Mario Villalobos Peñalosa

AGRADECIMIENTOS

A la Universidad Nacional Autónoma de México por brindarme la oportunidad de realizar mis estudios de posgrado, de manera especial al Programa de Posgrado en Ciencias de la Tierra junto a su personal por su soporte invaluable y colaboración para con los estudiantes.

Al Consejo Nacional de Ciencia y Tecnología (CONACyT) por la beca otorgada para la realización de mis estudios de doctorado.

A la Secretaría de Educación Superior, Ciencia, Tecnología e Innovación (Senescyt) por el apoyo otorgado para la realización del presente trabajo de investigación.

Al Dr. Mario Villalobos Peñalosa por todo su apoyo, guía y paciencia en la realización del presente proyecto y por todo el aprendizaje obtenido tanto en la ciencia como en lo personal.

A la Dra. Silvia Castillo Blum y la Dra. Margarita Gutiérrez Ruíz, por sus comentarios y sugerencias invaluables durante todo este tiempo.

A los miembros del jurado por la colaboración brindada con sus observaciones y sugerencias para este trabajo.

A la Dra. Teresa Pi y al Dr. Rodolfo Zanella, por su colaboración con este proyecto.

A mis amigos y compañeros de laboratorio, con quienes compartí un ambiente de trabajo muy agradable, y me brindaron su experiencia y amistad.

A los estudiantes y técnicos del LABQA por su colaboración desinteresada y amistad que valoro mucho.

A mis compañeros de aventura, mis casi hermanos: Pato, Pablito, Flavio y Gus, que han sido un pilar muy importante para mi desarrollo personal y profesional, ustedes junto a Henry han sido mi familia fuera de casa, mil gracias por estar ahí.

Al hermoso país de México por abrirme sus puertas para prepararme mejor y a toda su gente que me abrió su corazón y me ofreció una sincera amistad.

A toda mi familia, quienes me brindaron su amor y confianza, su fe en mi me ha permitido culminar con este sueño, de manera especial a mis padres, mi hermano y mis tíos Melania, Patricio, Felipe y Cecibel, gracias por su apoyo.

Y en especial, gracias a Dios, porque nunca me desamparó y siempre ha guiado mi camino.

DEDICATORIA

Este esfuerzo está dedicado al motor de mi vida, a mis padres Hilter y Rocío, simplemente no sería nada sin ellos, todo su amor y apoyo me ha dado las fuerzas para alcanzar mis sueños, a mi hermano Fabricio, cómo no dedicarle el trabajo que realizo, si es quien me da la seguridad de que puedo lograr lo que me proponga, él cubre mis espaldas, a mi hermoso sobrino, quien llena nuestras vidas de alegría, ¡gracias por rescatarme!, a mi cuñada, por tu ayuda y su cariño con mi familia, y a mi prometido Henry, por acompañarme en esta gran aventura, por ser mi soporte, por todas las buenas y malas ;)

CONGRESOS

El presente trabajo de investigación se desarrolló en el Laboratorio de Biogeoquímica Ambiental (LABQA), del Instituto de Geografía, y en el Laboratorio de Geoquímica Ambiental del Instituto de Geología de la Universidad Nacional Autónoma de México, bajo la asesoría del Dr. Mario Villalobos Peñalosa.

Los resultados de este trabajo se presentaron en:

Water-Rock Interaction Symposia WRI13. Session: Characterization of mineral surfaces and water/mineral interfacial processes, Guanajuato, Mexico, 16-20, 2010 [oral presentation],

Katherine Vaca and Mario Villalobos (2010) "*Adsorption versus precipitation: Behavior of As(V) in Goethite/Pb(II)/ Carbonate systems".*

Goldschmidt Conference 2011. Session: Geochemical Process in Mining Environments – Sponsored by MIBRAG, Prague, Czech Republic, August 14-19, 2011 [poster presentation],

Katherine Vaca and Mario Villalobos (2011) *"Arsenate precipitation: An alternative fate of as in soils contaminated with mine-related wastes".*

XXII Congreso Nacional de Geoquímica (INAGEQ 2012). Coatzacoalcos, Veracruz, Octubre 1-5, 2012 [presentación oral],

Katherine Vaca and Mario Villalobos (2012) *"Influencia del área superficial de la goetita en las regiones de predominio de especies adsorbidas y precipitadas de As(V) en presencia de Pb(II)"*

12th International Conference on the Biogeochemistry of Trace Elements. "Recent Developments in Surface Complexation Modeling: Trace Elements Speciation and Reactive Transport Modeling" (Sponsored by UGS-OVPR), Athens, Georgia USA, June 16-20, 2013 [oral presentation],

M. Villalobos and K.R. Vaca-Escobar (2013) *"Modeling two competing As(V) attenuation processes: Adsorption vs. solid formation in aqueous Goethite/As(V)/Pb(II) systems"*

Goldschmidt Conference 2013. "Recent Advances in Imaging Minerals and Rocks: Geochemical Processes at the Nanoscale", Florence, Italy, August, 25-30, 2013 [oral presentation],

Livi K, Villalobos M, Varela M, Villacis-Garcia M, Vaca-Escobar K & Sverjensky D (2013) *"The Relationship of Goethite Surface Structure, Habit and Adsorption Capacity"*

246th American Chemical Society National Meeting and Exposition. "Fate of Environmental Pollutants in Biogeochemical Interfaces" Symposium, Environmental Chemistry Division (co-sponsored by the Geochemistry Division), Indianapolis, Indiana, September 8-12, 2013 [poster presentation],

Katherine Vaca-Escobar and Mario Villalobos (2013) *"Arsenic(V) is more prone to precipitate than to adsorb to Fe oxides in the presence of divalent heavy metals"*

XXIV Congreso Nacional de Geoquímica (INAGEQ 2014). Cd. Delicias, Chihuahua, Octubre 6-10, 2014 [presentación oral],

Katherine Vaca y Mario Villalobos (2014) *"Condiciones geoquímicas que dictan la movilidad del As(V) en sistemas acuosos contaminados"*

Simposio OPEN LAB de Cristalografía y Prácticas en Difracción de Rayos X, Distrito Federal, México, Noviembre 18-21, 2014 [presentación poster],

Katherine Vaca-Escobar, Milton Villacís-García y Mario Villalobos (2014) "*Reactividad superficial de la goetita en función de sus caras cristalinas"*

ÍNDICE GENERAL

INDICE DE FIGURAS

ÍNDICE DE TABLAS

ABREVIATURAS

ASE	Área superficial específica medida en $m^2\ g^{-1}$
BET	Brunauer, Emmett y Teller
GOE 50	Goetita de área superficial específica 94 $m^2\ g^{-1}$
GOE 94	Goetita de área superficial específica 50 $m^2\ g^{-1}$
ICP-AES	Inductively Coupled Plasma-Atomic Emission Spectrometry – Espectroscopía de Emisión Atómica por Inducción de Plasma Acoplado
SCM	Surface complexation modeling – Modelo de complejación superficial
USEPA	United States Environmental Protection Agency

SIMBOLOGÍA EMPLEADA

C	Valor de capacitancia constante ($F\ m^{-2}$)
Cs	Peso del sorbente en contacto con un litro de solución ($g\ L^{-1}$)
F	Constante de Faraday (96480 $C\ mol^{-1}$)
I	Fuerza iónica ($mol\ L^{-1}$)
MINTEQA2	Programa computacional de especiación química de la USEPA
R	Constante ideal de los gases (8.314J $mol^{-1}\ K^{-1}$)
S_A	Área superficial del sorbente ($m^2\ g^{-1}$)
T	Temperatura absoluta (K)
ψ_o	Potencial eléctrico en el "plano 0" (V)
ψ_β	Potencial eléctrico en el "plano β" (V)
γ_1	Coeficiente de actividad termodinámica para iones de Z = 1

MECANISMOS GEOQUÍMICO-AMBIENTALES QUE DICTAN LA MOVILIDAD Y EL DESTINO DEL As(V) EN SISTEMAS ACUOSOS CONTAMINADOS: ADSORCIÓN vs. PRECIPITACIÓN

RESUMEN

La contaminación de suelo y agua subterránea con elementos potencialmente tóxicos es un problema generalizado alrededor del mundo. Los residuos minero-metalúrgicos liberan grandes cantidades de estos elementos al ambiente en especies altamente móviles. Recientemente, se ha encontrado en suelos mexicanos contaminados con estos tipos de desechos, que los iones arseniato [de As(V)] no se encuentran como especies adsorbidas a los óxidos de Fe presentes en los suelos (como se reporta de manera general en la literatura), sino mayoritariamente formando compuestos muy insolubles tales como arseniatos de plomo y de otros metales divalentes. Para entender este comportamiento, se ha aplicado un modelo termodinámico, considerando simultáneamente el proceso de precipitación y el de adsorción para dos goetitas con diferentes áreas superficiales específicas (94 y 50 m^2/g), y por tanto diferentes reactividades por área. El acoplamiento de procesos de adsorción y precipitación para un mismo componente, en este caso para arsénico (V), no se ha realizado en modelos de especiación geoquímica con anterioridad. El presente trabajo es un esfuerzo por llevar a cabo esto en sistemas contaminados, utilizando un enfoque de "abajo hacia arriba", es decir, desde sistemas sencillos a más complejos, describiéndolos progresivamente a través de sus interacciones fundamentales. El objetivo final es determinar las condiciones geoquímicas que favorecen los procesos de inmovilización de As(V) (adsorción o precipitación). Para este fin, se definió inicialmente un sistema de goetita (α-FeOOH) / As(V) / Pb(II) / carbonato, como una función de la relación As(V) / Fe(III), en un intervalo de pH de 4 – 9. El modelo predice que a partir de una relación molar muy baja de As(V) / Fe(III) (mayor a 0.02 a pH 7) el mecanismo de precipitación influye significativamente en la atenuación de As(V), y se convierte rápidamente en el proceso dominante sobre el mecanismo de adsorción. Este comportamiento fue corroborado mediante experimentos puntuales, los cuales brindan confianza en el modelo empleado. Una vez determinado el efecto de la presencia de plomo en el sistema, se estudió la influencia de: (i) la relación molar As(V)/Pb(II) empleada, (ii) la presencia de cloruros y sulfatos, y (iii) la presencia de cobre (II) en presencia y ausencia

de plomo (II). Se encontró que las condiciones que favorecen la precipitación son, en orden de importancia: presencia de Cl^-, proporciones altas de Pb/As, proporciones altas de As/Fe, la presencia simultánea de Pb(II) y Cu(II), y goetitas de alta área superficial. La adsorción se favorece en condiciones opuestas, y también en presencia de sulfatos pero sólo a valores bajos de pH en que precipita el sulfato de Pb(II). Finalmente, el proceso de precipitación es benéfico para la atenuación tanto de arsénico como de plomo.

ENVIRONMENTAL GEOCHEMICAL MECHANISMS THAT DETERMINE THE As(V) MOBILITY AND FATE IN CONTAMINATED AQUEOUS SYSTEMS: ADSORPTION VERSUS PRECIPITATION

ABSTRACT

Soil and groundwater contamination with potentially toxic elements is a world widespread problem. Mining and metallurgical wastes release large amounts of these elements to the environment in highly mobile species. Recently, it was found in Mexican soils contaminated with this kind of wastes, that the arsenate ions [of As(V)] are not found as adsorbed species onto iron oxides (as generally reported in the literature), but mostly formed very insoluble minerals such as lead and other divalent metal arsenates. To understand this behavior, a thermodynamic model was applied considering simultaneously precipitation and adsorption for two goethites with different surface specific areas (94 y 50 m^2/g), and therefore different reactivity per area. The coupling of adsorption and precipitation processes in geochemical speciation modeling of arsenic (V), has not been performed before modeling. The present work is an effort to accomplish this in contaminated systems, using a bottom-up approach, that is, from single to more complex systems, describing them progressively through their fundamentals interactions. The final objective is determinate the geochemical conditions that favor the As(V) immobilization processes (adsorption or precipitation). For this purpose, a system of goethite (α-FeOOH) / As(V) / Pb(II) / carbonate was initially defined, and studied as a function of the molar As(V) / Fe(III) ratio, in a pH range from 4 – 9. The model predicts that from very low molar As(V) / Fe(III) ratios (greater than 0.02 at pH 7) the precipitation mechanism influences significantly As(V) attenuation, and quickly becomes the dominant process over the adsorption mechanism. This behavior was confirmed through limited experimental spot checks, which provided confidence in the model used. Once the effect of lead(II) in the system was determined, the influence of the following geochemical conditions was studied: (i) the molar ratio As(V) / Pb(II), (ii) the presence of chloride and/or sulfate, and (iii) the presence of copper (II) in the presence and absence of lead (II). The conditions that favor precipitation were found to be, in order of importance: chloride presence, high Pb/As proportions, high As/Fe proportions, simultaneous presence of Pb(II) and Cu(II), and goethites with high specific surface area. Adsorption is favored in opposite conditions,

and also in the presence of sulfate, but only at low pH, in which Pb(II) sulfate precipitates. Finally, the precipitation process is beneficial for simultaneous arsenic and lead attenuation, potentially providing higher stability than the adsorption process.

CAPÍTULO 1

1. INTRODUCCIÓN

El arsénico es uno de los elementos tóxicos más comunes en el ambiente, se encuentra ampliamente distribuido en la corteza terrestre, con mayor frecuencia incorporado en sulfuros o como arseniatos metálicos, es constituyente de más de 245 minerales y está asociado con mayor frecuencia con minerales de cobre, oro, plomo y zinc en menas sulfurosas (Cullen y Reimer, 1989; Oremland y Stolz, 2003; Shen et al., 2013). Las erupciones volcánicas y otros procesos naturales son fuentes de altas concentraciones de arsénico en el ambiente (Smedley y Kinniburgh, 2002; Garelick et al., 2008), pero otras fuentes de contaminación de arsénico son las actividades humanas como la disposición de residuos industriales, especialmente mineros y metalúrgicos, la fundición de minerales compuestos por arsénico, la quema de combustibles fósiles y la aplicación de compuestos arsenicales en varios productos especialmente en los pasados 100 años (Garelick et al., 2008; Chang et al., 2009; Mirza et al., 2014).

Por lo tanto, la contaminación de agua y suelo por arsénico y metales pesados es un fenómeno altamente difundido alrededor del mundo (Vázquez et al., 2011; Lenoble et al., 2013), en especial alrededor de áreas de extracción de metales puesto que en medios óxicos se promueve la solubilidad de los contaminantes y su movilidad. Este problema es de gran preocupación ya que constituye un riesgo para los seres vivos por su alta toxicidad (Flemming y Trevors, 1989; Järup, 2003; Papanikolaou et al., 2005; Duruibe et al., 2007; Maderova et al., 2011; Bowell et al., 2014). Por ejemplo, las concentraciones de arsénico más altas reportadas para suelos cercanos a fundidoras de plomo fueron: 2 g kg^{-1}, para fundidoras de cobre: 0.55 g kg^{-1}, y de oro: 0.5 a 9.3 g kg^{-1} (Bissen y Frimmel, 2003), lo cual constituye un riesgo para la salud de seres humanos, animales y plantas (Sevilla y Mateus, 2008).

El drenaje ácido de minas generado por la disolución oxidativa de sulfuros es una de las mayores causas de movilización de arsénico alrededor del mundo, a partir de yacimientos ricos en arsénico como arsenopirita y pirita enriquecida en arsénico, cuyas

concentraciones alcanzan hasta cientos de mg L^{-1} (Asta et al., 2009). El arsénico proveniente de residuos minero metalúrgicos, a su vez, está acompañado de metales pesados, tales como plomo, cobre, zinc, etcétera, en concentraciones usualmente altas (Vaughan, 2006).

La movilidad del arsénico en el medio ambiente depende considerablemente de su interacción con los óxidos, oxihidróxidos e hidróxidos de metales (Hartley y Lepp, 2008; Mamindy-Pajany et al., 2009). Los minerales de óxidos de hierro, como la goetita y la ferrihidrita entre otros, han sido identificados en forma generalizada como las fases que dictan la movilidad de las especies oxidadas de arsénico [As(III) y As(V)] en suelos y aguas subterráneas, a través de procesos de sorción y/o coprecipitación con éstos (Lin y Puls, 2001; Stuben et al., 2001; Matera et al., 2003; Paktunc et al., 2004; Morin y Calas, 2006; Slowey et al., 2007; Mamindy-Pajany et al., 2009).

Como mecanismo alternativo de atenuación de As, se ha encontrado la asociación del As(V) con cationes de metales pesados como Pb(II) y Cu(II), para formar compuestos altamente insolubles en suelos contaminados con residuos minero-metalúrgicos (Gutierrez-Ruiz et al., 2005; Villalobos et al., 2010). Se encontró que la formación de arseniatos de metales pesados en dichos suelos se debe a que, aunque los contenidos de óxidos de Fe son normales (2% de Fe en peso, en promedio), las relaciones molares de As/Fe son relativamente altas (0.06 - 0.37), y las relaciones de As(V)/metales son cercanas a 1, y por lo tanto estos últimos compiten favorablemente contra los óxidos de Fe para enlazar e inmovilizar al As(V) debido a sus bajos valores de productos de solubilidad.

En el presente trabajo se investigaron las condiciones geoquímicas que determinan la formación ya sea de arseniatos metálicos, o de complejos de adsorción de arsénico(V) sobre un óxido de Fe(III) representativo de ambientes naturales, la goetita – α-FeOOH, para determinar los factores que favorecen uno u otro mecanismo.

Estos estudios son relevantes tanto para el entendimiento del comportamiento geoquímico ambiental del arsénico, como para el diseño de esquemas eficientes de remediación de sistemas contaminados con arsénico. La modelación termodinámica de fenómenos de adsorción conjuntamente con fenómenos de precipitación, debidamente validados, resultará en una herramienta útil para predecir el comportamiento geoquímico

ambiental del arsénico. Adicionalmente, se podrá determinar qué condiciones del sistema bajo estudio son susceptibles de modificar con la finalidad de asegurar el mayor porcentaje de inmovilización de arsénico y de otros elementos potencialmente tóxicos. La validación de la modelación termodinámica presentada en esta investigación es la base fundamental para el estudio de sistemas de mayor complejidad, en un esfuerzo por construir la descripción geoquímica fundamental de los sistemas naturales, con un enfoque llamado de "bottom-up" (de abajo hacia arriba).

1.1. OBJETIVOS

1.1.1 Objetivo General

Determinar las condiciones geoquímicas que favorecen la formación de arseniatos de Pb(II) y Cu(II), y aquellas que favorecen procesos de adsorción del As(V) a goetita, y la relación entre ellas, aproximándose gradualmente a la complejidad geoquímica en la composición de los medios naturales.

1.1.2 Objetivos Específicos

1. Determinar la influencia de las siguientes condiciones en el comportamiento de adsorción *vs*. precipitación del As(V):
    a. El área superficial específica (ASE) y la naturaleza de la goetita.
    b. El pH en un intervalo relevante al ambiente (4-9).
    c. La proporciones As/Fe y As/metal divalente totales [para Pb(II) y Cu(II)], tanto en forma individual como mezclada, especialmente en condiciones de subsaturación de los sitios superficiales disponibles para adsorción del As(V).
2. Caracterizar los sólidos de arseniatos de plomo.
3. Investigar el mecanismo de la reacción que simula de manera simplificada la mezcla de residuos con contenidos separados de Pb(II) y de As(V):

$$9Na_2HAsO_4 + 5Pb_3(OH)_2(CO_3)_2 \rightarrow 3Pb_5(AsO_4)_3OH + 7H_2O + 9Na_2CO_3 + H_2CO_3$$

1.2. HIPÓTESIS

a. Hipótesis general

La modelación termodinámica, acoplando reacciones de adsorción y de precipitación en sistemas representativos relativamente sencillos permitirá determinar las condiciones geoquímicas que favorecen la formación de arseniatos de Pb(II) y Cu(II), y aquellas que favorecen procesos de adsorción del As(V) a goetita, así como la relación entre ellas.

b. Hipótesis particulares

La goetita con menor ASE (i.e., con mayor tamaño de partícula), tendrá una mayor reactividad hacia la adsorción de arsénico al normalizarla por área.

La precipitación de arseniatos de metales se favorecerá en goetitas superficialmente menos reactivas, i.e., de tamaños de partícula pequeños.

Valores de pH altos favorecerán el mecanismo de precipitación de arseniatos metálicos, mientras que valores bajos favorecerán la adsorción del As(V).

Las relaciones molares As/Fe bajas favorecerán el proceso de adsorción, al igual que las relaciones As/Pb altas.

La presencia de cloruros favorecerá el mecanismo de precipitación de arseniato de Pb(II) por la formación de un mineral extremadamente insoluble.

Los arseniatos de metales mezclados $[(Pb,Cu)_x(AsO_4)_y(OH)_z]$ competirán con menor éxito que los arseniatos puros por secuestrar arsénico contra la adsorción, dadas sus solubilidades más altas.

El mecanismo de formación del $Pb_5(AsO_4)_3OH$ a partir de $Pb_3(OH)_2(CO_3)_2$ y Na_2HAsO_4, se llevará a cabo por incorporación del ión arseniato a la estructura de $Pb_3(OH)_2(CO_3)_2$, y no por mecanismos de disolución-precipitación mediante la siguiente ecuación:

$$9Na_2HAsO_4 + 5Pb_3(OH)_2(CO_3)_2 \rightarrow 3Pb_5(AsO_4)_3OH + 7H_2O + 9Na_2CO_3 + H_2CO_3$$

CAPÍTULO 2

2. METODOLOGÍA

La mayor parte del trabajo desarrollado en esta investigación involucra modelación termodinámica empleando los programas Visual MINTEQ (Gustafsson, 2010) y MINEQL (Westall, 1976; Schecher y McAvoy, 1992), además de validación mediante experimentos selectos de química húmeda.

2.1 Modelaciones Termodinámicas

Para el desarrollo de las modelaciones termodinámicas se emplearon dos programas de especiación química (Visual MINTEQ y MINEQL+), cuyas bases de datos fueron comparadas entre sí y actualizadas de tal manera que sus resultados sean consistentes y capaces de predecir de manera óptima el comportamiento de los contaminantes en el sistema. Su guía de uso se muestra en el Anexo A y los valores de las constantes actualizadas en la tabla 2.1 y Anexo B.

Tabla 2.1 Constantes de formación actualizadas [tomadas de Villalobos et al. (2010)].

NOMBRE	FÓRMULA	Log K_f
SÓLIDOS		
Schultenita	$PbHAsO_4$	23.97
Hidroximimetita	$Pb_5(AsO_4)_3OH$	62.115
Mimetita	$Pb_5(AsO_4)_3Cl$	83.571
Escorodita	$FeAsO_4.H_2O$	25.83
COMPLEJOS ACUOSOS		
	$PbHAsO_4^0$	14.03
	$PbH_2AsO_4^+$	19.73

2.1.1 Visual MINTEQ

La modelación termodinámica de los sistemas estudiados, considerando los procesos de adsorción y de precipitación conjuntamente, se desarrolló mediante el uso del programa Visual MINTEQ, para ello fue necesario incluir en el programa los parámetros propios del proceso de adsorción que son requeridos por el modelo, como son: dos capacitancias eléctricas (C_1 y C_2), el ASE del mineral, la concentración de sólidos, la fuerza iónica, y la presión parcial del CO_2 atmosférico. Los datos empleados en esta investigación se muestran en la tabla 2.2:

Tabla 2.2 Parámetros adicionales usados en los modelos de complejación superficial (Salazar-Camacho y Villalobos, 2010).

Parámetro	Valor	Unidades
C_1 (GOE94)	0.729	F m^{-2}
C_1 (GOE50)	1.17	F m^{-2}
C_2	0.200	F m^{-2}
Área superficial específica (GOE94)	94	m^2 g^{-1}
Área superficial específica (GOE50)	50	m^2 g^{-1}
Concentración de Sólidos	0.2	g L^{-1}
Fuerza Iónica	0.01	mol L^{-1}
Log P_{CO_2}	-3.5	Log (atm)

Junto con los datos mostrados anteriormente, se adicionó en la base de datos de Visual MINTEQ las ecuaciones de formación de complejos superficiales y sus constantes de afinidad, para arsénico, plomo, cloruros y carbonatos, cuyos valores fueron reportados por Villalobos et al. (2009) y Salazar-Camacho y Villalobos (2010), las cuales fueron adaptadas del modelo usado en este trabajo, basado en un estado estándar de 1.0 mol L^{-1}, a uno de 1.0 de fracción molar, cuyos valores se muestran en la tabla 2.3.

Tabla 2.3 Reacciones de complejación superficial ingresadas en Visual Minteq con las constantes de formación descritas por tipo de sitio superficial (Villalobos y Perez-Gallegos, 2008; Vaca-Escobar et al., 2012).

Ec.	***Ácido-base [c]:***	***REACCIONES [a]***	***Log K [b]***		
			FeOH	***Fe_2OH***	***Fe_3OH***
1	$SOH + H^+ \rightleftharpoons SOH_2^+$	$K = \frac{[SOH_2^+]}{\gamma_1[SOH][H^+]} e^{\frac{F}{RT}(\psi_0)}$	6.8	nr	7.66
2	$SOH \rightleftharpoons SO^- + H^+$	$K = \frac{\gamma_1[SO^-][H^+]}{[SOH]} e^{-\frac{F}{RT}(\psi_0)}$	-10.8	nr	-11.66
	Complejación de Electrolitos (esfera-externa):				
3	$SOH + H^+ + NO_3^- \rightleftharpoons SOH_2^+ \cdots NO_3^-$	$K = \frac{[SOH_2^+ \cdots NO_3^-]}{\gamma_1^2[SOH][H^+][NO_3^-]} e^{\frac{F}{RT}(\psi_0 - \psi_\beta)}$	8.02	nr	9.025
4	$SOH + H^+ + Cl^- \rightleftharpoons SOH_2^+ \cdots Cl^-$	$K = \frac{[SOH_2^+ \cdots Cl^-]}{\gamma_1^2[SOH][H^+][Cl^-]} e^{\frac{F}{RT}(\psi_0 - \psi_\beta)}$	8.4	nr	8.9
5	$SOH + Na^+ \rightleftharpoons SO^- \cdots Na^+ + H^+$	$K = \frac{[SO^- \cdots Na^+][H^+]}{[SOH][Na^+]} e^{\frac{F}{RT}(\psi_\beta - \psi_0)}$	-9.43	nr	-11.095

Continúa en la siguiente página

	Complejos de Esfera-interna:				
6	$SOH + Pb^{2+} \rightleftharpoons SOPb^{+} + H^{+}$	$K = \frac{[SOPb^{+}][H^{+}]}{\gamma_1^3[SOH][Pb^{2+}]} e^{\frac{F}{RT}(\psi_0)}$	0.64	nr	nr
7	$FeOH + SOH + H^{+} + AsO_4^{3-} \rightleftharpoons FeO^{-0.7}AsO_3^{-1.3\cdots}HOS + H_2O$	$K = \frac{[FeO^{-0.7}AsO_3^{-1.3\cdots}HOS]}{\gamma_1^{10}[FeOH]^{d}[H^{+}][AsO_4^{3-}]} e^{\left(-0.7\psi_0 - 1.3\psi_\beta\right)\frac{F}{RT}}$	21/20.7[e]	18.75[f]	nr
8	$FeOH + SOH + 2H^{+} + AsO_4^{3-} \rightleftharpoons FeO^{-0.7}AsO_3H^{-0.3\cdots}HOS + H_2O$	$K = \frac{[FeO^{-0.7}AsO_3H^{-0.3\cdots}HOS][H_2O]}{\gamma_1^{10}[FeOH][H^{+}]^2[AsO_4^{3-}]} e^{\left(-0.7\psi_0 - 0.3\psi_\beta\right)\frac{F}{RT}}$	nr	19.6[f]	nr
9	$SOH + H^{+} + CO_3^{2-} \rightleftharpoons SO^{-0.2}CO_2^{-0.8} + H_2O$	$K = \frac{[SO^{-0.2}CO_2^{-0.8}]}{\gamma_1^5[SOH][CO_3^{2-}][H^{+}]} e^{\frac{F}{RT}\left(-0.2\psi_0 - 0.8\psi_\beta\right)}$	13.55	13.32	nr
	Complejos de Esfera-externa:				
10	$SOH + Pb^{2+} + H_2O \rightleftharpoons SO^{-\cdots}PbOH^{+} + 2H^{+}$	$K = \frac{[SO^{-\cdots}PbOH^{+}][H^{+}]^2}{\gamma_1^2[SOH][Pb^{2+}]} e^{\frac{F}{RT}\left(\psi_\beta - \psi_0\right)}$	-10.1	-8.6	nr

[a] SOH puede ser los grupos FeOH, Fe_2OH o Fe_3OH.
[b] nr = grupo no reactivo.
[c] El log de las constantes de acidez usadas fueron establecidas mediante un ΔpKa de 4 alrededor del pH del PZNPC para cada tipo de sitio, estas son 8.8 y 9.66 para los grupos FeOH y Fe_3OH respectivamente.
[d] El exponente es 1cuando SOH es Fe_2OH y 2 cuando es FeOH.
[e] El log de la constante de formación usada fue 21 para GOE94 y GOE106, y 20.7 para GOE50 y GOE43. Esto difiere del valor de 21.6 ± 0.7 de Salazar-Camacho y Villalobos (2010) debido a que el estado estándar de las actividades de las especies superficiales en este último es 1.0 M, mientras el valor usado para la modelación en el presente trabajo es 1.0 en fracción mol.
[f] Los grupos Fe_2OH adyacentes a los grupos FeOH están presentes sólo en la cara (0 1 0), y su densidad corresponde a la mitad de todos los grupos FeOH presentes en esta cara. Además, los valores de la densidad de sitios reactivos hacia el enlace de As(V) fue la mitad del total de la densidad de sitios de FeOH en esta cara.

Otro parámetro importante que se debe describir son las densidades de sitios superficiales (n_s) en función de las caras específicas expuestas de los cristales de cada mineral, estos valores se muestran en la tabla 2.4.

Tabla 2.4 Análisis de la densidad de sitios de las dos goetitas usadas (Villalobos y Perez-Gallegos, 2008).

Goetita	Contribuciones de las caras (%)			Densidad de sitios superficiales reactivos (sitios nm^{-2})		
	101	001	010	≡FeOH	$\equiv Fe_2OH$	$\equiv Fe_3OH$
GOE94	70	30	0	3.12	0.00	3.12
GOE50	37	0	63	6.85	2.87	1.12

Las densidades de sitios superficiales totales de la tabla 2.4 para cada goetita provienen de las densidades de sitios cristalográficas de cada cara, multiplicadas por la fracción de cara cara cristalina contribuyente.

2.1.2 MINEQL+

La modelación termodinámica desarrollada para identificar los sólidos que se pueden formar en el sistema a través de diagramas de índice de saturación en función del pH se realizó mediante el uso del programa MINEQL, ya que dicho programa presenta una plataforma gráfica, la cual es de mucha utilidad para identificar las fases sólidas de manera más rápida. Para ello es necesario revisar y actualizar las bases de datos con las constantes de formación de arseniatos metálicos que se muestran en la tabla 2.2 y en el anexo B.

2.2 Parte Experimental

2.2.1 Reactivos

Todos los reactivos empleados para el desarrollo del trabajo experimental son grado analítico y sus fuentes se muestran en la tabla 2.5:

Tabla 2.5 Reactivos empleados en los experimentos de adsorción-precipitación.

Reactivo	Casa Comercial	Característica
Nitrato de Hierro nonahidratado	Sigma-Aldrich	98%
Hidróxido de Sodio	J. T. Baker	98.8%
Arseniato monoácido de sodio heptahidratado	Sigma-Aldrich	≥ 98%
Nitrato de plomo	J.T. Baker	99.3%
Yoduro de Potasio	J.T. Baker	100%
Borohidruro de Sodio	J.T. Baker	98%
Ácido Clorhídrico	J.T. Baker	36.5-38%
Nitrato de Sodio	Sigma Aldrich	≥ 97%
Ácido Nítrico	J.T. Baker	64.7%
Estándar As(V) al 2% en HCl	High Purity Standards	1000 mg L^{-1}
Estándar Pb(II) al 2% en HNO_3	High Purity Standards	1000 mg L^{-1}
Estándar Fe(II) al 2% en HNO_3	High Purity Standards	1000 mg L^{-1}
Solución Amortiguadora pH4	J.T. Baker	Biftalato de Potasio
Solución Amortiguadora pH7	J.T. Baker	Fosfato de Sodio y Potasio
Solución Amortiguadora pH10	J.T. Baker	Borato de Potasio
Agua de alta pureza	Desionizada	Resistividad: 17.3 MΩ.cm

2.2.2 Materiales

Los materiales empleados en la parte experimental de esta investigación se describen a continuación:

Como reactor se emplearon frascos de polipropileno de 250 mL de capacidad (Nalgene 3140-0250). Con la finalidad de diferenciar entre las fases adsorbidas y precipitadas se empleó una membrana tubular de diálisis de celulosa regenerada marca SPECTRA/POR 7 cuyas características son: un diámetro de 2.04 cm, una relación volumen/longitud de 3.3 mL cm^{-1}, la cual se mantiene preservada en solución de azida de sodio al 0.1% en peso y deja pasar moléculas con un peso molecular de 8000Da

(Spectrum Laboratories Inc.), es decir, presentan un tamaño de poro de 3nm (http://www.spectrapor.com/dialysis/PoreSize.html).

Además, se usaron barras de agitación cubiertas de teflón de 2.54 cm de largo por 0.64 cm de ancho (Cole-Parmer Instrument Co), para mantener una agitación constante.

Para la medición potenciométrica del pH durante los experimentos de adsorción-precipitación, se empleó el potenciómetro Beckman Φ720, con un electrodo combinado de vidrio (Hanna, HI 1143, Hanna Combination pH Electrode, 0-14 pH, glass body), cuya disolución interna es de KCl 3M (Hanna), con un flujo de 0.02 a 0.03 mL h^{-1}. Para limpiar y darle mantenimiento al electrodo, éste se debe sumergir en una disolución de HCl 0.1M durante media hora, para posteriormente colocar el electrodo en la disolución de almacenamiento (Electrode Storage Solution, Orion 910001) por lo menos una hora. Luego, el electrodo se calibra potenciométricamente con disoluciones amortiguadoras de concentración conocida. Esta calibración se lleva a cabo utilizando 3 diferentes soluciones amortiguadoras comerciales pH 4, 7 y 10 que comprendían el intervalo de pH de trabajo.

Para realizar los experimentos de adsorción-precipitación se emplearon dos goetitas de diferente ASE, sintetizadas y caracterizadas en trabajos anteriores mediante difracción de rayos X, determinación de área superficial BET, diversas microscopías electrónicas, y titulaciones potenciométricas ácido-base (van Geen et al., 1994; Ostergren et al., 2000; Villalobos et al., 2001), sus ASE son 94 m^2 g^{-1} llamada GOE94 y 50 m^2 g^{-1} llamada GOE50.

Debido a que no existía la cantidad necesaria de goetitas para realizar todos los experimentos considerados en el presente trabajo, se consideró necesario sintetizar muestras de goetita con diferente ASE, para ello se empleó el método de (Atkinson et al., 1967) con una pequeña variación, el cual se describe a continuación:

Se preparó agua desionizada y descarbonatada, la cual se empleó en todo el procedimiento de síntesis, para ello se hirvió agua desioinizada (Milli-Q) y mientras ésta se enfría, se dejó burbujear N_2 para eliminar el CO_2 disuelto.

En un recipiente de polipropileno de 1 L con 825 g de agua desionizada y descarbonatada se disuelven 50 g de $Fe(NO_3)_3.9H_2O$; separadamente, se preparan 200

mL de una solución libre de CO_2 de NaOH con una concentración de 2.5 M. La solución de NaOH se vierte sobre la solución de Fe(III) bajo flujo de N_2 y agitación continua, en donde se puede observar la formación inmediata de un precipitado color pardo rojizo, que corresponde a la formación intermedia de ferrihidrita. El pH final de la reacción es mayor a 12. La mezcla se calienta a 60°C, manteniendo esta temperatura por 24 h, luego de este período se puede observar el cambio de color del sólido a un amarillo ocre, característico de la goetita. Se neutralizan las suspensiones resultantes con HNO_3 y posteriormente se lavan con 1 L de agua desionizada libre de CO_2 para remover todas las sales que no reaccionaron, hasta una conductividad de 0.1 μS cm^{-1}. Durante la reacción se mantuvo una atmósfera inerte de N_2 con el fin de evitar una adsorción inicial de carbonato en la superficie de goetita (Fig. 2.1). Para secar las muestras, éstas se llevaron a 105°C hasta sequedad (hasta peso constante) por 48 h aproximadamente y se caracterizaron mediante difracción de Rayos-X y área superficial BET.

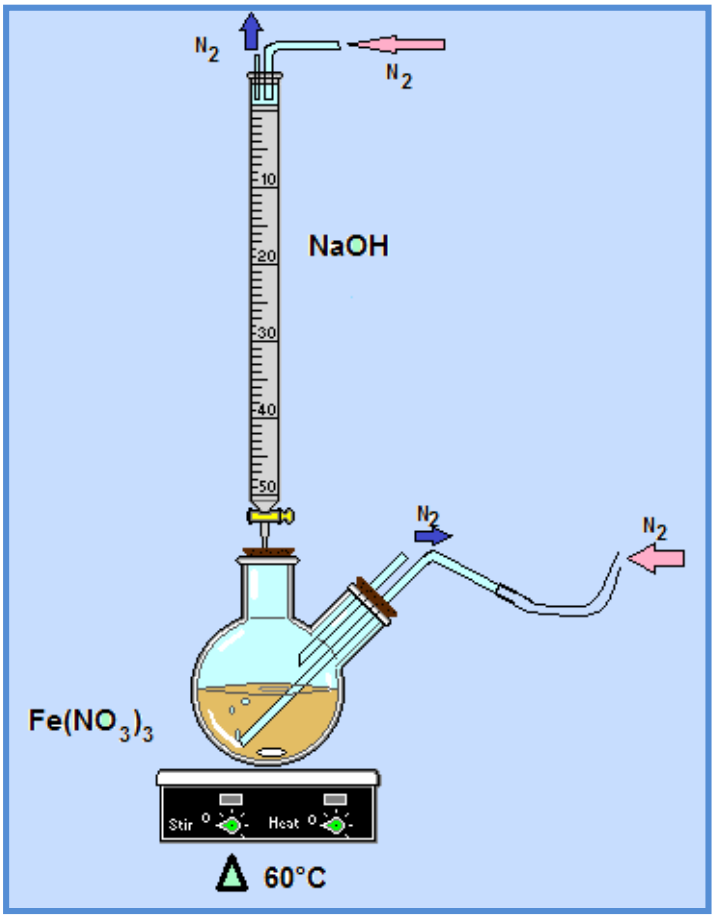

Fig. 2.1 Diagrama del sistema de síntesis de goetita.

Las condiciones experimentales como la velocidad de adición y el total de base añadida, la presencia de sorbatos, y el tiempo de añejamiento, son los responsables de la forma cristalina y del tamaño de las partículas de goetita sintetizadas, que son las características que afectan el ASE (Cornell et al., 1974; Cornell y Schwertmann, 2004a). De esta manera, la única diferencia en la síntesis de las goetitas en estudio fue la velocidad de adición de la solución de NaOH durante la precipitación inicial de la ferrihidrita. Una adición inmediata de la solución de NaOH da lugar a la formación de goetita de baja ASE (42.7 $m^2 g^{-1}$ - GOE43) y con una velocidad de adición de 1 mL min^{-1}, se obtiene goetita de alta ASE (106 $m^2 g^{-1}$ - GOE106).

Las goetitas de alta ASE (GOE106 y GOE94) tienen las mismas características entre sí, lo mismo ocurre entre las goetitas de baja ASE (GOE43 y GOE50), por lo que se emplean indistintamente en los experimentos de adsorción-precipitación.

2.2.3 Preparación de Reactivos

Antes de preparar los reactivos empleados fue necesario realizar la limpieza del material a utilizarse, lo cual es muy importante debido a las concentraciones tan bajas que se consideraron para el desarrollo de esta investigación. A continuación se detalla el procedimiento que se siguió:

El material debe sumergirse en solución jabonosa (Hyclin, detergente sin espuma, libre de fosfatos, aproximadamente 20 g de detergente por litro de solución), durante unos minutos para proceder con el lavado con escobillas y el enjuague repetido con agua corriente para remover todo el detergente, a continuación se lleva el material a una tina de lavado con HNO_3 al 10% por lo menos por 2 h. Se enjuaga el material perfectamente con agua destilada y después con agua desionizada (de 17.3MΩ.cm).

Las disoluciones necesarias para realizar los experimentos se prepararon con material previamente calibrado gravimétricamente, con la finalidad de obtener datos más confiables. La masa se midió con la balanza analítica digital Sartorius R200D (con una precisión de 0.00005 g).

Preparación de soluciones y suspensiones

1. *Suspensión de hidroxi-carbonato de plomo:* se pesó 0.6669 g de $Pb(NO_3)_2$, se diluyó adicionando 28 g de agua y se llevó a pH 7, con solución de NaOH 1M pesándolo, se dejó estabilizar durante un día dejando entrar CO_2 del aire, luego se llevó a un volumen de 100mL con agua desionizada y se pesó. Además se determinó la densidad.
2. *Suspensión de Hidroximimetita:* se pesaron 0.55694 g de $Pb(NO_3)_2$ y 0.31669 g de $Na_2HAsO_4.7H_2O$, se adicionó 50 mL de agua, se fijó el pH a 7 y se llevó la suspensión a 100mL. Los volúmenes se pesaron y se halló su densidad.
3. *Solución de $NaNO_3$ 1M:* se pesaron 8.497 g de $NaNO_3$ y se llevó a 100 mL de solución, tomando el peso de la solución.
4. *Solución de Na_2HAsO_4 $1x10^{-2}$ M:* se pesaron 0.31669 g de $Na_2HAsO_4.7H_2O$ y se lo llevó a 100 mL.
5. *Suspensión de Mimetita:* se pesaron 0.0557 g de $Pb(NO_3)_2$, 0.0317 g de $Na_2HAsO_4.7H_2O$ y 0.0012 g de NaCl, se adicionó 50 mL de agua, se fijó el pH a 7 y se llevó la suspensión a 100mL.

Los reactivos Na_2HAsO_4 y $Pb(NO_3)_2$ fueron secados a 130°C antes de su uso y su pureza fue comprobada mediante soluciones estándar de 1000 mg L^{-1} de Pb.

2.2.4 Experimentos de Adsorción-Precipitación

Los experimentos de adsorción-precipitación se diseñaron con base en lo encontrado mediante los modelos termodinámicas con el programa Visual MINTEQ. Las condiciones empleadas se escogieron debido a que los modelos termodinámicos predicen la existencia de tres zonas diferentes (mostradas a detalle en el capítulo 4), siendo representadas por cada condición establecida en los experimentos de adsorción-precipitación (tabla 2.6). En los experimentos 1, 2 y 3, la condición inicial se estableció partiendo del arseniato de plomo sólido, hidroximimetita $[Pb_5(AsO_4)_3OH]$, en una proporción molar con respecto a la goetita de acuerdo a lo indicado en la tabla 2.6. El cuarto experimento corresponde a las mismas condiciones que las del experimento 2 pero se partió del sólido hidrocerusita $[Pb_3(OH)_2(CO_3)_2]$ y de Na_2HAsO_4 para proveer

del As(V) necesario para cumplir con la relación As/Pb (igual a la de la hidroximimetita) y As/Fe.

Tabla 2.6 Condiciones experimentales iniciales.

Exp.	Concentración (M)		Relación As / Fe
	AsO_4^{3-}	Pb^{2+}	
1	$1.0x10^{-6}$	$1.67x10^{-6}$	0.0004
2	$2.6x10^{-4}$	$4.33x10^{-4}$	0.1155
3	$5.0x10^{-5}$	$8.33x10^{-5}$	0.0222
4	$2.6x10^{-4}$	$4.33x10^{-4}$	0.1155

Adicionalmente se desarrollaron experimentos de adsorción-precipitación que serán capaces de corroborar el comportamiento del As(V) predicho por el modelo empleado para el sistema As(V)/Pb(II)/CO_3^{2-}/GOE/Cl^-. Para ello las condiciones experimentales fueron:

Tabla 2.7 Condiciones experimentales iniciales para sistema con cloruros.

Exp.	Concentración (M)			Relación As / Fe
	AsO_4^{3-}	Pb^{2+}	Cl^-	
Cloruros 1	$2.00x10^{-5}$	$3.33x10^{-5}$	$1.0x10^{-5}$	0.009
Cloruros 2	$4.00x10^{-5}$	$6.67x10^{-5}$	$1.0x10^{-5}$	0.018

El procedimiento para la realización de los experimentos de adsorción-precipitación se detalla a continuación:

Se pesó cada reactor al inicio y después de cada adición para conocer el volumen final de las suspensiones. Se cortaron 10 cm del tubo de diálisis de celulosa regenerada, se lavaron con agua desionizada para quitar el exceso de azida de sodio que presenta el material como medio de preservación, a continuación se cerró un extremo del tubo, y se colocó dentro de un vaso de precipitación para poder pesarlo. Posteriormente se procedió a pesar la suspensión de hidroximimetita, de hidrocerusita ó de mimetita (para el experimento con cloruros), en las cantidades apropiadas para que las concentraciones finales fueran las descritas anteriormente.

La membrana se cerró de manera que no se existiera transferencia del sólido del interior de la membrana hacia la suspensión cuando se colocara dentro de ésta. Posteriormente se procedió a pesar la goetita, la cantidad necesaria para tener una

concentración de sólidos de 0.2 g L^{-1} (en este caso 0.05 g), a continuación se ajustó la fuerza iónica a 0.01 M con la solución de $NaNO_3$ 1 M.

Adicionalmente, para el experimento 4, fue necesario pesar la solución de Na_2HAsO_4 en el reactor de manera que la concentración de As(V) fuera la descrita en la tabla 3.6. Se adicionó una cantidad de agua desionizada (de modo que el volumen final sea cercano a 250 mL), y se ajustó el pH a 7, para simular condiciones ambientales.

Las suspensiones se llevaron a 250 mL, se colocó la barra magnética dentro del reactor, se cerraron los reactores y se colocaron sobre los agitadores magnéticos (marca Corning PC-420D), con una velocidad de agitación de 900 rpm. El sistema está cerrado, pero no de manera hermética, permitiendo de esta manera el intercambio de CO_2 con el ambiente.

El esquema del reactor empleado se muestra en la figura 2.2.

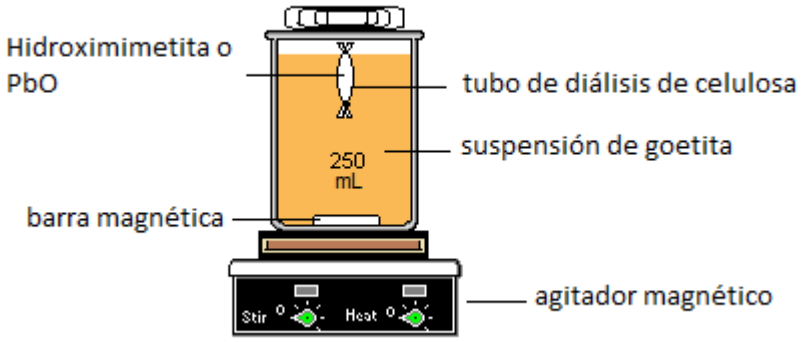

Figura 2.2 Esquema general de los reactores diseñados para los experimentos

Se ajustó el pH continuamente, para no alterar la condición establecida (pH 7), para ello se calibró el potenciómetro como se describió en secciones anteriores, antes de su uso.

Además de las condiciones descritas anteriormente, se prepararon varios blancos sin la presencia de goetita, en las concentraciones máximas correspondientes al experimento #4 (tabla 2.4), con la finalidad de identificar diferentes fenómenos: en el primero, se colocó en el tubo de diálisis hidroximimetita y se mantuvo en agitación para identificar que no exista formación del sólido fuera del tubo de diálisis y confirmar que los iones $H_2AsO_4^-$ y $HAsO_4^{2-}$ atraviesen el tubo; el segundo se preparó con solución de

Na_2HAsO_4 dentro del tubo de diálisis, para determinar si existía adsorción en el tubo de diálisis o en el recipiente, y el tercero se realizó partiendo del óxido de plomo en el tubo de diálisis y con una solución de Na_2HAsO_4, para identificar la formación de hidroximimetita dentro del tubo de diálisis. El sólido resultante se identificó mediante difracción de rayos X.

2.2.5 Monitoreo de los experimentos

Para tener un conocimiento detallado del proceso de adsorción-precipitación es necesario tomar muestras constantemente y analizarlas, para determinar cuando el sistema ha alcanzado el equilibrio y de esta manera conocer la cinética del proceso.

Con una jeringuilla de 10 mL se tomó una muestra de la suspensión de 10 mL cada 2 días hasta que los experimentos alcanzaron el equilibrio (aproximadamente 14 días). Dichas muestras se filtraron a través de membranas de nitrocelulosa de 0.05µm de diámetro de poro (Millipore 9004-70-0 filter tipe) que se encontraban sostenidas en un swinnex (Swinnex-Gasket, Millipore SX0002501). El filtrado se recogió, se pesó (se adicionan 60µL de $HCl_{(c)}$ para preservar la muestra), y se analizó con la finalidad de determinar la fracción de As(V) y Pb(II) soluble.

Mientras tanto el sólido separado (pasta), que se retiene sobre la membrana de nitrocelulosa, se lavó por tres ocasiones con agua destilada con el fin de remover la solución acuosa remanente. Luego se procedió a digerir completamente la goetita empleando 5 mL de HCl concentrado y por último a la disolución resultante se agregó agua desionizada hasta alcanzar un volumen de 25mL, para proceder a analizar las fracciones de As(V) y Pb(II) adsorbidos.

Una vez determinadas las fracciones solubles y adsorbidas tanto de As(V) como de Pb(II) se restan del valor inicial de concentración agregada de cada experimento para el cálculo indirecto de la concentración de especies precipitadas en cada sistema. Esto se muestra en la siguiente ecuación:

$$[i]_{TOTAL} = [i]_{(aq)} + [i]_{(ads)} + [i]_{(s)} \qquad \text{Ec. 11}$$

Donde, $[i]_{TOTAL}$ es la concentración molar añadida de As(V) o Pb(II), $[i]_{(aq)}$ es la concentración molar acuosa al equilibrio, $[i]_{(ads)}$ es la concentración molar adsorbida y $[i]_{(s)}$ es la concentración molar que corresponde a las especies precipitadas.

Esto fue posible dado que las fracciones precipitadas $[i]_{(s)}$ no atravesaron la membrana de diálisis, manteniéndose en el interior y físicamente separada de la goetita.

2.2.6 Métodos analíticos para la determinación de As y Pb

La determinación de arsénico se realizó por dos métodos, dependiendo del nivel de concentración esperado. Estos métodos se describen a continuación:

Para los sistemas donde se esperaban concentraciones altas de arsénico (provenientes de las fracciones adsorbidas), según los modelos termodinámicas, se empleó el método de espectrometría de emisión atómica acoplada a plasma inducido, con el equipo ICP-AES Thermo IRIS intrepid II XSP empleando una longitud de onda de 193.7 nm, cuyo plasma es de argón, el flujo de nebulizador fue de 0.5 L min^{-1} y un poder de radiofrecuencia de 1150 W.

Para esta determinación fue necesario realizar una curva de calibración en un intervalo de 1-6 mg L^{-1} a partir de una solución de 50 mg L^{-1} realizada a partir de la solución estándar comercial de 1000 mg L^{-1}. A los estándares se les adicionó una concentración alta de Fe(III), con la finalidad de igualar la matriz en las muestras provenientes de la digestión de goetita. Los estándares fueron acidificados con HCl al 5% en volumen.

Para las muestras con concentraciones menores a 1 mg L^{-1} de As(V) se realizó un tratamiento para poder emplear el método de espectrometría de absorción atómica por generación hidruros (AAS-GH). Esto se debe a que esta técnica nos permite medir concentraciones mucho más pequeñas (hasta 1 μg L^{-1}), el equipo empleado es el VARIAN SpectrAA110 con una longitud de onda de 193.7 nm y con llama de acetileno.

El tratamiento previo que se le da a las muestras es el que se describe a continuación:

Se tomaron 3 mL de la muestra, se adicionaron 0.5 mL de solución de KI (con una concentración de 20% peso/volumen), y 0.5 mL de HCl (en concentración de 50%

en volumen) se dejaron reposar las muestras hasta que tomaron un color amarillo intenso (aproximadamente por tres horas), y se procedió a llevar las muestras a 10 mL. Con esto, todo el As(V) presente se reduce a As(III).

Un tratamiento similar se siguió para la preparación de los estándares de la curva de calibración, partiendo de una solución de 250 μg L^{-1} de As, preparada a partir del estándar comercial de 1000 mg L^{-1}, se prepararon 25 mL de las soluciones de la curva de calibración en un intervalo de 1 a 30 μg L^{-1}, estableciendo una concentración final de KI de 1% peso/volumen y de HCl de 2.5 % en volumen.

Para la generación de hidruros es necesario preparar una solución de $NaBH_4$ de concentración 0.6% peso/volumen sobre una solución de NaOH de concentración 0.5% peso/volumen. Además en necesario preparar una solución 50:50 de HCl, ambas soluciones ingresarán al generador de hidruros junto con la muestra (como lo muestra la Fig. 2.3), para darse las reacciones de formación de arsina (AsH_3) que se muestran a continuación:

$$NaBH_4 + 3H_2O + HCl \rightarrow H_3BO_3 + NaCl + 8H^+ \qquad \text{Eq. 12}$$

$$As^{3+} + 8H^+ \rightarrow AsH_3 + 5/2\, H_2(exceso) \qquad \text{Eq. 13}$$

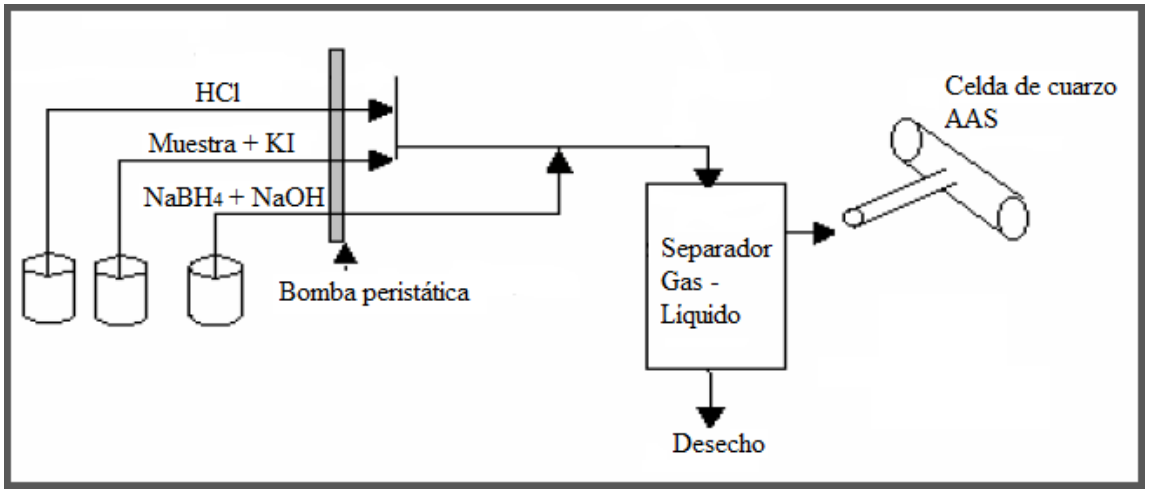

Figura 2.3 Representación esquemática del absorción atómica acoplada a generador de hidruros.

La determinación de la concentración de plomo se realizó mediante espectrometría de absorción atómica (AAS) con el equipo VARIAN SpectrAA110 con

las siguientes condiciones de trabajo: una longitud de onda de 217 nm, con una llama producida por aire/acetileno.

Los estándares para la curva de calibración se prepararon a partir de una solución de 100 mg L^{-1} preparada a partir de una comercial de 1000 mg L^{-1}, en un intervalo de concentraciones finales entre 0.1 y 5 mg L^{-1}. Al final los estándares fueron acidificados con HCl al 5% en volumen, al igual que las muestras.

2.2.7 Limpieza de goetita

Puesto que la goetita de estudio requiere un amplio trabajo de caracterización, se ha considerado muy importante recuperar el material para usarlo en experimentos posteriores, es por ello que es necesario realizar un proceso de lavado del material antes de su empleo en los experimentos de adsorción-precipitación, dicho proceso se detalla tanto para cationes, como para oxianiones:

a. *Goetita con cationes adsorbidos:* las suspensiones de goetita (cuya concentración de sólidos es 0.2 g L^{-1}) se ajustaron a valores de pH ligeramente menor a 4 (para evitar la posible disolución de goetita, esto último ocurre a pH< 3) adicionando una disolución de ácido nítrico 0.1 M, se estableció a una fuerza iónica de 0.1 M con $NaNO_3$ de modo que la sedimentación de la goetita sea más fácil, se agitó por 30 min y se centrifugó durante 10 min a una velocidad de 2000 rpm, se separó el sobrenadante, nuevamente se adicionó ácido nítrico y $NaNO_3$ en las concentraciones indicadas y se repitió el procedimiento 10 veces para asegurar la limpieza. Se adicionó agua desionizada y $NaNO_3$ cuya concentración final fue 0.1 M y se repitió el procedimiento descrito hasta que no se encontraron cationes en solución (determinada mediante la medición de conductividad ~ 0.1 $\mu S\ cm^{-1}$). Una vez concluido este proceso se ajustó la suspensión a pH neutro, lavándola con agua desionizada y centrifugándola durante 30 min a una velocidad de 3600 rpm.
b. *Goetita con oxianiones adsorbidos:* el procedimiento a realizar es muy similar al descrito en el punto anterior, la única diferencia radica en que las

suspensiones de goetita se deben llevar a pH 13 en lugar de a pH 4, esto se logra con solución 0.1 M de NaOH.

Una vez que se ha conseguido tener las goetitas libres de oxianiones y cationes, y con una mínima cantidad de agua, se procede a secarlas, colocándolas en la estufa en un vaso de precipitación a 105°C durante un día.

CAPÍTULO 3

3. DESCRIPCIÓN DE ARTÍCULOS PRESENTADOS

Para los experimentos desarrollados en la presente investigación se empleó goetita, cuyo método está descrito en:

1. Villacís-García, M., Ugalde-Arzate, M., Vaca-Escobar, K., Villalobos, M., Zanella, R., Martínez-Villegas, N., 2015. Laboratory synthesis of goethite and ferrihydrite of controlled particle sizes. Boletín de la Sociedad Geológica Mexicana (en prensa).

En donde se detalla el diseño de un método de síntesis y las condiciones empleadas para la obtención de goetitas con diferente ASE, necesarios en el desarrollo de la presente investigación ya que se emplearon goetitas de alta y de baja reactividad con la finalidad de corroborar el comportamiento que el modelo predice, dicha reactividad depende del ASE que presenta el óxido de hierro, como se ha demostrado en varias investigaciones desarrolladas anteriormente. Entre las condiciones empleadas, la más importante es el control de la velocidad de adición de hidróxido durante la hidrólisis de soluciones ácidas de Fe(III), encontrándose que con una adición rápida se producen goetitas de baja ASE y lo contrario produce goetitas de alta ASE.

Los resultados subsecuentes se obtuvieron con el modelo termodinámico, el cual fue validado con los resultados de experimentos de química húmeda, se determinaron las condiciones geoquímicas fundamentales que gobiernan la movilidad del As(V) en presencia de Pb(II) en el sistema goetita (α-FeOOH)/As(V)/Pb(II)/carbonato en un intervalo de pH de relevancia ambiental, cuyos resultados se reportan en los artículos científicos que se mencionan a continuación:

2. Vaca-Escobar, K., Villalobos, M., Ceniceros-Gomez, A.E., 2012. Natural arsenic attenuation via metal arsenate precipitation in soils contaminated with metallurgical wastes: III. Adsorption versus precipitation in clean As(V)/goethite/Pb(II)/carbonate systems. Applied Geochemistry 27, 2251-2259.

Donde se reportó que desde una baja relación molar As(V)/Fe(III) (0.012 a pH 7) el mecanismo de precipitación influye en la atenuación del As(V), y rápidamente se vuelve el proceso dominante sobre el mecanismo de adsorción. Los resultados del modelo, pese a ser obtenidos usando un valor promedio de las constantes de afinidad, permiten identificar de manera apropiada las condiciones cuantitativas de predominancia de cada mecanismo y las condiciones en las cuales prevalecen las fracciones relativamente grandes de especies adsorbidas, precipitadas y disueltas de As(V).

3. Vaca-Escobar, K., Villalobos, M., Pi-Puig, T., Zanella, R., 2015. Approaching the geochemical complexity of As(V)-contaminated systems through thermodynamic modeling. Chemical Geology (en prensa).

En el cual se aplicó el modelo termodinámico con una complejidad mayor en comparación con lo realizado con anterioridad. Para esto se diferenciaron los tipos de sitios presentes en el mineral goetita, se emplearon dos goetitas de diferente ASE y se evaluó la influencia de las relaciones molares empleadas [As(V)/Pb(II)], el pH y la presencia de iones cloruro y sulfato, y se encontró que las condiciones que favorecen la precipitación son, en orden de importancia: presencia de Cl^-, proporciones altas de Pb/As, proporciones altas de As/Fe, y goetitas de alta ASE; y las condiciones opuestas favorecen la adsorción, así como también la presencia de sulfatos a pH bajo.

4. Vaca-Escobar, K., Villalobos, M., 2015. Modeling the additive effects of Pb(II) and Cu(II) on the competitive attenuation of As(V) through solid precipitation versus adsorption to goethite. Boletín de la Sociedad Geológica Mexicana (en prensa).

En el cual, con la finalidad de acercarse a las diferentes condiciones que se tienen en sistemas reales, se determinó la influencia que tiene en el sistema bajo estudio: la presencia de un metal diferente al estudiado, para ello se empleó Cu(II) en lugar de Pb(II) usando varias relaciones molares As(V)/Cu(II), y la presencia simultánea de Pb(II) y Cu(II) en diferentes relaciones molares As(V)/Pb(II)/Cu(II), encontrándose que se tiene un mayor porcentaje de especies precipitadas en el sistema binario con Pb(II) que en el con Cu(II) y se favorece aún más el proceso de precipitación con la presencia en el sistema ternario con una relación de As(V)/Pb(II)/Cu(II) = 1/1/1.

México, D.F., 18 de Marzo, 2015

A QUIEN PUEDA INTERESAR

En mi calidad de editor en jefe del *Boletín de la Sociedad Geológica Mexicana*, me complace hacer constar que el manuscrito intitulado "*Laboratory synthesis of goethite and ferrihydrite of controlled particle sizes*", sometido por M. Villacís-García, M. Ugalde-Arzate, K. Vaca-Escobar, M. Villalobos, R. Zanella, y N. Martínez-Villegas ha sido aceptado para su publicación en el número de nuestra revista, "From micro to molecular scale investigations in geochemistry", tras su revisión por dos árbitros expertos independientes y un editor a cargo.

Saludos cordiales,

Dr. Antoni Camprubí
Editor en Jefe, Boletín de la Sociedad Geológica Mexicana

Laboratory synthesis of goethite and ferrihydrite of controlled particle sizes

Milton Villacís-García[a], Mariana Ugalde-Arzate[a], Katherine Vaca-Escobar[a], Mario Villalobos[a,*], Rodolfo Zanella[b] and Nadia Martínez-Villegas[c]

[a] Environmental Bio-Geochemistry Group, Earth Sciences Graduate Program, Geochemistry Department, Instituto de Geología, Universidad Nacional Autónoma de México (UNAM), Coyoacán, Ciudad Universitaria, México 04510, D.F.

[b] Centro de Ciencias Aplicadas y Desarrollo Tecnológico, Universidad Nacional Autónoma de México (UNAM), Coyoacán, Ciudad Universitaria, México 04510, D.F.

[c] IPICyT, Instituto Potosino de Investigacion Cientifica y Tecnologica, Camino a la Presa San Jose No. 2055, Col. Lomas 4a Secc., 78216 San Luis Potosi, SLP, Mexico

* Address correspondence: Tel: (52-55)5622-4336; FAX: (52-55)5622-4352. E-mail address: mar.villa@stanfordalumni.org (M. Villalobos)

ABSTRACT

Iron oxihydroxides, such as goethite and ferrihydrite, are highly abundant and ubiquitous minerals in geochemical environments. Their surface reactivity is high towards adsorption of anions and cations of environmental relevance because of their small particle sizes. For this reason these minerals are extensively studied in environmental geochemistry, and also are very important for environmental and industrial applications. In the present work, we report the synthesis and characterization of goethites and ferrihydrites of controlled particle sizes, because it has been shown that their surface reactivity is highly dependent on their crystal sizes, even after normalizing by specific surface area. In order to investigate the reasons for this changing reactivity it is necessary to work with reproducible particle sizes of these minerals. We investigated here the experimental condition to synthesize goethite samples of four different specific surface areas: *ca*. 40, 60, 80 and 100 $m^2 g^{-1}$, through the controlled speed of hydroxide addition during hydrolysis of acid Fe(III) solutions. In the case of 2-line ferrihydrite, samples with two different particle sizes were prepared by changing the aging time under the pH conditions of synthesis (pH = 7.5). The synthesized minerals were identified and characterized by: X-ray Diffraction, N_2 adsorption BET specific surface area, Transmission Electron Microscopy, Attenuated Total Reflectance Fourier Transform Infrared Spectroscopy, and maximum Cr(VI) adsorption.

KEYWORDS:

Synthesis, iron oxides, specific surface area, goethite, ferrihydrite, particle size.

RESUMEN

Los oxihidróxidos de hierro, como la goetita y ferrihidrita, son minerales altamente abundantes y ubicuos en ambientes geoquímicos. Su reactividad superficial es alta hacia la adsorción de aniones y cationes de relevancia ambiental dados sus pequeños tamaños de partícula. Por esta razón estos minerales son estudiados extensamente en geoquímica ambiental, y también son muy importantes en aplicaciones ambientales e industriales. En el presente trabajo reportamos la síntesis y caracterización de goetitas y ferrihidritas de tamaño de partícula controlado dado que se ha demostrado que su reactividad superficial es altamente dependiente de sus tamaños cristalinos, aún después de normalizar por su área superficial específica. Para investigar las razones de estos cambios de reactividad es necesario trabajar con tamaños de partícula reproducibles de estos minerales. Aquí presentamos las condiciones experimentales para sintetizar muestras de goetita de cuatro diferentes áreas superficiales específicas: *ca*. 40, 60, 80 and 100 $m^2 g^{-1}$, a través de la velocidad controlada de adición de hidróxido durante la hidrólisis de soluciones ácidas de Fe(III). En el caso de ferrihidrita de 2 lineas, se prepararon muestras con dos tamaños diferentes de partícula cambiando el tiempo de añejamiento bajo las condiciones de pH de síntesis (pH=7.5). Los minerales sintetizados se identificaron y caracterizaron por: Difracción de Rayos X, área superficial específica por adsorción de N_2 BET, Microscopía de Transmisión Electrónica, Espectroscopía de Infrarrojo de Transformada de Fourier con Reflectancia Total Atenuada, y adsorción de Cr(VI) máxima.

PALABRAS CLAVE:

Síntesis, óxidos de hierro, área superficial específica, goetita, ferrihidrita, tamaño de partícula.

1. Introduction

Iron oxides, oxyhydroxides, and hydroxides (henceforth referred to as "iron oxides", for simplicity) are widely distributed in soils and rocks, lakes, rivers, on the seafloor, air and in organisms (Adegoke *et al.*, 2013). Because of their abundance and reactivity these minerals play an important role and are extensively studied in numerous disciplines, including environmental science, geochemistry, geology, engineering, and health sciences (Schwertmann and Cornell, 2007), in an attempt to understand their different physical, chemical and mineralogical properties. According to Guo and Barnard (2013) there are 14 species of iron oxides and ten of these occur in nature, being the most abundant goethite (α-FeOOH), hematite (α-Fe_2O_3), and magnetite (Fe_3O_4), followed by ferrihydrite [$Fe_{10}O_{14}(OH)_2$] (Michel *et al.*, 2011), maghemite (γ-Fe_2O_3) and lepidocrocite (γ-FeOOH). These iron oxides are responsible for the mobility and fate of numerous chemical species in soils and aquatic environments through adsorption processes, particularly onto goethite and ferrihydrite (Maji *et al.,* 2008; Swedlund *et al.,* 2009; Villalobos and Antelo, 2011), or through adsorption followed by reduction mechanisms as is the case of susceptible species on magnetite (Villacís-García *et al.,* 2014).

The present work reports the laboratory procedures required for the synthesis of goethite and ferrihydrite of controlled particle sizes, and their essential characterization, especially focusing on their surface properties. This is important because both minerals have shown considerable changes in surface reactivity as a function of their particle size, often following trends that are non-intuitive or not easily predictable. Therefore, working with

samples of controlled particle sizes is essential to ultimately understand the relationship between particle size and reactivity, as a function of morphological and surface structural changes.

Goethite is an abundant constituent of terrestrial soils, sediments, and oolitic iron ores, being a major weathering product of all rock types. It is predominant in younger sedimentary deposits, giving the rocks a yellow color (Prasad *et al*., 2006)**.** Goethite particles show high specific surface areas and strong affinities for surface binding of oxyanions and heavy metals (Fendorf *et al*., 1997; Villalobos and Leckie, 2001; Antelo *et al*., 2005; Granados-Correa *et al*., 2011; Perelomov *et al*., 2011).

Synthetic goethite nanoparticles are acicular and are often aggregated into bundles or rafts of oriented crystallites (Varanda *et al*., 2002). The precipitation technique is probably the simplest and most efficient chemical pathway to obtain iron oxide particles. Iron oxides (goethite, magnetite or maghemite) are usually prepared by addition of alkali to iron salt solutions and keeping the precipitated solids in suspension for aging (Guyodo *et al*., 2003; Jaiswal *et al*., 2013).

In recent years, important differences in the reactivity of goethite have been found, in an inverse relationship with its specific surface area (SSA). There appears to be two categories of goethites: ideal crystals with high specific surface area (>80 $m^2 g^{-1}$) that behave equally when adsorption data are normalized by SSA; and goethites of low specific surface area (< 80 $m^2 g^{-1}$), which show progressively higher surface reactivity as SSA decreases (Villalobos and Perez-Gallegos, 2008). The controlled synthesis of goethites of desired SSAs is therefore useful to investigate this anomalous geochemical behavior, which

is apparently caused by changes in the distribution of the goethite crystal faces exposed, because some faces are considerably more reactive than others (Villalobos *et al.*, 2009; Salazar-Camacho and Villalobos, 2010).

One of the most popular procedures for goethite preparation in the laboratory is the precipitation method proposed by Atkinson *et al.* (1967) and variations from it. The mechanisms of goethite formation involves deprotonation and hydrolysis of Fe(III) in solution, followed by nucleation and crystallization (Kosmulski *et al*., 2004). The length/width ratio of the crystals varies widely, as a result of changes in precipitation conditions; for example, the crystal size of goethite decreased as the temperature fell from 70 to 4°C, increasing the specific surface area (SSA) by an order of magnitude (Schwertmann *et al*., 1985; Montes-Hernandez *et al*., 2011). Conversely, stirring conditions can promote the growth of goethite crystals (Schwertmann and Stanjek, 1998). More recently, the use of surfactants and other organic compounds for goethite synthesis has also been applied to control its size and shape (Zamiri *et al*., 2014).

However, it is clear that even small changes in one chosen method, such as the Atkinson method, may have important repercussions on the resulting particle sizes, as evaluated by specific surface area (SSA). Table 1 shows a compilation of such changes with resulting SSA values varying from 8 to 105 $m^2 g^{-1}$. In the present work we adopted the Atkinson *et al*. (1967) method and investigated the effect of base addition rate on the resulting goethite SSA, at fixed volumes, concentrations and other synthetic conditions; evaluating in tandem the reproducibility of the results.

In the case of ferrihydrite (FH), this nanomineral is precursor to the other prevalent Fe(III) oxide minerals, goethite and hematite (Schwertmann *et al.,* 2004; Cudennec and Lecerf,

2006), which form by oriented aggregation crystal growth of ferrihydrite nanoparticles (Burrows *et al.*, 2013). However, ferrihydrite itself is widespread as suspended material in the aqueous fraction of soils and weathered rocks, in precipitates around cold and hot springs, especially those supporting iron-metabolizing bacteria, and in acid mine effluents, especially as they neutralize (Childs, 1992; Fortin and Langley, 2005).

In the goethite synthesis ferrihydrite is the initial precipitate that results from the rapid hydrolysis of Fe(III) solutions, before aging to goethite at higher temperature. Its crystal size and order are usually lower than those of any other Fe oxide except feroxyhyte and schwertmannite, and it is considered a nanomineral because its particle sizes range only from 2 to 9 nm (Hiemstra, 2013). For this reason ferrihydrite shows very broad and few X-ray diffraction (XRD) bands, and the two particular varieties of this mineral are named according to the number of XRD bands they show: 6-line ferrihydrite shows 6 –8 broad peaks and a higher crystallinity, and 2-line ferrihydrite shows only two very broad peaks and a lower crystallinity, but a higher reactivity. In natural environments all forms of ferrihydrite are widespread usually as young Fe oxides, and they play an important role as active adsorbents as a result of their very high SSA (Schwertmann and Cornell, 2007). Nevertheless, the actual reactive SSA is not known because upon drying for the experimental BET nitrogen adsorption determination, ferrihydrite nanoparticles aggregate considerably and thus yield values that are considerably lower than those found under aqueous suspension conditions. To date, no experimental method has been devised to determine the SSA of ferrihydrite under aqueous conditions.

Some of the conditions imposed in synthetic procedures to obtain ferrihydrite are compiled in Table 2, but no systematic work has been performed to determine resulting particle sizes or SSAs as a function of experimental conditions.

We limited the present research to the controlled synthesis of 2-line ferrihydrites because the reactivity of the more crystalline 6-line variety is expected to be very different. Given the difficulties for accurate determinations of particle sizes and SSAs of ferrihydrite in aqueous suspension, we complemented TEM observations with indirect parameters related to surface reactivity differences.

2. Materials and methods

2.1 Goethite synthesis.

Goethite was synthesized following the basic protocol of Atkinson *et al*. (1967), to yield 8-9 g of goethite: 50 g of $Fe(NO_3)_3.9H_2O$ (Sigma-Aldrich) were weighed and dissolved in 825 g of deionized water (Milli-Q). Water used for synthesis solutions was previously boiled and bubbled in N_2 to eliminate CO_2. Separately, 200 ml of a 2.5M NaOH (Sigma-Aldrich) CO_2-free solution were prepared. This NaOH solution was poured over the Fe(III) solution under N_2 flow, while continuously stirring. From the conditions compiled in Table 1 it was clear that similar pH, aging times, and temperatures produced goethites with important differences in SSA. The small goethite particles synthesized by Hiemstra and van Riemsdijk (1996) by slow addition of base gave us a clue about the importance of the speed of NaOH addition in the hydrolysis of aqueous Fe(III) and the resulting particle sizes, so we focused on this parameter for the current investigation. The speed of base addition into the Fe(III) solution, was inversely proportional to the resulting goethite SSA (Table 3).

For example, for the lowest SSA obtained through this control parameter, the complete NaOH solution was added at once in the reactor, and for the highest SSA values, the base addition rate was 1 mL min^{-1}. After final NaOH addition (pH >12), the stirring was maintained for 30 min. The reactor was then placed in an oven at 60 ^{o}C for 24 h, to allow the initial ferrihydrite precipitate to age to goethite. Goethite precipitates were repeatedly washed, shaken, and centrifuged. Dilute HNO_3 was used to drop the pH to 7 for the initial washes. For the sequential washes deionized water was used until a conductivity value of 0.1 μS cm^{-1} was obtained.

2.2 Ferrihydrite synthesis:

100 mL of a 0.2M $FeCl_3 \cdot 6H_2O$ (Sigma-Aldrich) were prepared and placed in a 250 mL Nalgene flask. The solution was vigorously stirred while a 1M NaOH solution was added relatively quickly to bring the pH to 6.5; the NaOH addition was continued dropwise until the pH reached a value of 7.5 (Schwertmann and Cornell, 2007; Li *et al.*, 2010).

The resulting suspension was divided into two batches that were named FFh and AFh, for fresh and aged ferrihydrites, respectively. The former was immediately and repeatedly washed, centrifuged and decanted until the conductivity was about 10 μS cm^{-1} and freeze dried (dyalisis was avoided in order to minimize further particle aging). The AFh batch was aged for 48 h at room temperature with continuous stirring, after which it was also washed and freeze dried as above. Both products were stored as dry solids at room temperature.

2.3 XRD identification.

Goethite and ferrihydrite X-ray powder diffraction (XRD) analyses were performed using a Shimadzu - XRD-6000 diffractometer equipped with a copper tube and a graphite monochromator. Samples were disaggregated with an agate pestle and mortar, and were mounted in aluminum holders and placed in the diffractometer. XRD patterns were collected in an angular range of 2Θ from 4° to 70° with a rate of 1° min^{-1}. Phase identification was made with a PDF database using Shimadzu software.

2.4 ATR-FTIR Measurements.

The goethite and ferrrihidryte dried samples were characterized using an infrared spectrometer Nicolet-IS10, THERMO-SCIENTIFIC with a diamond GladiATR accessory from PIKE Technology, using the Omnic 9 software, which allows IR analysis in a wavelength range between 450 and 4000 cm^{-1}. For each analysis, a background of the free diamond crystal was collected and used to correct for the presence of the internal reflection element and air. A small quantity of each dry sample was placed over the diamond surface.

2.5 Specific Surface Area Determination.

The specific surface areas (SSAs) of goethite and ferrihydrite were calculated by the Brunauer-Emmett-Teller (BET) method on a Quantachrome Autosorb 1. Before nitrogen adsorption, 200-250 mg of the dry and (mortar-) dispersed solid powders were placed on a Quantrachrome 9 mm cell, and outgassed at 105 °C for 24 h to remove adsorbed water. Nitrogen adsorption isotherms were programmed with a 44 data point collection, of which

the first 11 were used for SSA calculations, by using a nonlinear least-squares regression method to fit the interval data in the experimental isotherms.

2.6 Transmission electron microscopy (TEM)

Transmission electron microscopy (TEM) images were obtained using a Tecnai G2 F30 S-Twin TEM instrument. The TEM operates at 300 kV using a field emission gun in Schottky mode as an electron source. The samples for TEM analysis were prepared by placing 3 mg of the dried (mortar- disaggregated) solid iron oxide in 10 mL of absolute ethanol, and ultrasonication for 45 minutes for goethite and 6 hours for ferrihydrite. Four drops of the slurry were deposited on a holey-carbon-coated copper grid for analysis.

2.7 Cr(VI) adsorption maxima.

Maximum Cr(VI) adsorption was determined following the procedures reported by Mesuere and Fish (1992), Vangeen *et al*. (1994) and Villalobos and Pérez-Gallegos (2008). 50 mL of a $4x10^{-3}$ M Cr(VI) solution were prepared from $K_2Cr_2O_7$ (JT Baker) and placed in a high density polypropylene reactor to which the iron oxide solid was added to yield a concentration of 1.8 g L^{-1} for goethite, and 0.3 g L^{-1} for ferrihydrite. The ionic strength was fixed to 0.1 M with $NaClO_4$ (Sigma-Aldrich) and the pH was fixed to pH 4 with diluted $HClO_4$ (Sigma–Aldrich). The suspension was immersed in an ultrasonic bath for approximately 1 min. to ensure an adequate disaggregation and dispersion of the solid. The suspension was then placed in an orbital shaker for 72 h, but the pH of the suspension required frequent readjustments to pH 4. This procedure was made at least in triplicate, but for the extreme SSA goethites it was done in replicates of 10 to 15 because we are

particularly interested in continuing work with these goethites. Aqueous Cr(VI) concentrations at equilibrium were analyzed, after filtering appropriate suspension aliquots through 0.05 μm nitrocellulose membranes, by UV-visible spectroscopy. Using a standard curve of 5-70 mg Cr(VI) L^{-1} at pH 4 direct colorimetric measurements were made at λ= 348 nm (Akiyama *et al.,* 2003) using a Jenna-Analitycs SPECORD 210 PLUS Uv/Vis spectrophotometer (detection limit = 0.3 mg L^{-1}). The difference from the total Cr(VI) added initially was assumed to be the maximum adsorbed Cr(VI) concentration.

3. Results and Discussion

3.1 Goethite synthesis

Figure 1 shows photographs of the experimental set-up (a), and products obtained (b-c) during goethite synthesis, in which CO_2 exclusion was maintained throughout the high-pH stages of the aqueous suspensions. The initial precipitate formed was a dark red suspended ferrihydrite, which upon aging turned to an ochre color goethite suspension. The different goethites varied from darker color hues for the high-SSA samples to lighter hues for the low-SSA samples.

3.2 Goethite characterization

3.2.1 Specific surface area (SSA)

SSA is used in this work as a proxy for particle size. Goethite particles are acicular, or recently described more accurately as blades or laths (Livi *et al.*, 2013), and thus, an average size parameter is difficult to define and measure directly. However, we may use

the log-linear relationship between SSA and the geometric average particle size [eq. (1)], as an alternative method to report changes in particle sizes for goethite, based solely on SSA.

$$\text{Log SSA} = \text{Log}\,(k/\delta) - \text{Log}\,r \qquad (1)$$

Where k is a constant related to the particle shape, δ is the specific gravity of the solid, and r is an average size parameter (Parks, 1990). For highly symmetrical shapes, such as spheres or cubes, k=3 and r is the sphere radius or the radius of the cube sides; but the k value for the goethite lath is unknown. Since both k and δ are expected to be approximately constant with goethite size changes, SSA changes are sufficient to indicate particle size differences in our samples, and no further efforts were devoted to calculate actual size values.

Table 3 shows the SSA values obtained for four different NaOH rate additions during goethite synthesis, ranging from 42 m^2/g to 105 m^2/g, as additions of 2.5 M NaOH were gradually slowed down from an instantaneous addition of the 200 mL to 1 mL min^{-1} (i.e., to 3.33 h to add the 200 mL), respectively. These values indicate that goethite particle laths are progressively smaller as the NaOH addition rate is decreased.

3.2.2 X-ray diffraction (XRD)

The XRD patterns of all samples synthesized correspond to pure goethite according to the JCPDS PDF data base (JCPDS 29-713) used for phase identification, and no other Fe oxide phases were identified (Figure 2). The samples were analyzed under the same diffractometer conditions. Differences in their relative crystallinities may be observed from changes in the peaks widths and heights. Sharper and taller peaks, denoting higher

crystallinity, are observed as SSA decreases, except when going from the 101 to the 83 m^2 g^{-1} goethites, which seem to show very similar peak widths and heights.

3.2.3 Transmission electron microscopy (TEM)

TEM images are shown for the two extreme sizes of goethites synthesized: GOE101 and GOE43 (Figure 3). In both cases the typical goethite lath shapes may be identified. GOE101 shows small ideal nanocrystals of lengths between 100 and 200 nm and widths of approximately 50 nm (Figure 3a and b). GOE43 shows particles that seem to have grown in aggregated form, reaching 1μm lengths with widths of around 200 nm (Figure 3c and d).

3.2.4 ATR-FTIR

The main ATR-FTIR spectra (Figure 4) are similar among all goethites. The peaks found at 621-632 cm^{-1} are associated to the FeO_6 octahedral lattice (Ruan et al., 2001). The peaks at 786-791 cm^{-1}, and at 886-897 cm^{-1} are assigned to Fe-O-H bending vibrations (Montes-Hernandez *et al*., 2011 and Zamiri et al., 2014). There is a small peak around 1650 cm^{-1} that corresponds to bending modes of hydroxyl (Prasad et al., 2006). The broad peaks centered around 3101-3118 cm^{-1} correspond to the stretching of goethite hydroxyls and surface H_2O molecules (Prasad et al., 2006). In the goethite sample with SSA of 43 m^2 g^{-1} the presence of leftover NO_3^- from incomplete washing may be detected at around 1400 cm^{-1}.

A close-up of the region between 1200-1700 cm^{-1} (Figure 5), shows the presence of adsorbed water bending vibrations at 1651-1654 cm^{-1}, and of adsorbed carbonate with peaks of the asymmetric and symmetric O–C–O stretch vibrations at 1499-1509 cm^{-1}, and

at 1307-1322 cm^{-1}, respectively (Villalobos and Leckie, 2001). The adsorbed nitrate on GOE43 (Figure 5a) blocked the potential carbonate peaks on this sample.

3.2.5 Cr(VI) adsorption

Maximum chromate adsorption was evaluated at pH 4 (Table 4). The results show that the goethite with the lowest SSA (GOE43) has the highest adsorption capacity (4.4 μmol m^{-2}), while the other three goethites don't show much differences in adsorption capacities, between 2.8 and 3.0 μmol m^{-2}. These latter values are slightly larger than the Cr(VI) adsorption maximum reported previously for a 94 m^2 g^{-1} goethite of 2.6 μmol m^{-2} under the same conditions (Villalobos and Perez-Gallegos, 2008). However the latter reported a considerably larger Cr(VI) adsorption maximum of 8.1 μmol m^{-2} for a 50 m^2 g^{-1} goethite, suggesting that the increase in reactivity for the more reactive goethites may not be a sole function of SSA. The increase in surface reactivity of large goethites is related to a higher proportion of crystal faces that contain a larger value of reactive surface site density (Villalobos et al., 2009; Salazar-Camacho and Villalobos, 2010).

3.3 Ferrihydrite synthesis

The experimental set-up for ferrihydrite synthesis is very similar as that described in the goethite section. Samples of 2-line ferrihydrite were synthetized according to one variation of the method of Schwertmann and Cornell (2007), adding carefully 1 M NaOH in 100 mL of 0.2 M $FeCl_3$ until pH 7.5, by continuous stirring (Schwertmann and Cornell, 2007; Li, *et al.*, 2010). To obtain different particle sizes the predominant experimental variable is pH,

and a high value of it produces surface charges that bring on growth by oriented aggregation (Burrows, *et al.,* 2013*)*. Therefore, the longer the product remains in its synthesis medium rich in OH^- groups, the greater the resulting particle size.

After the synthesis, products were repeatedly centrifuged and washed to remove the remaining salts. In this step an indirect evidence of different resulting particles size was observed, as presumably larger AFh particles were easily separated from the solution, in contrast to FFh particles. Furthermore, the final products had slightly different colors, AFh being the darkest.

3.4 Ferrihydrite characterization

3.4.1 SSA

Experimental BET results showed that the fresh ferrihydrite (FFh) had a higher SSA (311 m^2/g) than the aged ferrihydrite (AFh) (258 m^2/g). The uncertainties for these determinations were ±5 m^2/g.

Nevertheless, it is widely believed that SSA determined from dry samples of ferrihydrite considerably underestimates the actual SSA under aqueous suspension conditions, because of the high aggregation expected upon drying from such small nanoparticles (Villalobos and Antelo, 2011). Therefore, the previous values are only indicative of SSA of dry FH aggregates.

3.4.2 XRD

The identity of the synthesis products was confirmed by XRD (Figure 6), showing almost identical patterns for both FFh and AFh, with the two bands characteristic of two-line ferrihydrite centered at 35 and 63º 2θ (Schwartmann and Cornell, 2007**).** Perhaps the only difference observed is a slightly taller band at 35º for the aged sample. This would mean that the width of this peak at mid-height would be slightly lower, which is coincident with an expected larger crystal size of the aged sample. These differences, however, are too small to be analyzed quantitatively.

3.4.3 Particle Size

The TEM images for these samples show the extreme state of aggregation despite the attempts to disaggregate them using ultrasound for extended periods (6 h) (Figure 7). Close-ups of the border regions of aggregates show an important difference between both samples. For AFh (Figure 7a) particles of approximately 5 nm may be detected, in contrast to FFh (Figure 7b), where particle size seems to be around 2nm.

Because of this extreme particle aggregation, direct and accurate particle size measurements in ferrihydrites are at best difficult and prone to high uncertainties. Therefore, we believe BET SSA measurements yield a more accurate average picture that relates directly to the sizes present, according to equation (1), and we may use these measurements to investigate more accurately size difference between both synthesized samples. BET SSA values for our samples were 311 m^2/g and 258 m^2/g, for FFh and AFh, which strongly suggests a definitive size difference between the samples.

However, as stated before, the obtained BET SSA values are indicative of the exposed surface area of the dry aggregates, not of the individual particles, and do not reflect the SSA

values expected under aqueous suspension. To approach the latter, we used the relationships reported by Wang *et al.* (2013), between particle size and phosphate adsorption capacity, and in turn between the latter and BET SSA of a series of ferrihydrites, to cross-calculate the relationship between particle size and BET SSA of our ferrihydrites. The linear relationship obtained is shown in Fig. 8, and we may interpolate our BET SSA values, to obtain particle sizes of 3.4 and 4.2 nm for FFh and AFh respectively.

A cautionary note should be mentioned in the fact that the data for the above linear relationship was reported together for FH samples of both 2 lines and 6 lines. If, from these size measurements we back-calculate the SSA of the individual particles expected, using the specific mass gravity of 3.56 g/cm^3 and a spherical shape (Villalobos and Antelo, 2011), we obtain values of 494 and 400 m^2/g for individual particles of FFh and AFh, respectively.

3.4.4 ATR-FTIR

Ferrihydrite identification was also attained by ATR- FTIR spectroscopy, which shows the characteristic bands for this material as reported previously by Hausner *et al.* (2009), and no major distinction between the FFh and AFh (Figure 9). Three predominant regions may be identified in the spectra: (i) near 3150 cm^{-1} the O-H stretching signals appear in a very broad band, related to structural hydroxide as well as adsorbed H_2O; (ii) between 1650 and 1300 cm^{-1}, deformation water bending vibrations appears near 1630 cm^{-1}, and the asymmetric and symmetric stretching of C-O from adsorbed carbonate may be observed, respectively at 1465 and 1345 cm^{-1} (Bargar, *et al.*, 2005; Hausner, *et al.*, 2009); (iii) Fe–O lattice stretching modes appear at 705; 565; 480; and 420 cm^{-1}. However, factors such as

the degree of crystallinity, and extent of particle aggregation have all been shown to influence the infrared spectrum of iron oxide minerals, and therefore for 2-line ferrihydrite those signals are not well defined (Hausner *et al*., 2009).

3.4.5 Cr (VI) Adsorption

Maximum chromate adsorption was evaluated at pH 4. As with goethite, the solid concentrations were set to achieve similar aqueous concentrations of surface area between the two minerals. The results are shown in mmol of Cr(VI) adsorbed per gram of ferrihydrite (Table 5). Surprisingly, both yield very similar values of 1.50-1.58 mmol g^{-1}. In this case, it is not accurate to normalize by experimental surface area because of the strong aggregation during the BET analysis. However, if we use the back-calculated SSAs from the linear relationship previously found (*cf.* section *3.4.3*) (Wang *et al.,* 2013), of 400 and 494 m^2/g for AFh and FFh, respectively, we obtain values of 3.95 and 3.04 μmol m^{-2}, respectively. These values are larger than those obtained for goethite, except for the largest particle sized sample (*cf*. Table 4), and suggest that the surface of the aged sample is more reactive than that of the fresh sample, i.e., larger FH particle sizes are more reactive, which is an unexpected result, but shows a similar trend as for goethite. Nevertheless, this needs to be confirmed through other adsorption measurements, for example by acid-base titrations to obtain proton adsorption data.

4. Conclusions

The rate of OH^- addition to the $Fe(NO_3)_3$ solution was the crucial factor to synthesize goethites of different particle sizes, the higher the speed, the larger the resulting particles.

Under these rate controlled conditions we were able to synthesize goethites with specific surface areas (SSAs) ranging from *ca*. 40 $m^2 g^{-1}$ to 100 $m^2 g^{-1}$. We confirmed that as SSA decreases (i.e., particle size increases), the surface reactivity of the goethite particles increased, when adsorbed concentrations are reported per surface area. For ferrihydrite, we found that the aging time at the synthesis pH of 7.5 was the most important factor to control the final particle size. Indirect calculations yielded particle sizes obtained of 3.4 and 4.2 nm, for freshly prepared, and for 48-h aged ferrihydrite.

5. Acknowledgements

The authors wish to thank Dr. Teresa Pi Puig at the Geology Institute – UNAM for the X-ray Diffraction measurements, Dr. Lucy Mora Palomino at the Geology Institute – UNAM for access to ultracentrifuge, freezer and lyophilizer equipment, and Dr. Jesús Ángel Arenas Alatorre, for his guidance in preliminary TEM images of ferrihydrite. We thank students and technicians from LABQA at the Chemistry School, UNAM for their help with handling the analytical equipment and techniques. M. V.-G. and K. V.-E. are grateful to the CONACyT and Senescyt for the Ph.D. student fellowships received. M. U.-A. thanks the CONACyt for the Master's student fellowship received. This project was funded by UNAM-PAPIIT Project IT100912. Finally, we appreciate the comments from two anonymous reviewers who helped improve the manuscript for publication.

6. References

1 Adegoke, H.I., Adekola, F.A., Fatoki, O.S., Ximba, B.J., 2013, Sorptive Interaction of
2 Oxyanions with Iron Oxides: A Review: Polish Journal of Environmental Studies,
3 22, 7-24.

4 Akiyama, E., Markworth, A. J., McCoy, J. K., Frankel, G. S., Xia, L., McCreery, R. L.,
5 2003, Storage and release of soluble hexavalent chromium from chromate
6 conversion coatings on Al alloys - Kinetics of release: Journal of the
7 Electrochemical Society, 150, B83-B91.

8 Antelo, J., Avena, M., Fiol, S., Lopez, R., Arce, F., 2005, Effects of pH and ionic strength
9 on the adsorption of phosphate and arsenate at the goethite-water interface: Journal
10 of Colloid Interface Science, 285, 476-486.

11 Antelo, J., Fiol, S., Pérez, C., Mariño, S., Arce, F., Gondar, D., López, R., 2010, Analysis
12 of phosphate adsorption onto ferrihydrite using the CD-MUSIC model: Journal of
13 Colloid and Interface Science 347, 112-119.

14 Atkinson, R. J., Posner, A. M. and Quirk, J. P., 1967, Adsorption of potential-determining
15 ions at the ferric oxide-aqueous electrolyte interface: The Journal of Physical
16 Chemistry, 71, 550-559.

17 Bargar, J.R., Kubicki, J.D., Reitmeyer, R., Davi, J.A., 2005, ATR-FTIR characterization of
18 inner-sphere and outer-sphere carbonate surface complexes on hematite:
19 Geochimica et Cosmochimica Acta, 69, 1527-1542.

20 Burrows, N., Hale, C., Penn, L., 2013, Effect of pH on the kinetics of crystal growth by
21 oriented aggregation: Crystal Growth and Design, 13, 3396-3403.

22 Cudennec, Y., Lecerf, A., 2006, The transformation of ferrihydrite into goethite or
23 hematite, revisited: Journal of Solid State Chemistry, 179, 716-722.

24 Childs, C.W., 1992, Ferrihydrite: A review of structure, properties and occurrence in
25 relation to soils: Zeitschrift für Pflanzenernährung und Bodenkunde, 155, 441-448.

1 Fendorf, S., Eick, M.J., Grossl, P., Sparks, D.L., 1997, Arsenate and Chromate Retention
2 Mechanisms on Goethite. 1: Surface Structure: Environmental Science &
3 Technology, 31, 315-320.

4 Fortin, D., Langley, S., 2005, Formation and occurrence of biogenic iron-rich minerals:
5 Earth-Science Reviews, 72, 1-19.

6 Granados-Correa, F., Corral-Capulin, N.G., Olguin, M.T., Acosta-Leon, C.E., 2011,
7 Comparison of the Cd(II) adsorption processes between boehmite (gamma-AlOOH)
8 and goethite (alpha-FeOOH). Chemical Engineering Journal. 171, 1027-1034.

9 Guyodo, Y., Mostrom, A., Penn, R.L., Banerjee, S.K., 2003, From Nanodots to Nanorods:
10 Oriented aggregation and magnetic evolution of nanocrystalline goethite:
11 Geophysical Research Letters, 30, 191-194.

12 Guo, H.B., Barnard, A.S., 2013, Naturally occurring iron oxide nanoparticles: morphology,
13 surface chemistry and environmental stability: Journal of Materials Chemistry A, 1,
14 27-42.

15 Hausner, D.B., Bhandari, N., Pierre-Louis, A. M., Kubicki, J. D., Strongin, D. R., 2009,
16 Ferrihydrite reactivity toward carbon dioxide: Journal of Colloid and Interface
17 Science, 337, 492-500.

18 Hiemstra, T., 2013, Surface and mineral structure of ferrihydrite: Geochimica et
19 Cosmochimica Acta, 105, 316-325.

20 Hiemstra, T., van Riemsdijk, W.H., 1996, A surface structural approach to ion adsorption:
21 The charge distribution (CD) model: Journal of Colloid and Interface Science, 179,
22 488-508.

23 Hofmann, A., van Beinum, W., Meeussen, J.C.L., Kretzschmar, R., 2005, Sorption kinetics
24 of strontium in porous hydrous ferric oxide aggregates II. Comparison of
25 experimental results and model predictions: Journal of Colloid and Interface
26 Science, 283, 29-40.

1 Jaiswal, A., Banerjee, S., Mani, R., Chattopadhyaya, M.C., 2013, Synthesis,
2 characterization and application of goethite mineral as an adsorbent: Journal of
3 Environmental Chemical Engineering, 1, 281-289.

4 Kosmulski, M., Durand-Vidal, S., Maczka, E., Rosenholm, J.B., 2004, Morphology of
5 synthetic goethite particles: Journal of Colloid and Interface Science, 271, 261-269.

6 Li, Z., Zhang, T., Li, K., 2011, One- step synthesis of mesoporous two-line ferrihydrite for
7 effective elimination of arsenic contaminants from natural water: Dalton
8 Transactions, 40, 2062-2066.

9 Livi, K. J. T., Villaobos M., Varela M., Villacís-García M., Vaca-Escobar K., Sverjensky
10 D. A., 2013, The relationship of goethite surface structure, habit and adsorption
11 capacity: Goldschmidt Conference Abstracts.

12 Maji, S.K., Pal, A., Pal, T., 2008, Arsenic removal from real-life groundwater by
13 adsorption on laterite soil: Journal of Hazardous Materials, 151, 811-820.

14 Michel F. M., Ehm L., Antao S. M., Lee P. L., Chupas P. J., Liu G., Strongin D. R.,
15 Schoonen M. A. A., Phillips B. L. and Parise J. B., 2007, The structure of
16 ferrihydrite, a nanocrystalline material: Science, 316, 1726–1729.

17 Mesuere, K., Fish, W., 1992; Chromate and oxalate adsorption on goethite. 1. Calibration
18 of surface complexation models: Environmental Science & Technology, 26, 2357-
19 2364.

20 Montes-Hernandez, G., Beck, P., Renard, F., Quirico, E., Lanson, B., Chiriac, R., Findling,
21 N., 2011, Fast precipitation of acicular goethite from ferric hydroxide gel under
22 moderate temperature (30 and 70 degrees C). Crystal Growth & Design, 11, 2264-
23 2272.

24 Parks G.A., 1990, Surface energy and adsorption at mineral-water interfaces: An
25 introduction, in Hochella, M.F. Jr., White A.F. (eds.), Mineral-Water Interface
26 Geochemistry: Chantilly – USA, Mineralogical Society of America, 133-175.

1 Perelomov, L.V., Pinskiy, D.L., Violante, A., 2011, Effect of organic acids on the
2 adsorption of copper, lead, and zinc by goethite: Eurasian Soil Science, 44, 22-28.

3 Prasad, P.S.R., Shiva Prasad, K., Krishna Chaitanya, V., Babu, E.V.S.S.K., Sreedhar, B.,
4 Ramana Murthy, S., 2006, In situ FTIR study on the dehydration of natural goethite:
5 Journal of Asian Earth Sciences, 27, 503-511.

6 Rout, K., Mohapatra, M., Anand, S., 2012; 2-line ferrihydrite: synthesis, characterization
7 and its adsorption behaviour for removal of Pb(II), Cd(II), Cu(II) and Zn(II) from
8 aqueous solutions: Dalton transactions, 41, 3302-3312.

9 Ruan, H.D., Frost, R.L., Kloprogge, J.T., 2001, The behavior of hydroxyl units of synthetic
10 goethite and its dehydroxylated product hematite: Spectrochimica Acta Part a-
11 Molecular and Biomolecular Spectroscopy, 57, 2575-2586.

12 Salazar-Camacho, C., Villalobos, M., 2010, Goethite surface reactivity: III. Unifying
13 arsenate adsorption behavior through a variable crystal face - Site density model:
14 Geochimica et Cosmochimica Acta, 74, 2257-2280.

15 Schwertmann, U., Cambier, P., Murad, E., 1985, Properties of goethites of varying
16 crystallinity: Clays and Clay Minerals, 33, 369-378.

17 Schwertmann, U., Cornell, R.M., 2007, Iron Oxides in the Laboratory: Weinheim, Wiley-
18 VCH Verlag GmbH.

19 Schwertmann, U., Stanjek, H., 1998, Stirring effects on properties of Al goethite formed
20 from ferrihydrite: Clays and Clay Minerals, 46, 317-321.

21 Schwertmann, U., Stanjek, H., Becher, H.-H., 2004, Long-term in vitro transformation of 2-
22 line ferrihydrite to goethite/hematite at 4, 10, 15 and 25°C: Clay Minerals, 39, 433-
23 438.

24 Swedlund, P.J., Webster, J.G., Miskelly, G.M., 2009, Goethite adsorption of Cu (II), Pb
25 (II), Cd (II), and Zn (II) in the presence of sulfate: Properties of the ternary
26 complex: Geochimica et Cosmochimica Acta, 73, 1548-1562.

Vangeen, A., Robertson, A.P., Leckie, J.O., 1994, Complexation of carbonate species at the goethite surface - implications for adsorption of metal-ions in natural-waters: Geochimica et Cosmochimica Acta, 58, 2073-2086.

Varanda, L.C., Morales, M.P., Jafelicci, M., Serna, C.J., 2002, Monodispersed spindle-type goethite nanoparticles from Fe-III solutions: Journal of Materials Chemistry, 12, 3649-3653.

Villacís-García, M., Villalobos, M., Gutiérrez-Ruiz, M., 2014, Optimizing the use of natural and synthetic magnetites with very small amounts of coarse Fe(0) particles for reduction of aqueous Cr(VI): Journal of Hazardous Materials. *In press.*

Villalobos, M., Antelo, J., 2011, A unified surface structural model for ferrihydrite: Proton charge, electrolyte binding, and arsenate adsorption: Revista Internacional de Contaminación Ambiental, 27, 139-151.

Villalobos, M., Cheney, M.A., Alcaraz-Cienfuegos, J., 2009, Goethite surface reactivity: II. A microscopic site-density model that describes its surface area-normalized variability: Journal of Colloid and Interface Science, 336, 412-422.

Villalobos, M., Leckie, J.O., 2001; Surface complexation modeling and FTIR study of carbonate adsorption to goethite: Journal of Colloid and Interface Science, 235, 15-32.

Villalobos, M., Perez-Gallegos, A., 2008, Goethite surface reactivity: A macroscopic investigation unifying proton, chromate, carbonate, and lead(II) adsorption: Journal of Colloid and Interface Science, 326, 307-323.

Wang, X., Li, W., Harrington, R., Liu, F., Parise, J.B., Feng, X., Sparks, D.L. 2013, Effect og ferrihydrite crystalite size on phosphate adsorption reactivity: Environmental Science and Technology, 47, 10322-10331.

Weidler, P.G., Schwinn, T., Gaub, H.E., 1996, Vicinal faces on synthetic goethite observed by atomic force microscopy: Clays and Clay Minerals, 44, 437-442.

Zamiri, R., Ahangar, H.A., Zakaria, A., Zamiri, G., Bahari, H.R., Drummen, G.P.C., 2014, Hydrothermal synthesis of goethite (alpha-FeOOH) nanorods in the presence of ethylenediamine:thiourea: Journal of Nanoparticle Research, 16, 2332-2342.

Zhang, J.S., Stanforth, R., 2005, Slow adsorption reaction between arsenic species and goethite (alpha-FeOOH): Diffusion or heterogeneous surface reaction control: Langmuir, 21, 2895-2901.

7. Tables

Table 1. Summary of conditions commonly employed in goethite synthesis.

Reagents	Concentration	Condition	Aging	Cleaning	SSA[a] ($m^2 g^{-1}$)	Reference
$Fe(NO_3)_3.9H_2O$ KOH	50 g / 825 ml H_2O 200 ml (2.5 N)	OH^- addition to pH 12	Heated 60°C for 24 hours	Dialyzed	70.9	Atkinson *et al*., 1967
$Fe(NO_3)_3.9H_2O$ NaOH	450 g / 8.3 L H_2O 900 ml (5 N)	OH^- addition to pH 12	Heated 60°C for 24 hours	Dialyzed	45	Vangeen *et al*., 1994
Fe nitrate NaOH	0.5 M 2.5 M	Slow neutralizing to pH 12	Heated 60°C for 90-100 hours	Dialyzed	105	Hiemstra and van Riemsdijk, 1996
$Fe(NO_3)_3.9H_2O$ KOH	100 ml (1 M) 180 ml (5 M)	OH- addition and dilution to 2L	Heated to 68°C for 2 months	Washed and freeze dried	7.9	Weidler *et al*., 1996
$Fe(NO_3)_3.9H_2O$ NaOH	1 mol 4 mol	OH^- addition	Heated 60°C for 24 hours	Neutralized and Dialyzed	70	Villalobos and Leckie, 2001
$Fe(NO_3)_3.9H_2O$ NaOH	4 L (0.1 M) 800 ml (5 M)	OH^- dropwise	Heated 60°C for 72 hours	Dialyzed	70.8	Antelo *et al.*, 2005
$Fe(NO_3)_3.9H_2O$ NaOH	50g / 825ml H_2O 200ml (2.5 N)	OH^- addition to pH 12	Heated 60°C for 72 hours	Washed	27	Zhang and Stanforth, 2005

[a] As determined by the nitrogen-adsorption BET method

Table 2. Summary of synthesis conditions reported for 2-line ferrihydrite synthesis.

Reagents	Concentration	Condition	Aging	Cleaning	SSA[a] (m^2 g^{-1})	Reference
$Fe(NO_3)_3.9H_2O$ NaOH	0.1 M 1 M	OH^- addition to pH 8	20°C for 48 hours	Dialyzed and freeze dried	337	Antelo *et al*., 2010
$Fe(NO_3)_3.9H_2O$ KOH	0.2 M 1 M	OH^- addition to pH 8	for 10 days	Dialyzed 15 hours	650[b]	Hofmann *et al*., 2005
$Fe(NO_3)_3.9H_2O$ KOH	40g /500 ml H_2O 330 ml (1 M)	OH^- addition to pH 7-8 Last 20ml	Only vigorous stiring and centrifugation	Dialyzed rapidly and Freeze dried	200-320	Schwertmann and Cornell, 2007
$FeC_6H_5O_7$ NH_3	500ml (0.3 M) 10 M	20 NH_3 drops / min Till pH 12	Heated to 90°C For 24 hours	Filtered off, washed and dried	175.8	Rout *et al*., 2012

[a] As determined by the nitrogen-adsorption BET method
[b] Value used for surface complexation modeling purposes, but is not the experimental BET value.

Table 3. Rate of NaOH addition and stirring used to obtain goethites of varying SSA.

Rate of addition NaOH	Rate of stirring (rpm)	SSA obtained[a] (m^2 g^{-1})
Immediate	60[b]	41.5 ±4
10ml min^{-1}	200	64 ±2
5ml min^{-1}	200	83 ±2
1ml min^{-1}	200	101 ±5

[a] Nitrogen adsorption BET values from replicates of three to five independent syntheses.
[b] Stirring speed promotes particle disaggregation, and thus formation of small final particle sizes. 60 rpm is the minimum speed for the suspension to rotate as a whole at this total volume, and which helps to yield larger particles.

Table 4. Maximum Cr(VI) adsorption onto goethite. [Cr(VI)] initial = $4x10^{-3}$ M, I= 0.1 M $NaClO_4$ at pH 4.

Sample	SSA[a] (m^2 g^{-1})	Cr(VI) (μmol m^{-2})
GOE 43	42.7	4.39 ±0.27
GOE 63	62.6	3.03 ±0.28
GOE 83	83.3	2.87 ±0.21
GOE 101	101.1	2.89 ±0.035

[a] The experimental error in the SSA determination by nitrogen adsorption BET measurements, for any individual goethite batch is 2-3 m^2 g^{-1}.

Table 5. Maximum Cr(VI) adsorption onto ferrihydrite. [Cr(VI)] initial = $4x10^{-3}$ M, I= 0.1 M $NaClO_4$ at pH 4.

Sample	Cr(VI) (mmol g^{-1})
FFh	1.50 ±0.23
AFh	1.58 ±0.39

8. Figure captions

Figure 1. a) Experimental set-up for goethite synthesis and fresh ferrihydrite precipitate after NaOH addition; b) Goethites obtained after aging: GOE50-labelled on the left corresponds to GOE43, and GOE94-labelled on the right to GOE101; c) clean and dried goethite (GOE43) before dispersing with mortar.

Figure 2. XRD patterns of goethite samples of different SSAs.

Figure 3. TEM images of GOE101 a) and b), and GOE43 c) and d), at two different magnifications.

Figure 4. ATR-FTIR goethite measurements (complete spectra).

Figure 5. ATR-FTIR spectra amplified in the range between 1200 and 1700cm^{-1} for a) GOE 43, b) GOE 63, c) GOE 83, and d) GOE 101.

Figure 6. XRD patterns of AFh and FFh.

Figure 7. TEM images of (A) AFh and (B) FFh.

Figure 8. Linear relationship between particle size and BET_{SSA}, recalculated from data by Wang *et al.* (2013).

Figure 9. ATR-FTIR spectra of FFh and AFh.

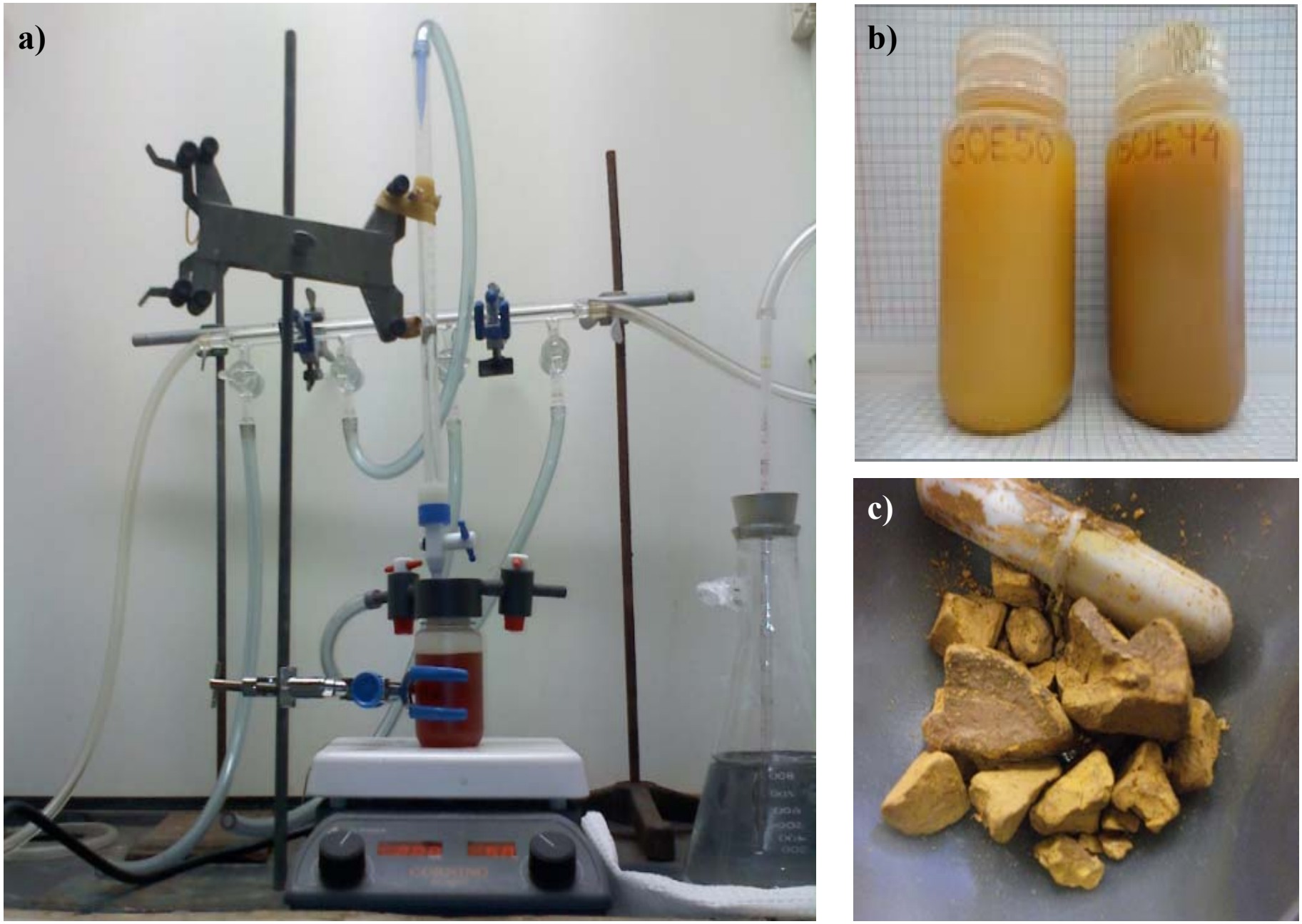

Figure 1

Villacis-Garcia, et al.

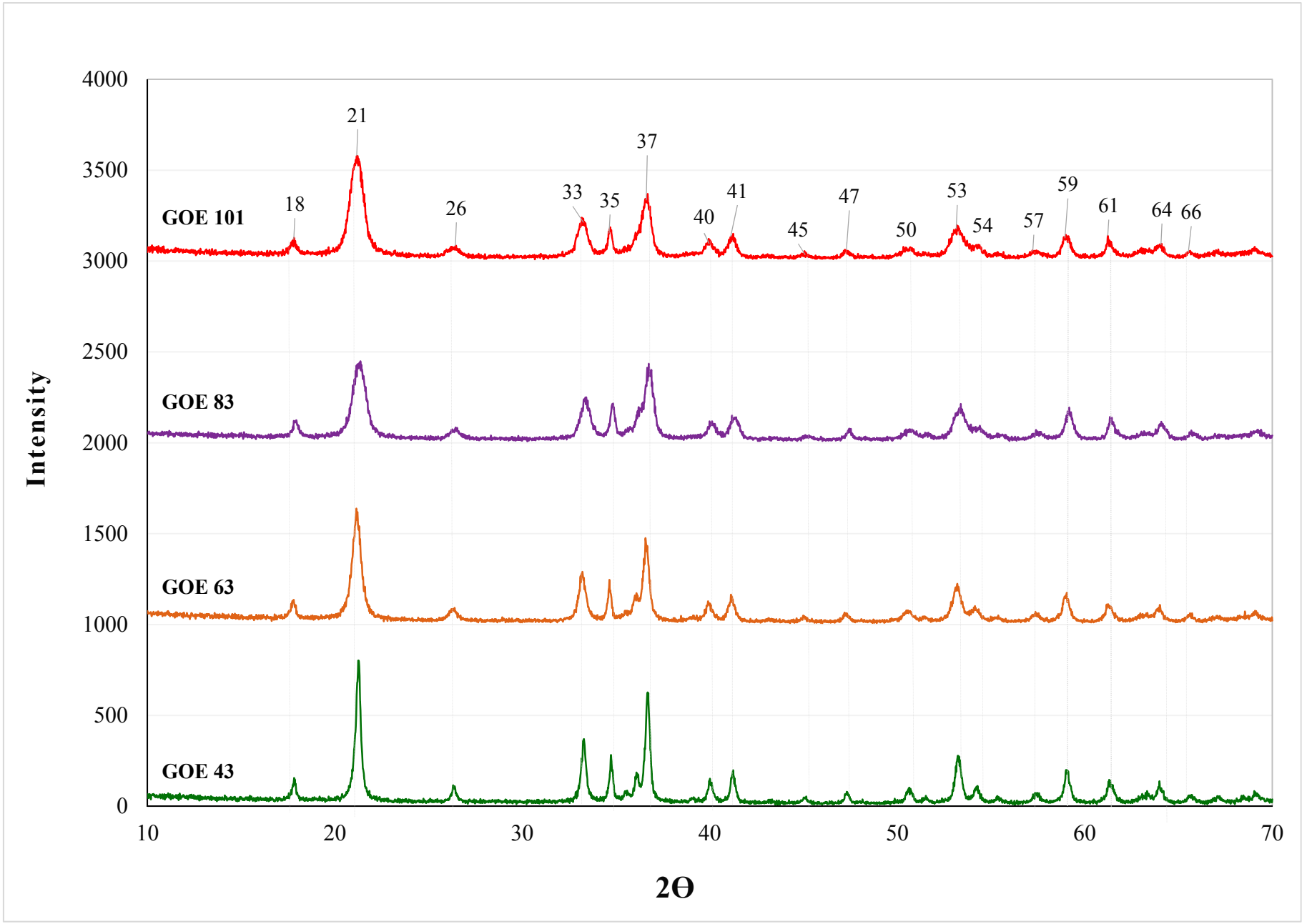

Figure 2

Villacis-Garcia, et al.

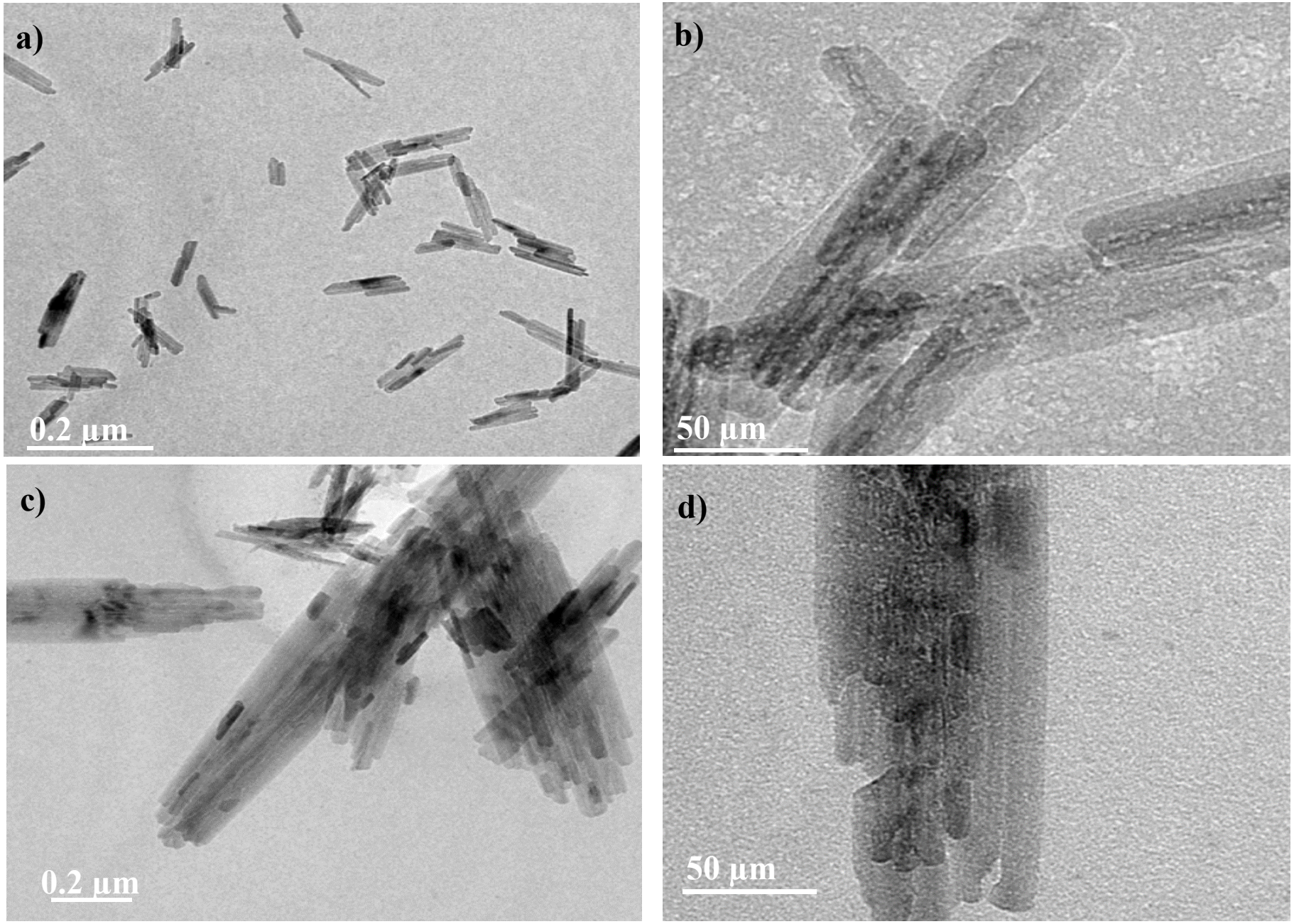

Figure 3

Villacis-Garcia, et al.

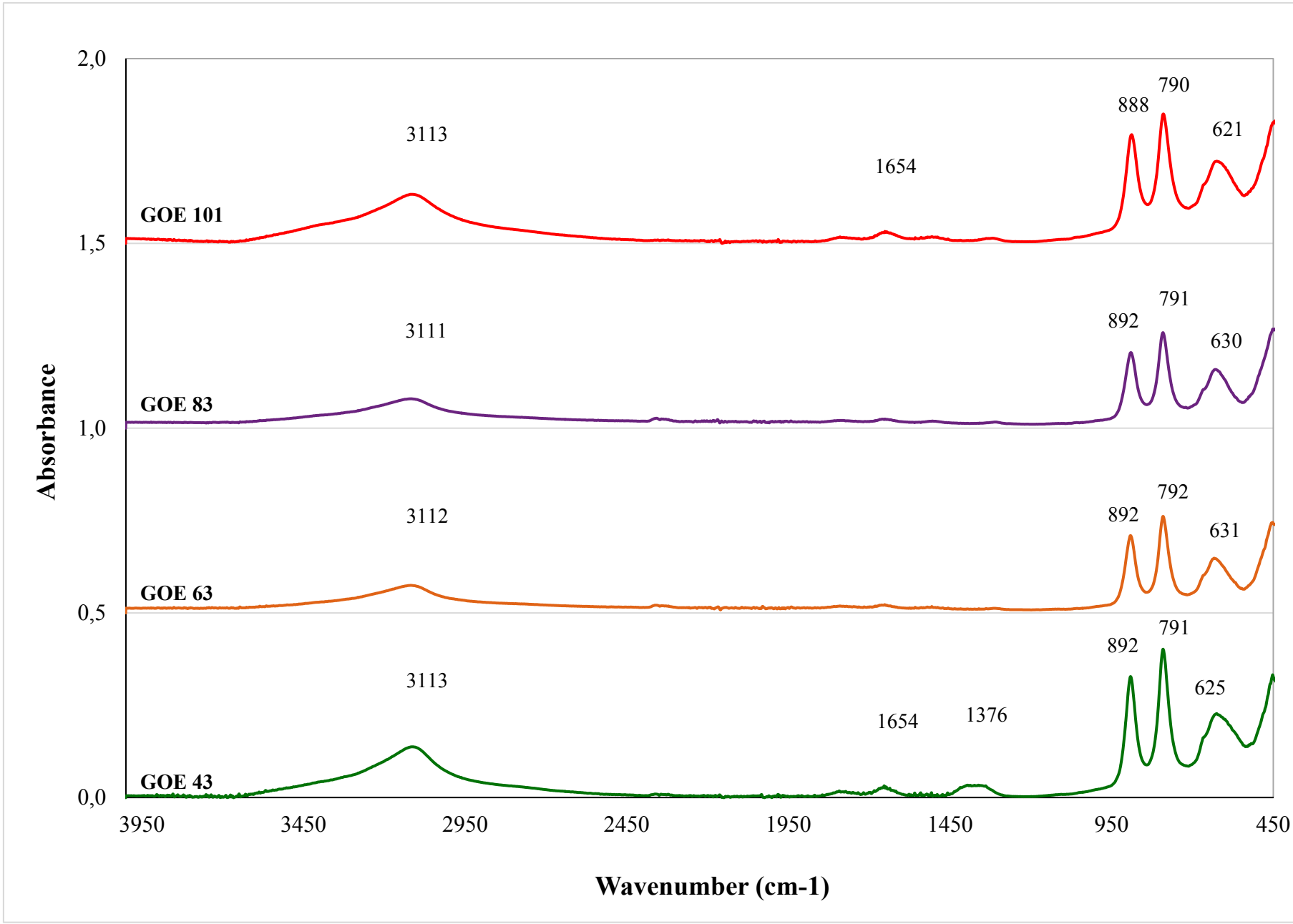

Figure 4

UNAM, 2015

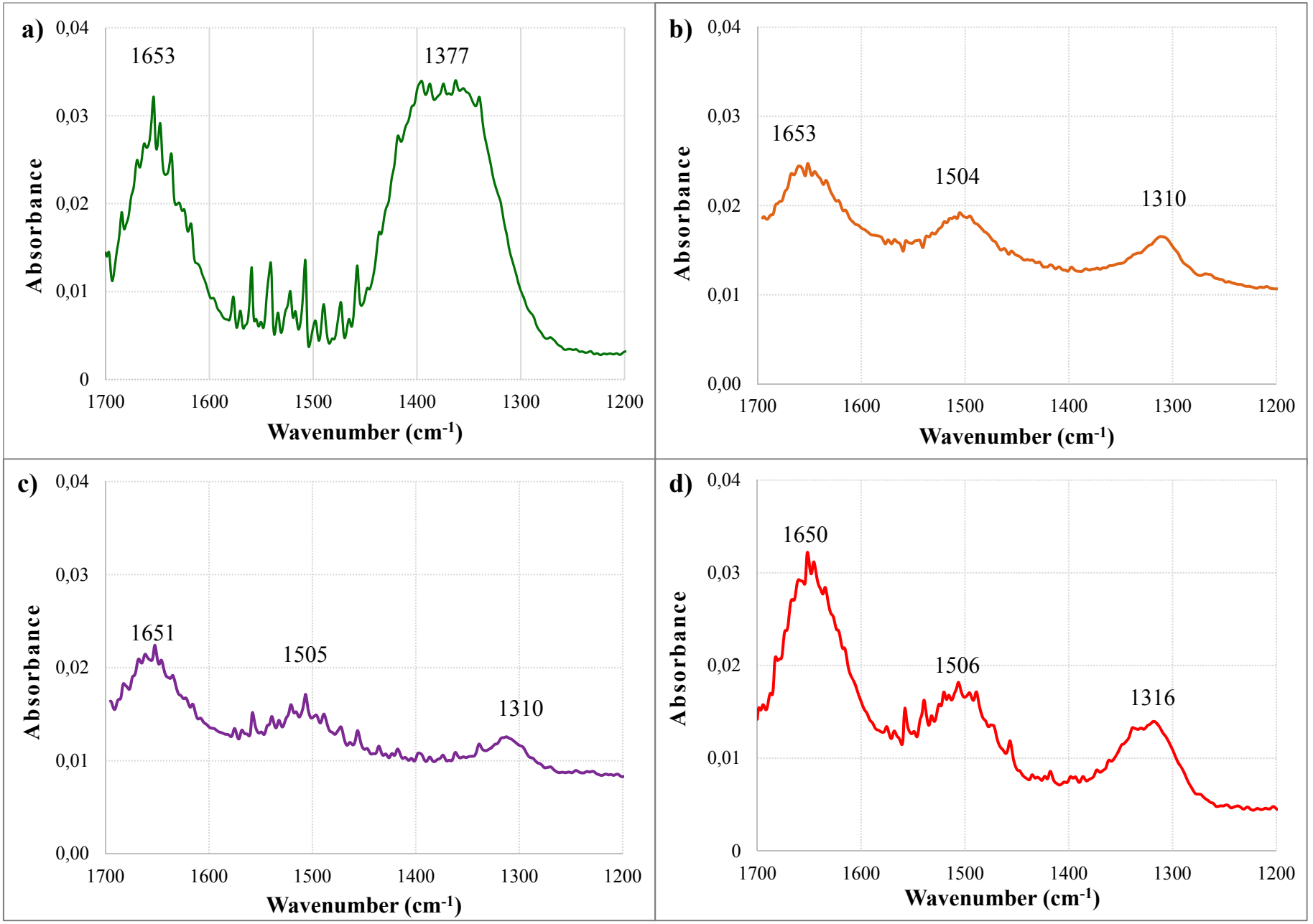

Figure 5

Villacis-Garcia, et al.

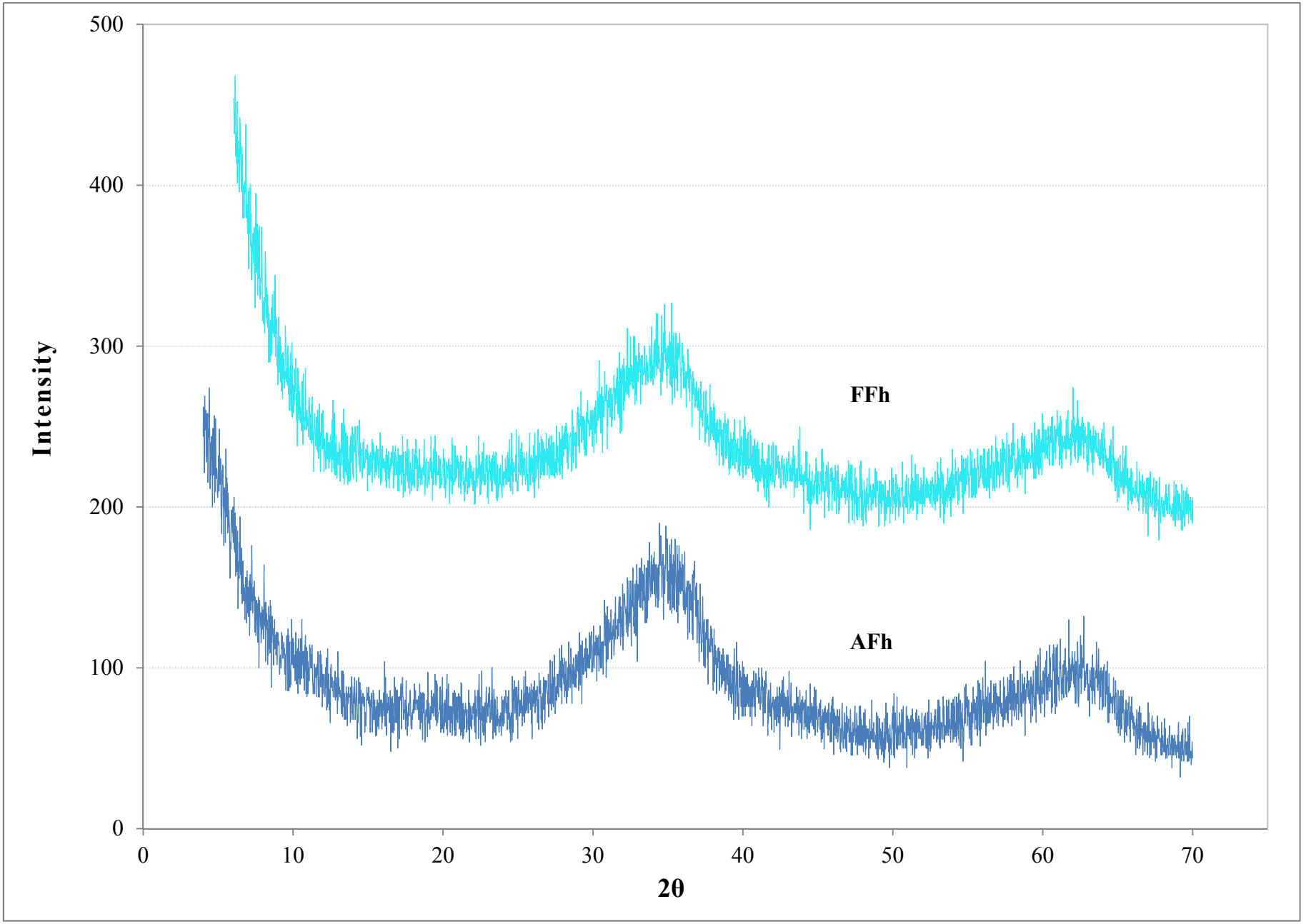

Figure 6

Villacis-Garcia, et al.

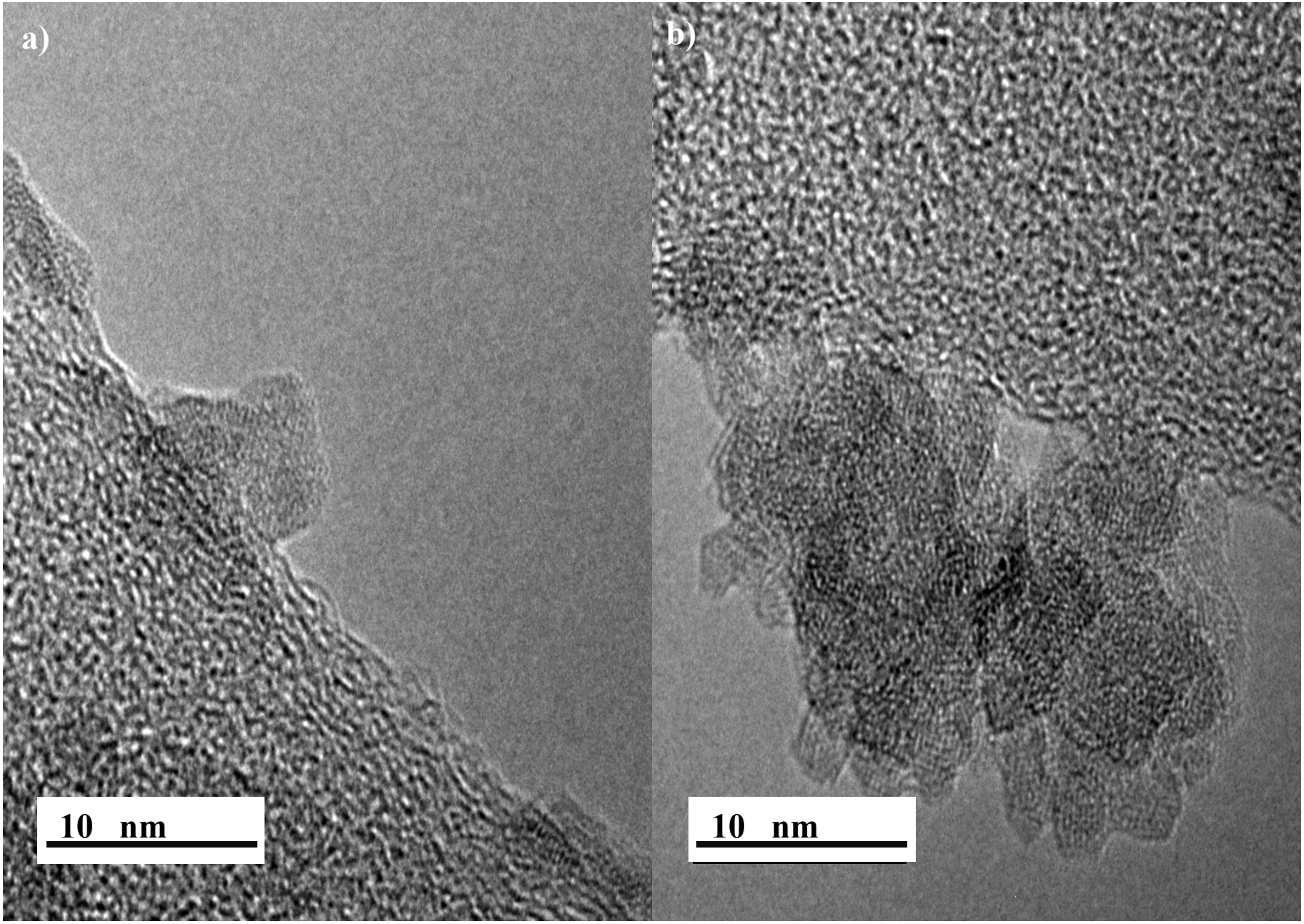

Figure 7

Villacis-Garcia, et al.

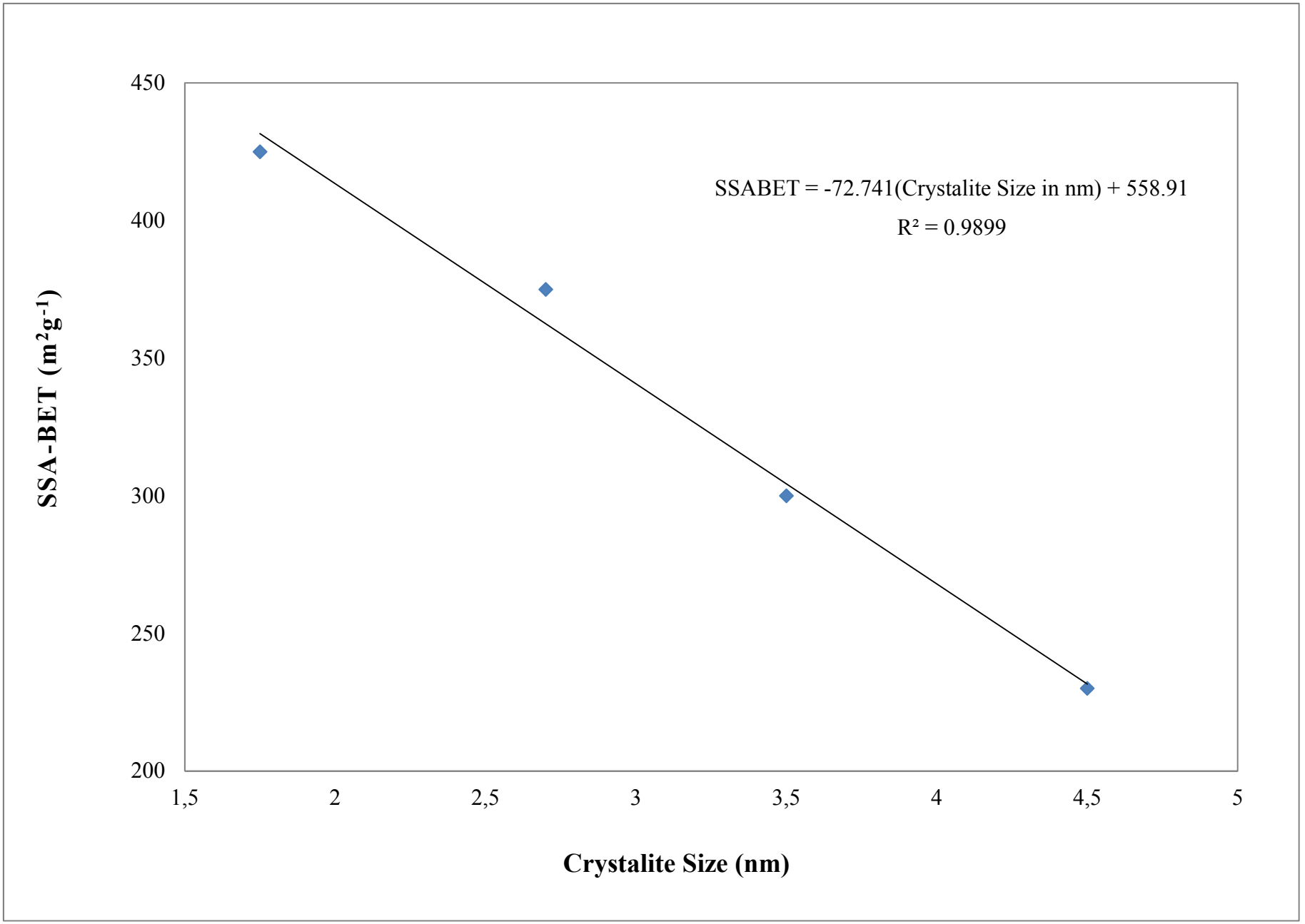

Figure 8

Villacis-Garcia, et al.

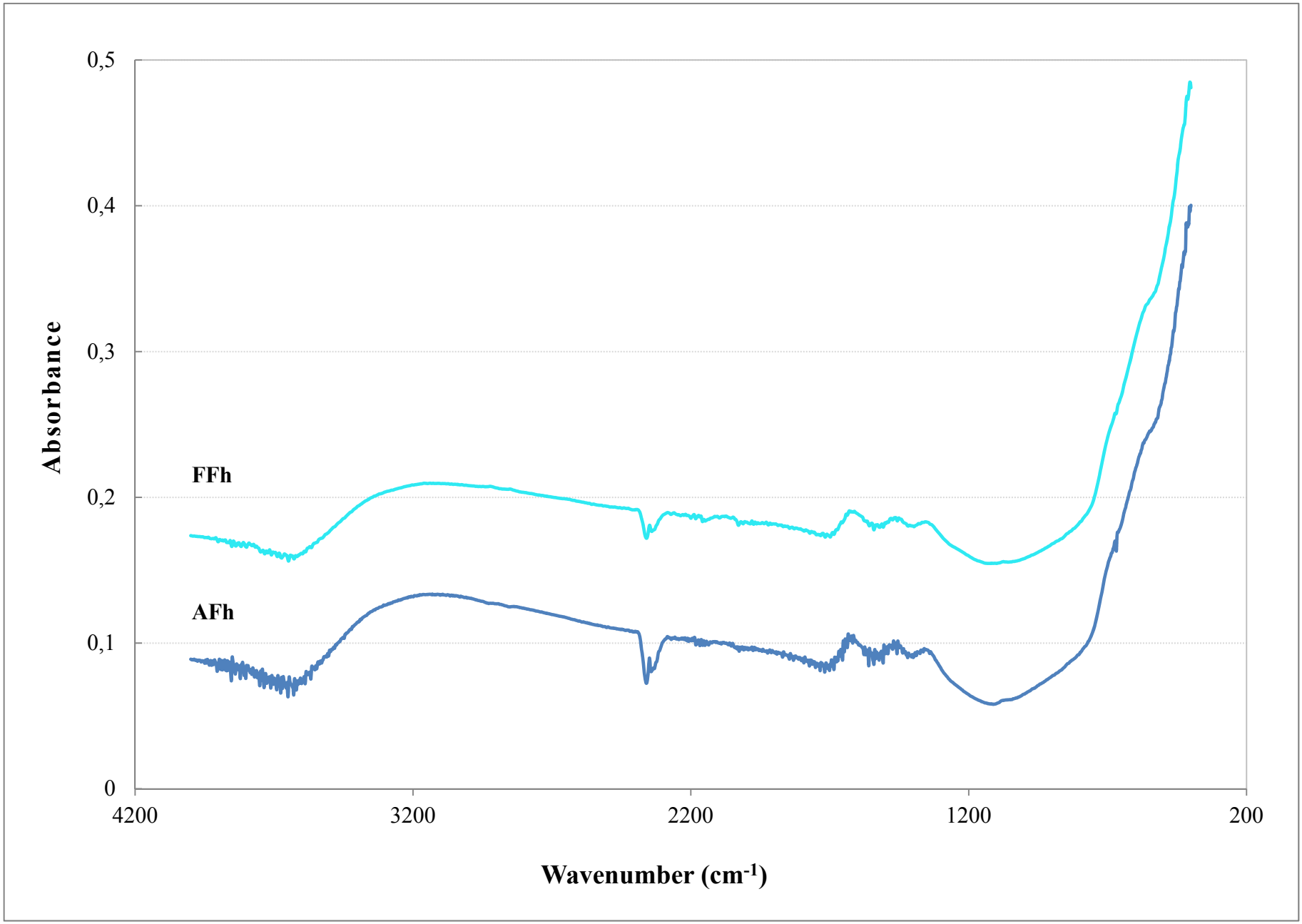

Figure 9

Villacis-Garcia, et al.

Applied Geochemistry 27 (2012) 2251–2259

Contents lists available at SciVerse ScienceDirect

Applied Geochemistry

journal homepage: www.elsevier.com/locate/apgeochem

Natural arsenic attenuation via metal arsenate precipitation in soils contaminated with metallurgical wastes: III. Adsorption versus precipitation in clean As(V)/goethite/Pb(II)/carbonate systems

Katherine Vaca-Escobar [a], Mario Villalobos [b,*], Agueda E. Ceniceros-Gómez [a]

[a] Environmental Bio-Geochemistry Group, Facultad de Química, Universidad Nacional Autónoma de México (UNAM), Coyoacán, Ciudad Universitaria, México 04510, D.F., Mexico
[b] Environmental Bio-Geochemistry Group, Instituto de Geología, Universidad Nacional Autónoma de México (UNAM), Coyoacán, Ciudad Universitaria, México 04510, D.F., Mexico

ARTICLE INFO

Article history:
Available online 28 January 2012

ABSTRACT

Soil contamination with As and potentially harmful metals is a widespread problem around the world especially from mining and metallurgical wastes, which release substantial amounts of these elements to the environment in potentially mobile species. Recently, it has been found that in various Mexican soils contaminated with these types of wastes, arsenate is not in the form of sorbed species on Fe oxides present in the soils, as generally reported in the literature, but in the form of very insoluble compounds such as Pb, Cu and Ca arsenates. Here a thermodynamic model is applied and validated with the results from wet chemical experiments to determine the fundamental geochemical conditions governing the mobility of As in the presence of Pb. For this purpose, a relatively simple but fundamental system of goethite (α-FeOOH)/As(V)/Pb(II)/carbonate was defined as a function of the As(V)/Fe(III) ratio, in a pH range of 5–10. The speciation model included the simultaneous inclusion of triple layer surface complexation and arsenate precipitation equilibria. The model predicts that from very low total As(V)/Fe(III) molar ratios (0.012 at pH 7) the precipitation mechanism significantly influences the attenuation of As(V), and rapidly becomes the dominant process over the adsorption mechanism. Model results identify the quantitative conditions of predominance for each mechanism and describe the transition conditions in which relatively large fractions of adsorbed, precipitated and dissolved As(V) species prevail. Experimental measurements at selected As(V)/Fe(III) ratios and pH confirmed the predictions and validated the coupled thermodynamic model utilized.

1. Introduction

Arsenic is a ubiquitous element in the earth's crust but can be highly toxic to humans, animals and plants when rendered bioavailable (Ng, 2005). The presence of As in high concentrations in natural surface environments is attributed to both anthropogenic and natural sources (Violante et al., 2006). It is a very common element in mining and metallurgical wastes together with metals such as Pb, Cu and Zn, with high concentrations (Vaughan, 2006). Additionally, it is also released to the environment in large quantities through agricultural activities (Plant et al., 2004; O'Day, 2006). The environmental geochemistry of As is of wide interest because its behavior shows a complex dependence on its chemical speciation. In natural systems, As may be found in one of four different oxidation states: (−III), (0), (III) and (V) (Pierce and Moore, 1982). The most reduced species are stable in underground conditions away from the atmosphere, for example in sulfidic environments. At the high Eh values encountered in aerated soils and in oxygenated waters, protonated arsenate [As(V)] species become stable, while in mildly reducing conditions in soils and waters, protonated arsenious [As(III)] species are stable (Pierce and Moore, 1982; Francesconi and Kuehnelt, 2002). In some regions of the world, groundwater enriched in As poses a serious health problem (Nordstrom, 2002), and much effort is devoted to investigating suitable remediation schemes (Morin and Calas, 2006; Kumpiene et al., 2009).

The fate of As in aerated environments, as inorganic arsenates, has been almost invariably related to its immobilization through adsorption to Fe oxides (Foster et al., 1998; La Force et al., 2000), or coprecipitation processes with Al and Fe oxides (Waychunas et al., 1993; Foster et al., 1998; La Force et al., 2000; Lee et al., 2005; Violante et al., 2006; Catalano et al., 2008; Asta et al., 2009; Carabante et al., 2009; Mamindy-Pajany et al., 2009; Weng et al., 2009). One of the most abundant and stable Fe oxides in nature under temperate and humid conditions is goethite (α-FeOOH) (Bigham et al., 2002), whose surface reactivity has been extensively studied and its synthetic preparations have served as references for many of the "surface complexation models" (SCMs) developed (see for example Hayes et al., 1990; Van Riemsdijk and Hiemstra, 2006;

* Corresponding author. Tel.: +52 55 5622 4336; fax: +52 55 5622 4352.
E-mail address: mariov@geologia.unam.mx (M. Villalobos).

0883-2927/$ - see front matter © 2012 Elsevier Ltd. All rights reserved.
doi:10.1016/j.apgeochem.2012.01.011

Table 1
Reaction equations and formation constants used for modeling.

Equation	Reaction		Log K
Solid species			
1	$5Pb^{2+} + H_2O + 3AsO_4^{3-} \rightleftharpoons Pb_5(AsO_4)_3OH + H^+_{(Hydroxymimetite)}$		62.115
2	$Pb^{2+} + H^+ + AsO_4^{3-} \rightleftharpoons PbHAsO_{4\,(Schultenite)}$		23.969
3	$10Pb^{2+} + 6CO_3^{2-} + 7H_2O \rightleftharpoons Pb_{10}(OH)_6O(CO_3)_6 + 8H^+_{(Plumbonacrite)}$		8.760
4	$3Pb^{2+} + CO_3^{2-} + 2H_2O \rightleftharpoons Pb_3O_2CO_3 + 4H^+$		−11.02
5	$2Pb^{2+} + CO_3^{2-} + H_2O \rightleftharpoons Pb_2OCO_3 + 2H^+_{(Shannonite)}$		0.558
6	$3Pb^{2+} + 2CO_3^{2-} + 2H_2O \rightleftharpoons Pb_3(OH)_2O(CO_3)_2 + 2H^+_{(Hydrocerrusite)}$		18.77
7	$2Na^+ + CO_3^{2-} + H_2O \rightleftharpoons Na_2CO_3 \cdot H_2O_{(Thermonatrite)}$		−0.637
8	$2Na^+ + CO_3^{2-} + 10H_2O \rightleftharpoons Na_2CO_3 \cdot 10H_2O_{(Natron)}$		1.311
9	$Pb^{2+} + CO_3^{2-} \rightleftharpoons PbCO_{3\,(Cerrusite)}$		13.13
10	$2Pb^{2+} + 3H_2O \rightleftharpoons Pb_2O(OH)_2 + 4H^+$		−26.188
11	$Pb^{2+} + H_2O \rightleftharpoons PbO + 2H^+_{(Massicot)}$		−12.894
12	$Pb^{2+} + H_2O \rightleftharpoons PbO + 2H^+_{(Litharge)}$		−12.694
13	$Pb^{2+} + 2H_2O \rightleftharpoons Pb(OH)_2 + 2H^+$		−8.15
14	$Pb^{2+} + 1.3H_2O \rightleftharpoons PbO : 0.3H_2O + 2H^+$		−12.98
15	$2AsO_4^{3-} + 6H^+ \rightleftharpoons As_2O_5 + 3H_2O$		34.694
Aqueous species			
16	$AsO_4^{3-} + H^+ \rightleftharpoons HAsO_4^{2-}$		11.6
17	$AsO_4^{3-} + 2H^+ \rightleftharpoons H_2AsO_4^-$		18.35
18	$3H^+ + AsO_4^{3-} \rightleftharpoons H_3AsO_4$		20.6
19	$Pb^{2+} + 2H^+ + AsO_4^{3-} \rightleftharpoons PbH_2AsO_4^+$		19.736
20	$Pb^{2+} + H^+ + AsO_4^{3-} \rightleftharpoons PbHAsO_4$		14.038
21	$Pb^{2+} + 2H_2O \rightleftharpoons Pb(OH)_2 + 2H^+$		−17.897
22	$Pb^{2+} + 2NO_3^- \rightleftharpoons Pb(NO_3)_2$		1.4
23	$Pb^{2+} + NO_3^- \rightleftharpoons PbNO_3^+$		1.17
24	$Pb^{2+} + H_2O \rightleftharpoons PbOH^+ + H^+$		−7.597
25	$4Pb^{2+} + 4H_2O \rightleftharpoons Pb_4(OH)_4^{4+} + 4H^+$		−19.988
26	$2Pb^{2+} + H_2O \rightleftharpoons Pb_2(OH)^{3+} + H^+$		−6.397
27	$Pb^{2+} + 3H_2O \rightleftharpoons Pb(OH)_3^- + 3H^+$		−28.091
28	$Pb^{2+} + 4H_2O \rightleftharpoons Pb(OH)_4^{2-} + 4H^+$		−39.699
29	$3Pb^{2+} + 4H_2O \rightleftharpoons Pb_3(OH)_4^{2+} + 4H^+$		−23.888
30	$2H^+ + CO_3^{2-} \rightleftharpoons H_2CO_3$		16.681
31	$H^+ + CO_3^{2-} \rightleftharpoons HCO_3^-$		10.329
32	$H^+ + Na^+ + CO_3^{2-} \rightleftharpoons NaHCO_3$		10.079
33	$Pb^{2+} + H^+ + CO_3^{2-} \rightleftharpoons PbHCO_3^+$		13.200
34	$Na^+ + CO_3^{2-} \rightleftharpoons NaCO_3^-$		1.270
35	$Pb^{2+} + CO_3^{2-} \rightleftharpoons PbCO_3$		6.478
36	$Pb^{2+} + 2CO_3^{2-} \rightleftharpoons Pb(CO_3)_2^{2-}$		9.938
Adsorbed species[a]			
37	$SOH + H^+ \rightleftharpoons SOH_2^+$	$K = \frac{[SOH_2^+]}{\gamma_1[SOH][H^+]} e^{\frac{F}{RT}(\psi_0)}$	7.2
38	$SOH \rightleftharpoons SO^- + H^+$	$K = \frac{\gamma_1[SO^-][H^+]}{[SOH]} e^{-\frac{F}{RT}(\psi_0)}$	−11.2
39	$SOH + H^+ + NO_3^- \rightleftharpoons SOH_2^{+\cdots}NO_3^-$	$K = \frac{[SOH_2^{+\cdots}NO_3^-]}{\gamma_1^2[SOH][H^+][NO_3^-]} e^{\frac{F}{RT}(\psi_0-\psi_\beta)}$	8.68
40	$SOH + Na^+ \rightleftharpoons SO^{-\cdots}Na^+ + H^+$	$K = \frac{[SO^{-\cdots}Na^+][H^+]}{[SOH][Na^+]} e^{\frac{F}{RT}(\psi_\beta-\psi_0)}$	−9.82
41	$SOH + H^+ + CO_3^{2-} \rightleftharpoons SO^{-0.2}CO_2^{-0.8} + H_2O$	$K = \frac{[SO^{-0.2}CO_2^{-0.8}]}{\gamma_1^2[SOH][CO_3^{2-}][H^+]} e^{\frac{F}{RT}(-0.2\psi_0-0.8\psi_\beta)}$	12.82
42	$SOH + Pb^{2+} \rightleftharpoons SOPb^+ + H^+$	$K = \frac{[SOPb^+][H^+]}{\gamma_1^3[SOH][Pb^{2+}]} e^{\frac{F}{RT}(\psi_0)}$	0.691
43	$SOH + Pb^{2+} + H_2O \rightleftharpoons SO^{-\cdots}PbOH^+ + 2H^+$	$K = \frac{[SO^{-\cdots}PbOH^+][H^+]^2}{\gamma_1^2[SOH][Pb^{2+}]} e^{\frac{F}{RT}(\psi_\beta-\psi_0)}$	−10.4
44	$2SOH + H^+ + AsO_4^{3-} \rightleftharpoons SO^{-0.7}AsO_3^{-1.3\cdots}SOH + H_2O$	$K = \frac{[SOAsO_3^{2-\cdots}SOH]}{\gamma_1^{10}[SOH]^2[H^+][AsO_4^{3-}]} e^{(-0.7\psi_0-1.3\psi_\beta)\frac{F}{RT}}$	21.2

[a] The constants reported by Salazar-Camacho and Villalobos (2010) were adapted to simplify their more complex model construction. The values of the affinity constants obtained are averages that describe the original binary systems for the 94 $m^2\,g^{-1}$ goethite, including acid–base titration data and the ion adsorption data. Evidently, these constants will only be valid for ideal goethites of high specific surface area, and not for preparations of specific surface areas below 80 $m^2\,g^{-1}$ because these goethites are more reactive due to a higher proportion of more reactive crystal faces.

Mathur and Dzombak, 2006). These have reached a considerable level of development and sophistication in their description of the physicochemical processes that occur across the mineral solid-water interface. Salazar-Camacho and Villalobos (2010) reported a model that describes quantitatively the arsenate adsorption behavior for any goethite preparation as a function of pH and ionic strength, by using one basic surface arsenate stoichiometry, with two affinity constants. The model combines a face distribution-crystallographic site density model for goethite with tenets of the Triple Layer and CD-MUSIC surface complexation models, and is self-consistent with its adsorption behavior towards protons, electrolytes, and other ions investigated.

Table 2
Parameters used in surface complexation modeling.

Parameter	Value	Units
C_1	0.729	F m^{-2}
C_2	0.200	F m^{-2}
Specific surface area	94	m^2 g^{-1}
Solids concentration	0.2	g L^{-1}
Ionic strength	0.01	mol L^{-1}
Log PCO_2	−3.5	Log (atm)
Density of surface sites	6.25	sites nm^{-2}

Table 3
Modeling and experimental concentrations imposed for adsorption–precipitation reactions. Goethite 0.2 g L^{-1}, 0.01 M $NaNO_3$.

Exp no.	Total concentration (M)		As/Fe ratio (mol/mol)	As and Pb sources
	As(V)	Pb(II)		
1	1.0×10^{-6}	1.67×10^{-6}	0.0004	Hydroxymimetite
2	2.6×10^{-4}	4.33×10^{-4}	0.1155	Hydroxymimetite
3	5.0×10^{-5}	8.33×10^{-5}	0.0222	Hydroxymimetite
4	2.6×10^{-4}	4.33×10^{-4}	0.1155	PbO + NaH_2AsO_4

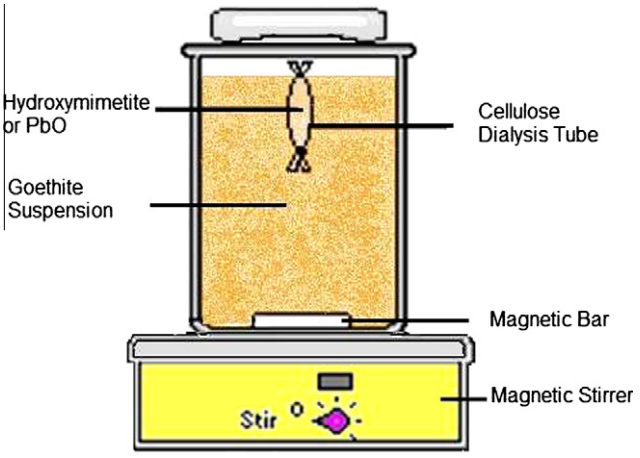

Fig. 1. Reactor sketch.

Nevertheless, the present authors have found previously that in situations where the metal contents that accompany As are high (as in many mining and metallurgical wastes), formation of highly-insoluble heavy metal arsenates (such as dulfite, hydroxymimetite, and bayldonite) is the predominant immobilization mechanism, over adsorption processes (Gutierrez-Ruiz et al., 2005; Drahota and Filippi, 2009; Villalobos et al., 2010). It was found that despite normal major contents of total Fe (2% weight average) in these soils, the formation of solid Pb and Cu arsenate minerals is still preferred because of the relatively high contents of total Pb (0.5% weight average) and Cu (0.2% weight average) accompanying As (0.3% weight average) in the contaminated soils, and the extremely low solubility products of these arsenates.

This third article in this series is devoted to investigating the thermodynamic conditions that determine the environmental geochemical conditions of arsenate mobility in aqueous environments, focusing on the competition between Pb arsenate formation and adsorption mechanisms to Fe oxide. For this purpose, a clean system composed of As(V)/Pb(II)/goethite/carbonate at an ionic strength of 0.01 M (fixed with $NaNO_3$), in equilibrium with the atmosphere was used, at pH values between 5 and 10. The results of this work are crucial for understanding the environmental geochemistry of As, and for the conceptual design of efficient remediation schemes of As-contaminated environments.

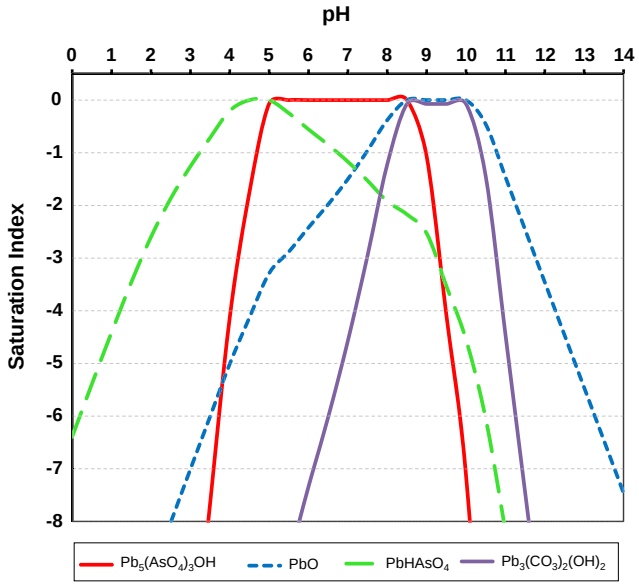

Fig. 2. Regions of solids precipitation (hydroxymimetite, shultenite and Pb oxide and carbonate) in the absence of goethite, from their saturation indices in the system composed of $[AsO_4^{3-}]_{TOTAL} = 4 \times 10^{-5}$ M, $[Pb^{2+}]_{TOTAL} = 6 \times 10^{-5}$ M and I = 0.01 M $NaNO_3$, these values correspond to an As/Fe molar ratio = 0.019 if goethite were present (at 0.2 g L^{-1}).

2. Methods

2.1. Thermodynamic modeling

Speciation modeling was performed by using the chemical equilibrium program MINEQL+, version 4.5, which was updated with the appropriate Pb arsenate formation constants (Villalobos et al., 2010), and adapted with recently reported surface complexation constants for As(V) and Pb(II) adsorption to goethite using the combined tenets of the Triple-Layer and CD-MUSIC models (Salazar-Camacho and Villalobos, 2010). The corresponding reaction equations, including all aqueous and solid species used, are described in Table 1.

Other parameters required by the model are: two electrical capacitances (C1 and C2) and densities of surface sites (ns) depending on the specific crystal faces exposed of each goethite mineral (Villalobos and Perez-Gallegos, 2008). The data used in this investigation are presented in Table 2.

The total concentrations used were defined from the stoichiometric ratio in hydroxymimetite ($Pb_5(AsO_4)_3OH$, which is the stable arsenate mineral composed solely of Pb in the soils investigated previously, (Villalobos et al., 2010) such that a Pb/As molar ratio of 5/3 was fixed (Eq. 1 in Table 1), while the As/Fe (and thus Pb/Fe) molar ratio was varied (Table 3). Three different values were chosen to represent: (i) very low As soil concentrations (As/Fe = 0.0004), (ii) intermediate soil concentrations (As/Fe = 0.0222), and (iii) high soil concentrations (As/Fe = 0.1155). The latter more representative of actual average contamination scenarios previously investigated in a smelter affected field (Villalobos et al., 2010). Values for pH were manually fixed between 5 and 10 by using 0.01 N HNO_3 and 0.01 N NaOH. In the model, pH may be set to the desired value.

2.2. Adsorption–precipitation experiments

All reagents used were analytical grade. Solutions and suspensions were prepared using high-purity ion-exchanged water (nanopure, 18.2 MΩ cm).

(1) PbO suspension: Weigh accurately 0.6669 g of $Pb(NO_3)_2$, dissolve in 28 mL H_2O and fix pH to 7 with 1 M NaOH, then allow to stabilize for 1 d and add H_2O to 100 mL.
(2) Hydroxymimetite suspension: Weigh accurately 0.55694 g of $Pb(NO_3)_2$ and 0.31669 g of $Na_2HAsO_4{\cdot}7H_2O$, add 50 mL H_2O, fix pH to 7, and then add H_2O to 100 mL. The precipitate obtained was characterized by X-ray diffraction after equilibrating for 48 h and its identity confirmed to be hydroxymimetite.

A previously-synthesized ideal 94 $m^2\,g^{-1}$ goethite was used (obtained from a modified version of the Atkinson Method, Atkinson et al., 1967), which was previously characterized by X-ray diffraction, BET surface area determination, electron microscopy and acid–base potentiometric titrations (Van Geen et al., 1994; Ostergren et al., 2000; Villalobos et al., 2001).

Laboratory experiments were performed at pH 7 to compare with the modeling results obtained. The conditions tested were the same as those applied in the model and reported in Table 3. The systems were kept open to atmospheric CO_2, with an ionic strength of 0.01 M $NaNO_3$ and goethite dosage of 0.2 g L^{-1}. At pH values above the first pKa of carbonate, the systems are expected to contain mostly HCO_3^- ions. These, however are not expected to exert strong competition for binding to the surface versus arsenate adsorption, due to their relatively low affinity.

A relatively simple reactor set-up was designed to experimentally determine the As and Pb speciation in the systems (Fig. 1) under the different conditions listed in Table 3. A 10 cm cellulose membrane dialysis tube (MWCO = 8000 Da) closed on both ends was placed inside the goethite suspension, itself inside a 250 mL polycarbonate bottle. Each tube was filled prior to closing the other end with volumes ranging from 0.025 mL to 6.5 mL, depending on the experiment, of a suspension of either hydroxymimetite (experiments #1–3) or PbO (experiment #4) (Table 3). For the latter, As(V) was added to the system in the form of NaH_2AsO_4 (Merck). The idea is that the dialysis membrane only lets ions and water molecules pass through its walls in the aqueous suspension, such that precipitation and adsorption processes may be physically separated easily because the goethite material is found only in the external suspension, and thus adsorption reactions take place only outside the tubing.

pH was measured potentiometrically using a Φ720 Beckman pH meter with a combined glass electrode (Orion Ross Combination pH Electrode, pH 0–14, glass body).

The suspension in the reactor was continuously stirred (900 rpm), and aliquots (10 mL) of the goethite (outside) suspension were sampled as a function of time and analyzed separately for total aqueous and total adsorbed As(V) and Pb(II), in order to monitor the process and establish the required times to reach equilibration conditions for the different experiments. The aliquots were filtered through nitrocellulose membranes of 0.05 μm pore size. The filtered solution was analyzed for As using Hydride Generation – AA Spectroscopy (Varian SPECTRAA110) (detection limit of 1 μg L^{-1} or 0.013 μM), and for Pb(II) by ICP-AES (Thermo IRIS intrepid II SPX) (detection limit of 0.05 mg L^{-1} or 0.24 μM). The solid retained on the filter membrane was slightly washed with nanopure water and was dissolved with concentrated HCl (36%) and made up to 25 mL with water to yield a final pH of 1 (no $PbCl_2$ precipitates were formed). The solutions were analyzed both for As(V) and Pb(II) (as adsorbed fractions on goethite) by ICP-AES (As detection limit of 0.02 mg L^{-1} (=0.26 μM).

The precipitated fractions were calculated indirectly from the following mass balance equation:

$$[\text{Total species}] = [\text{Adsorbed species}] + [\text{Dissolved species}] + [\text{Precipitated species}]$$

This equation may be applied experimentally only if it is assumed that any precipitated species were present exclusively inside the dialysis tubing, and this is possible because none of the systems were prepared from all soluble salts of both components As(V) and Pb(II) simultaneously. At equilibrium, the dissolved concentrations were assumed to be equal inside and outside the dialysis tubing, and this condition was reached when no further variation in the analyzed concentrations was obtained with time.

3. Results and discussion

3.1. Thermodynamic models

A simple As(V)–Pb(II) aqueous system with a molar As/Pb ratio of 3/5 predicts formation of the solid mineral hydroxymimetite [$Pb_5(AsO_4)_3OH$] in a pH range of 5–8.5 at total concentrations corresponding to an As/Fe molar ratio = 0.019 for a hypothetical 0.2 g L^{-1} goethite (Fig. 2). In the open CO_2 system investigated, Pb oxide and carbonate solids form above pH 8.5, dissolving the As-containing hydroxymimetite, but then dissolve again above pH 10 through the formation of aqueous hydroxylated and carbonated complexes.

Fig. 3 shows the predicted speciation diagram of As in the system that included goethite at pH 7, as a function of the As/Fe (goethite) molar ratio. There are three important regions in the diagram: the first one occurs at low molar As/Fe ratios (<0.02), in which adsorption processes (to goethite) are dominant. The second region, at As/Fe ratios around 0.02, in which both adsorption and precipitation processes contribute similarly; and the third region (As/Fe > 0.02) where precipitation processes (as hydroxymimetite) rapidly become dominant. In fact, the model predicts a very steep positive slope for these precipitation processes from very low As/Fe, and a steep negative slope for adsorption processes with increasing As/Fe.

In the case of Pb(II) (Fig. 4) the behavior is very similar to As(V), except that the dissolved species are always negligible (as is expected for Pb(II) at this pH), and thus Pb(II) is found either as an adsorbed species and/or as a precipitate (hydroxymimetite) at any Pb/Fe ratio. Adsorbed species when predominant are mostly found as the inner-sphere complex listed in Table 1 (not shown).

At pH values between 5 and 9.5 the general speciation behavior is the same as that shown at pH 7 (Figs. 3 and 4), except that the point at which adsorbed and precipitated species coincide moves to higher As/Fe (or Pb/Fe) ratios with increasing pH (Fig. 5). This essentially means that as pH increases the region of predominance of adsorbed As(V) species increases as well. At pH values from 5 to 7, this increase is very small, but after pH 7.5 the slope with pH rises considerably, reaching an As/Fe ratio close to 0.06 at pH 9.5, below which adsorption is the dominant mechanism of As(V) immobilization.

The model explains this behavior as follows: as pH increases the onset of precipitation occurs at increasing As/Fe ratios (Fig. 6). An As(V) speciation diagram in the absence of adsorption for example at a hypothetical 0.019 As/Fe (Fig. 7) shows that as pH increases above 8, hydroxymimetite dissolves (and PbO precipitates), releasing As(V) to the aqueous phase at a fast pace (note the positive slope of the total aqueous As curve in the log–log diagram) (This pH of hydroxymimetite dissolution will actually increase as the As/Fe ratio is increased but the example shown in Fig. 7 is illustrative of the phenomenon observed). Notwithstanding, experimental adsorption data for As(V) to goethite in the absence of Pb(II) show also that As(V) desorbs with increasing pH (Fig. 8), however, this happens at a slower rate than As(V) dissolution from the Pb–arsenate. The net result is, on the one hand the predominance of adsorption over precipitation as pH increases (Figs. 5 and 6), but on the other an increase in the total aqueous As(V) concentrations

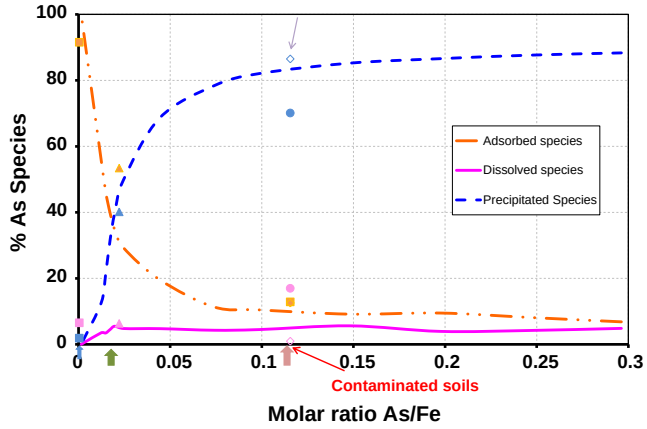

Fig. 3. As(V) species distribution in the presence of Pb(II) and goethite at pH 7 (line: model prediction; symbols: experimental data – squares correspond to As/Fe = 0.0004, triangles to As/Fe = 0.0222, diamonds to As/Fe = 0.1155 initially using hydroxymimetite, and circles to As/Fe = 0.1155 using initially Pb oxide and a soluble Na arsenate salt) (total As/Pb is always 3/5).

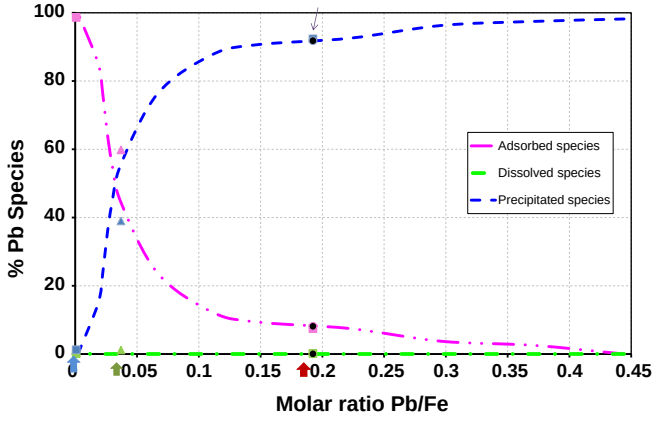

Fig. 4. Pb(II) species distribution in the presence of As(V) and goethite at pH 7 (line: model prediction; symbols: experimental data – squares correspond to Pb/Fe = 0.00067, triangles to As/Fe = 0.037, diamonds to As/Fe = 0.1925 using initially hydroxymimetite, and circles to As/Fe = 0.1925 initially using Pb oxide and a soluble Na arsenate salt) (total As/Pb is always 3/5).

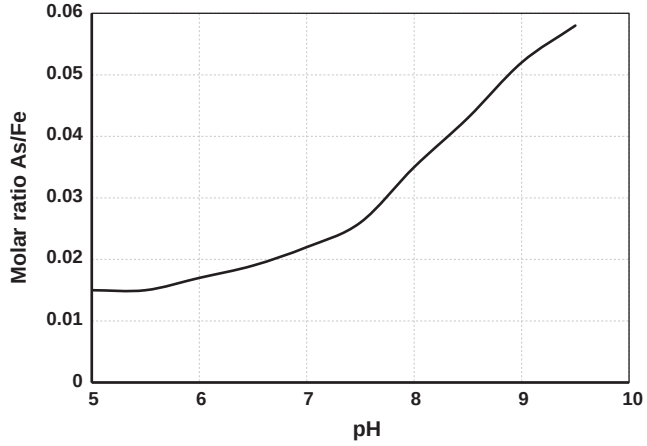

Fig. 5. As/Fe molar ratios at which an equal contribution of As(V) adsorbed and precipitated species occur, as a function of pH.

with pH (not shown) because both the precipitation and the adsorption mechanisms decrease in absolute terms (albeit at different rates) with pH.

At pH 10, no solid Pb(II) arsenate forms (because all Pb(II) precipitates as PbO – see Fig. 7), and thus, at very low As/Fe ratios, most As(V) present is adsorbed (Fig. 9). However, As(V) quickly desorbs as the As/Fe ratio increases to yield aqueous As(V) as the predominant species, although As(V) adsorbed species still contribute around 10% throughout the higher range of As/Fe ratios investigated.

Analyzing the modeled data from the perspective of the adsorption mechanism, the competitive effect that Pb(II) exerts may be shown in an adsorption "isotherm" plotted as a function of the As/Fe molar ratio (Fig. 10). It is evident that the model does not yield a perfect match, but it shows the correct trend of the experimental data. The clear decrease in As(V) adsorption predicted in the presence of Pb(II) is observed at all As/Fe ratios, and even at the highest As/Fe ratios modeled (0.15), no surface site saturation was predicted, which underscores the strength of the arsenate precipitation mechanism under high concentrations of Pb(II).

3.2. Adsorption–precipitation experiments

The previous modeling was validated with experimental data, for which the systems at the intermediate pH 7 were chosen. The experimental distribution of As(V) and Pb(II) species is summarized in Table 4 as a percentage of the total added. These are plotted in Figs. 3 and 4 to compare with thermodynamic model predictions.

Experimental results are discussed separately for each experimental condition (As/Fe ratio), since both the kinetics and equilibrium of adsorption and precipitation/dissolution were investigated and compared with the model. Experiment #1 corresponds to scenarios of very low contamination of As(V) and Pb(II) in soils. Experiments #2 and #4 correspond to a condition of high oversaturation of surface sites with respect to As(V) [and Pb(II)] added, and match the average contents found in soils contaminated with metallurgical wastes (Villalobos et al., 2010). Total As(V) concentration in experiment #3 was set to match the concentration at which goethite surface site saturation would occur by adsorbed As(V) if no Pb(II) were present (Salazar-Camacho and Villalobos, 2010).

3.2.1. Experiment #1. As/Fe ratio = 0.0004

Under these conditions the hydroxymimetite placed initially inside the dialysis tubing (Fig. 1) completely dissolved, and most of the liberated As(V) from this dissolution adsorbed onto goethite (Fig. 3) after crossing the dialysis membrane. The major part of the process was relatively fast, <24 h. However, the final balance

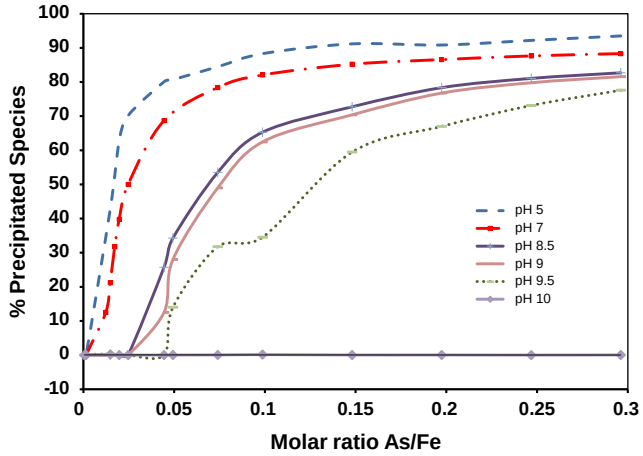

Fig. 6. Precipitated As(V) species distribution at several pH values as a function of the As/Fe molar ratio.

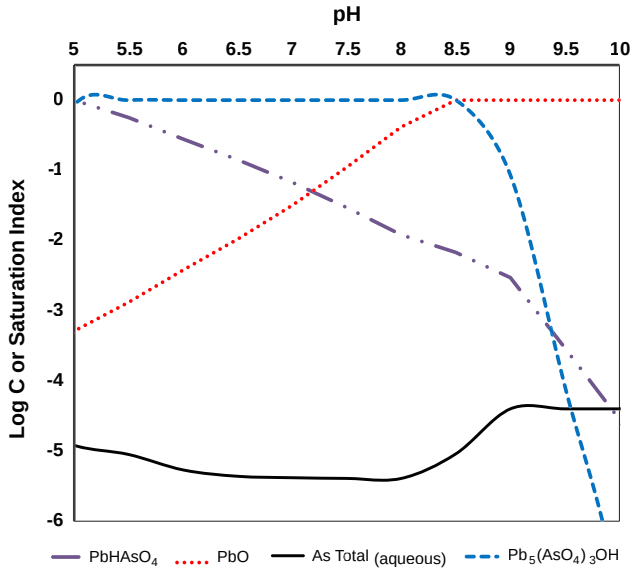

Fig. 7. Total aqueous As(V) and solid species distribution in the presence of Pb(II) (As/Pb = 3/5) without adsorption, obtained with $[AsO_4^{3-}]_{TOTAL} = 4.2 \times 10^{-5}$ M, which corresponds to an As/Fe molar ratio = 0.019 if goethite were present (0.2 g L^{-1}).

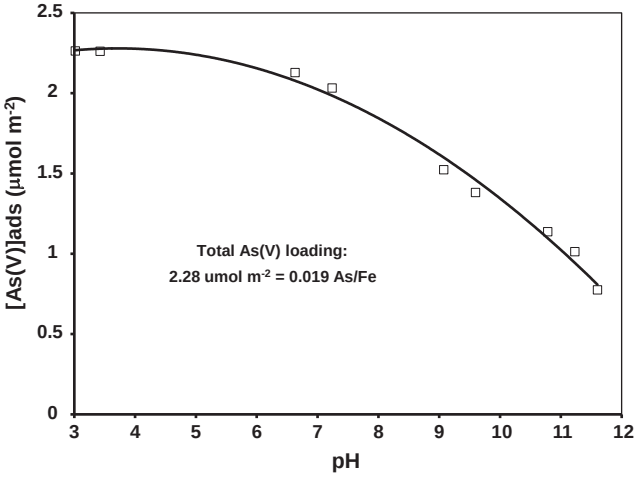

Fig. 8. pH-edge arsenate adsorption data for ideal goethite in absence of Pb(II) (taken from Stachowicz et al., 2008).

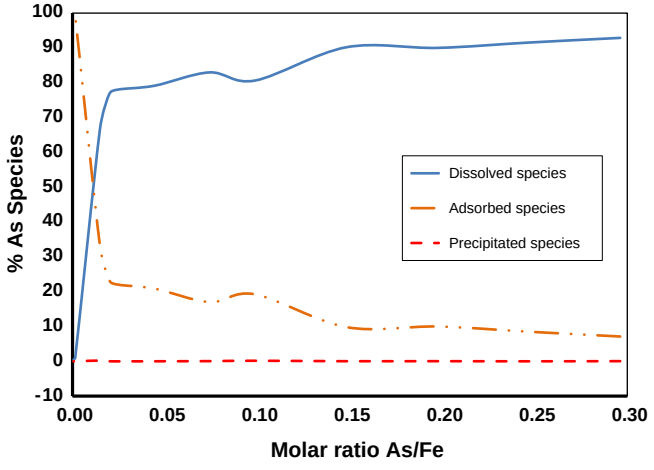

Fig. 9. As(V) species distribution model in the presence of Pb(II) and goethite at pH 10 as a function of the total As/Fe molar ratio.

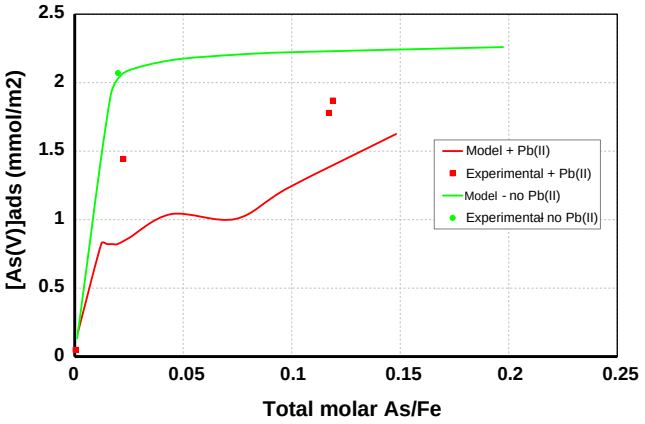

Fig. 10. Effect of Pb(II) on As(V) adsorption on an ideal goethite at pH 7 and total molar As/Pb = 3/5. The experimental point in the absence of Pb(II) (green circle) was obtained from Hiemstra and Van Riemsdijk (2000). The experimental points in the presence of Pb(II) (red squares) were generated in the present work. (For interpretation of the references to colour in this figure legend, the reader is referred to the web version of this article.)

of the last small fraction to reach equilibrium was reached after 7 days (data not shown). For Pb(II), the same situation was observed as with As(V) (Fig. 4) but no aqueous Pb(II) was detected. It is noteworthy that no precipitated species (e.g., PbO) were detected either (not shown). In contrast Pb (II) rapidly adsorbed on goethite, despite the latter having a net-positively charged protonated surface at pH 7 (pH_{ZPC} = 9.2, Villalobos et al., 2003), allowing the complete dissolution of the solid.

The possibility of a ternary As(V)–Pb(II) surface complex formation was not included in the model, but apparently these are not necessary, since the model, which considers binary independent Pb(II) and As(V) surface complexes exclusively, closely described the experimental data. Although the model results are not perfect, but it is believed that given the complexity of the processes being described and the relative simplicity of the adsorption model used, the trend of the predicted results is quite close to that of the experimental one.

The overall results of predominance of adsorption processes under this As/Fe condition may be explained as a result of an excess of reactive goethite surface sites present, with respect to As(V) and Pb(II) species (in the µmolar range), yielding a very strong driving force for ionic adsorption on the solid surface.

3.2.2. Experiment #2. As/Fe ratio = 0.1155

The significant increase in the As (and Pb)/Fe ratio, with respect to the previous experiment results in the predominance of the precipitation processes (Table 4, Figs. 3 and 4), with less than 13% of adsorbed As(V) species, less than 10% of adsorbed Pb(II) species, and negligible values of dissolved species. In this case, the kinetics were somewhat slower, taking 9 days to reach equilibrium (data not shown), even though the initial condition of the system had all As(V) and Pb(II) present in the hydroxymimetite precipitate inside the dialysis tubing (Fig. 1), which stays predominantly at equilibrium.

3.2.3. Experiment #3. As/Fe ratio = 0.0222

Under these conditions equivalent contributions of adsorption and precipitation processes were obtained for both As(V) (Fig. 3) and Pb(II) (Fig. 4), leading to an equilibrium time of 7 days (data not shown). Dissolved species were very low, 6.4% for As(V) and negligible for Pb(II). The corresponding total concentrations were 50 and 83 µmolar for As(V) and Pb(II), respectively (Table 3).

Table 4
As(V) and Pb(II) species distribution at equilibrium (7–9 days) from experiments at pH 7 [total concentration of dissolved carbonate (as HCO_3^-) = 60 μM].

Exp no.	As/Fe ratio	As(V) species (% of initial concentration)			Pb(II) species (% of initial concentration)			Symbol
		Adsorbed	Aqueous	Precipitated	Adsorbed	Aqueous	Precipitated	
1	0.0004	91.6	6.6	1.9	98.6	0.1	1.3	Squares
2	0.1155	12.6	0.97	86.5	8.1	0.06	91.8	Diamonds
3	0.0222	53.4	6.4	40.2	59.8	1.2	39.0	Triangles
4	0.1155	12.9	17.0	70.1	7.5	0.2	92.4	Circles

Note: The symbols refer to those used in Figs. 3 and 4.

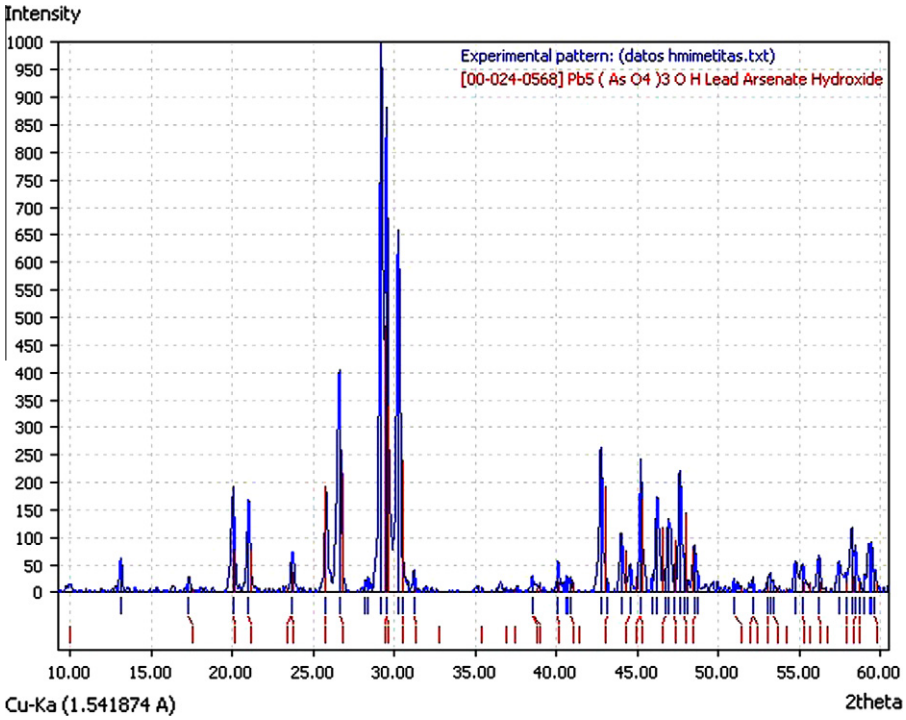

Fig. 11. X-ray diffraction pattern of solid inside dialysis tube at the end of experiment #4, and comparison with hydroxymimetite pattern from the crystallographic database. Note that this same diffraction pattern was obtained for the solid initially placed inside the tube of experiment #1–3.

3.2.4. Experiment #4. As/Fe ratio = 0.1155

This experiment was designed to simulate a pollution scenario from independent waste sources of As(V) and Pb(II), with aqueous As(V) in the outside suspension, and solid PbO inside the dialysis tubing, respectively. The ratios were set to match exactly those of experiment #2, to compare and evaluate the degree of similarity in equilibrium conditions obtained. As expected, the kinetic behavior was very different from that in experiment #2 since As (V) was initially in solution. However, at equilibrium (about 9 days), the species reached similar values shown for experiment #2 (Table 4, Figs. 3 and 4).

The X-ray diffraction pattern of the solid inside the dialysis tubing at the end of the experiment confirmed the complete transformation of PbO to hydroxymimetite (Fig. 11), and the analysis results of this experiment yield information on the mechanism involved in this transformation. Since As(V) precipitation occurred exclusively within the dialysis membrane, it is speculated that hydroxymimetite formation probably occurs via incorporation of As(V) to the PbO solid, and not by dissolution and reprecipitation phenomena (unless these latter stay very localized within the dialysis membrane). In the latter case some Pb(II) ion leakage towards the outside goethite suspension would have been expected (Fig. 1), with total concentration higher than that obtained in experiment #2 (which was not the case – compare the sum of adsorbed and aqueous Pb(II) from both experiments – Table 4), and thus detectable As(V) (as hydroxymimetite) in the goethite suspension. The presence of this solid in the goethite suspension would have overestimated the indirectly calculated adsorbed fractions outside the membrane in the suspension sampled. In contrast, adsorbed As(V) concentrations were remarkably similar in both experiments.

The close similarity obtained between experimental and modeled data at equilibrium, at pH 7 (Figs. 3 and 4), validates the modeling exercise. The modeling tested included highly involved surface complexation descriptions (Table 1) coupled with precipitation phenomena. This validation helped to acquire confidence in the predictive capability of the model at pH conditions other than seven presented in this work, and is promising for investigations at other conditions, such as variable As/Pb ratios, and the presence of other competing metals ions, such as Cu(II) and Zn(II), which will be engaged in future work.

Previous studies in which the fate of arsenate was identified as adsorbed to Fe oxides may be explained by the present investigation from the high proportions of Fe oxides with respect to total As(V) and metals normally present in those systems. This essentially means that Fe oxides being major components in most soil systems will tend to make adsorption the dominant process, unless the concentrations of As(V) and metals surpass a specific As/Fe threshold, which in the case of goethite is in the range of

0.015–0.06, depending on pH (provided the metal concentrations are also high).

The results from the relatively simple system defined agree well with the findings in the contaminated soils from the two previous articles of this series, and thus validated the simplifying approach followed. This approach allows better identification of the main contributing variables to the competing processes investigated, by excluding in the modeling all the complexity of the natural heterogeneous systems.

Nevertheless, it is also clear that the surface complexation modeling requires improvement by incorporating the possibility of different types of sites with different affinities on the goethite surface (Salazar-Camacho and Villalobos, 2010). The evidence of this is clearer when comparing the predicted adsorption behavior to the experimental data in Fig. 10. The model overestimates the effect of Pb arsenate precipitation on the adsorption of arsenate on goethite. However, although the accurate absolute values of the adsorption quantities are not reproduced by the model, the model shows the correct trend and significant competitive effect that the precipitation process exerts over the adsorption pathway. This renders the modeling method employed a confident tool to predict the geochemical behavior of As in the presence of metals, for future applications to more complex conditions as present in natural contaminated systems.

4. Conclusions

Thermodynamic modeling of the goethite/As(V)/Pb(II)/carbonate systems closely described the experimental behavior observed, by incorporating into the speciation program surface affinity constants obtained from the individual binary goethite systems, simultaneously with updated Pb arsenate solid formation constants. Model and experimental results showed that adsorption processes are only predominant at very low As/Fe molar ratios, while Pb(II) arsenate precipitation quickly begins competing as this ratio increases, preventing goethite surface site saturation with As(V). Under a limited range of As/Fe ratios both processes contribute in similar proportions. At higher As/Fe ratios, corresponding to the real contaminated soil scenarios investigated previously, Pb arsenate precipitation is the dominant process and no surface site saturation with As(V) occurred even at the highest As/Fe ratios investigated. This was evident in the experiments departing either from hydroxymimetite or from $PbO + Na_2HAsO_4$. Increasing pH over the range from 5 to 9.5 yielded a small increase in the predominance region of the adsorption process. However, overall Pb arsenate precipitation prevailed under most As/Fe conditions. The precipitation process seems to offer an advantageous mechanism for arsenate [and Pb(II)] attenuation in contaminated environments where both elements occur in similar total contents, with a high stability based on the pH range of hydroxymimetite stability.

Acknowledgments

We thank students and technicians from LAFQA at the Chemistry School, UNAM for their help with handling the analytical equipment and techniques, in particular ICP-AES and Atomic Absorption Spectroscopy. We are grateful to CONACyT for the student fellowship received and for the funding through Project # CB-2010-01-153723. Finally, we greatly appreciate the comments of two reviewers and the guest editors of this special issue, who helped improve the manuscript considerably.

References

Asta, M.P., Cama, J., Martínez, M., Giménez, J., 2009. Arsenic removal by goethite and jarosite in acidic conditions and its environmental implication. J. Hazard. Mater. 171, 965–972.
Atkinson, F., Posner, A., Quirk, J., 1967. Adsorption of potential-determining ions at the ferric oxide-aqueous electrolyte interface. J. Phys. Chem. 71, 550–558.
Bigham, J.M., Fitzpatrick, R.W., Schulze, D.G., 2002. Soil mineralogy with environmental applications. In: Dixon, J.B., Schulze, D.G. (Eds.), SSSA Book Series, vol. 7. Soil Sci. Soc. Am, Madison, WI, pp. 323–366.
Carabante, I., Grahn, M., Holmgren, A., Kumpiene, J., Hedlund, J., 2009. Adsorption of As(V) on iron oxide nanoparticle films studied by in situ ATR-FTIR spectroscopy. Colloids Surf. A 346, 106–113.
Catalano, J., Park, C., Fenter, P., Zhang, Z., 2008. Simultaneous inner- and outer-sphere arsenate adsorption on corundum and hematite. Geochim. Cosmochim. Acta 72, 1984–2004.
Drahota, P., Filippi, M., 2009. Secondary arsenic minerals in the environment: a review. Environ. Int. 35, 1243–1255.
Foster, A.L., Brown Jr, G.E., Tingle, T.N., Parks, G.A., 1998. Quantitative arsenic speciation in mine tailings using X-ray absorption spectroscopy. Am. Mineral. 83, 553–568.
Francesconi, K.A., Kuehnelt, D., 2002. Arsenic compounds in the environment. In: Frankenberger, W. (Ed.), Environmental Chemistry of Arsenic. Marcel Dekker, Inc., New York, pp. 51–94.
Gutierrez-Ruiz, M., Villalobos, M., Romero, F., Fernandez-Lomelin, P., 2005. Natural attenuation of arsenic in semiarid soils contaminated by oxidized arsenic wastes. In: O'Day, P.A., Vlassopoulos, D., Meng, X., Benning, L.G. (Eds.), Advances in Arsenic Research: Integration of Experimental and Observational Studies and Implications for Mitigation. Am. Chem. Soc. Symp. Series 915, 235–252 (Chapter 17).
Hayes, K., Redden, G., Ela, W., Leckie, J.O., 1990. Surface complexation models: an evaluation of model parameter estimation using FITEQL and oxide mineral titration data. J. Colloid Interface Sci. 142, 448–469.
Hiemstra, T., Van Riemsdijk, W.H., 2000. Adsorption on goethite in relation to different types of surface sites. J. Colloid Interface Sci. 225, 94–104.
Kumpiene, J., Ragnvaldsson, D., Lövgren, L., Tesfalidet, S., Gustavsson, B., Lättström, A., Leffler, P., Maurice, C., 2009. Impact of water saturation level on arsenic and metal mobility in the Fe-amended soil. Chemosphere 74, 206–215.
La Force, M.J., Hansel, C.M., Fendorf, S., 2000. Arsenic speciation, seasonal transformations, and co-distribution with iron in a mine waste influenced palustrine emergent wetland. Environ. Sci. Technol. 34, 3937–3943.
Lee, P.K., Kang, M.J., Choi, S.H., Touray, J.C., 2005. Sulfide oxidation and the natural attenuation of arsenic and trace metals in the waste rocks of the abandoned Seobo tungsten mine, Korea. Appl. Geochem. 20, 1687–1703.
Mamindy-Pajany, Y., Hurel, C., Marmier, N., Roméo, M., 2009. Arsenic adsorption onto hematite and goethite. Compt. Rend. Chim. 12, 876–881.
Mathur, S.S., Dzombak, D.A., 2006. Surface complexation modelling: goethite. In: Lützenkirchen, J. (Ed.), Surface Complexation Modelling. Academic Press, Elsevier, Amsterdam, pp. 443–468.
Morin, G., Calas, G., 2006. Arsenic in soils, mine tailings, and former industrial sites. Elements 2, 97–101.
Ng, J.C., 2005. Environmental contamination of arsenic and its toxicological impact on humans. Environ. Chem. 2 (3), 136–160.
Nordstrom, D.K., 2002. Worldwide occurrences of arsenic in ground water. Science 296, 2143–2145.
O'Day, P.A., 2006. Chemistry and mineralogy of arsenic. Elements 2, 77–83.
Ostergren, J., Trainor, T., Bargar, J., Brown, T., Parks, G., 2000. Inorganic ligand effects on Pb(II) sorption to goethite (α-FeOOH). J. Colloid Interface Sci. 225, 466–482.
Pierce, M.L., Moore, C.B., 1982. Adsorption of arsenite and arsenate on amorphous iron hydroxide. Water Res. 16, 1247–1253.
Plant, J.A., Kinniburgh, D.G., Smedley, P.L., Fordyce, F.M., Klinck, B.A., 2004. Arsenic and Selenium. In: Lollar, B.S. (Ed.), Environmental Geochemistry. Holland, H.D., Turekian, K.K., (Exec. Eds), Treatise on Geochemistry, vol. 9. Elsevier, Amsterdam, 17–66.
Salazar-Camacho, C., Villalobos, M., 2010. Goethite surface reactivity: III. Unifying arseniate adsorption behavior through a variable crystal face- Site density model. Geochim. Cosmochim. Acta 74, 2257–2280.
Stachowicz, M., Hiemstra, T., van Riemsdijk, W.H., 2008. Multi-competitive interaction of As(III) and As(V) oxyanions with Ca^{2+}, Mg^{2+}, PO_4^{3-}, and CO_3^{2-} ions on goethite. J. Colloid Interface Sci. 320, 400–414.
Van Geen, A., Robertson, A., Leckie, J.O., 1994. Complexation of carbonate species at the goethite surface. implications for adsorption of metal ions in natural waters. Geochim. Cosmochim. Acta 58, 2073–2086.
Van Riemsdijk, W.H., Hiemstra, T., 2006. The CD-MUSIC model as a framework for interpreting ion adsorption on metal (hydr) oxide surfaces. In: Lützenkirchen, J. (Ed.), Surface Complexation Modelling. Academic Press, Elsevier, Amsterdam, pp. 251–268.
Vaughan, D.J., 2006. Arsenic. Elements 2, 71–75.
Villalobos, M., Perez-Gallegos, A., 2008. Goethite surface reactivity: a macroscopic investigation unifying proton, chromate, carbonate, and lead(II) adsorption. J. Colloid Interface Sci. 326, 307–323.
Villalobos, M., García-Payne, D., López-Zepeda, J., Ceniceros-Gómez, A., Gutiérrez-Ruiz, M., 2010. Natural arsenic attenuation via metal arsenate precipitation in soils contaminated with metallurgical wastes: I. Wet chemical and thermodynamic evidences. Aquat. Geochem. 16, 225–250.

Villalobos, M., Trotz, M.A., Leckie, J.O., 2001. Surface complexation modeling of carbonate effects on the adsorption of Cr(VI), Pb(II), and U(VI) on goethite. Environ. Sci. Technol. 35, 3849–3856.

Villalobos, M., Trotz, M.A., Leckie, J.O., 2003. Variability in goethite surface site density: evidence from proton and carbonate sorption. J. Colloid Interface Sci. 268, 273–287.

Violante, A., Ricciardella, M., Del Gaudio, S., Pigna, M., 2006. Coprecipitation of arsenate with metal oxides: nature, mineralogy, and reactivity of aluminum precipitates. Environ. Sci. Technol. 40, 4961–4967.

Waychunas, G.A., Rea, B.A., Fuller, C.C., Davis, J.A., 1993. Surface chemistry of ferrihydrite: Part 1. EXAFS studies of the geometry of coprecipitated and adsorbed arsenate. Geochim. Cosmochim. Acta 57, 2251–2269.

Weng, L., Van Riemsdijk, W., Hiemstra, T., 2009. Effects of fulvic and humic acids on arsenate adsorption to goethite: experiments and modelling. Environ. Sci. Technol. 43, 7198–7204.

Chemical Geology 410 (2015) 162–173

Contents lists available at ScienceDirect

Chemical Geology

journal homepage: www.elsevier.com/locate/chemgeo

Approaching the geochemical complexity of As(V)-contaminated systems through thermodynamic modeling

Katherine Vaca-Escobar [a], Mario Villalobos [a,*], Teresa Pi-Puig [b], Rodolfo Zanella [c]

[a] Environmental Bio-Geochemistry Group, Earth Sciences Graduate Program, Universidad Nacional Autónoma de México (UNAM), Coyoacán, Ciudad Universitaria, 04510 DF, Mexico
[b] X-ray Diffraction Laboratory, Geochemistry Department, Instituto de Geología, Universidad Nacional Autónoma de México (UNAM), Coyoacán, Ciudad Universitaria, 04510 DF, Mexico
[c] Centro de Ciencias Aplicadas y Desarrollo Tecnológico, Universidad Nacional Autónoma de México (UNAM), Coyoacán, Ciudad Universitaria, 04510 DF, Mexico

ARTICLE INFO

Article history:
Received 25 September 2014
Received in revised form 5 June 2015
Accepted 7 June 2015
Available online 12 June 2015

Editor: Carla M Koretsky

Keywords:
Arsenate
Lead
Adsorption
Precipitation
Goethite
Surface complexation

ABSTRACT

Arsenate mobility in oxic environments is largely controlled by its adsorption to iron (hydr)oxides, but precipitation as heavy metal arsenates represents a potentially significant competing mechanism. Predicting As geochemical behavior in heterogeneous contaminated systems where various simultaneous equilibria are taking place may be achieved in a thermodynamically sound manner by coupling adsorption and solid-aqueous equilibria, provided that accurate equilibrium constants are employed; especially challenging is the surface complexation model segment.

The influence of adsorption and precipitation processes on As(V) mobility was modeled in the presence of Pb(II) and goethite by varying the As/Fe and As/Pb ratios, the goethite particle size, pH, and the inclusion of chloride and sulfate ions. A bottom-up approach is adopted here to gradually approximate the geochemical complexity of real contaminated scenarios. A unified surface complexation model for goethites of different particle sizes was used, which accounts for differences in their reactivity, and was coupled with a thermodynamic speciation model for aqueous and solid-phase equilibria.

The geochemical conditions found that favor As(V) precipitation as Pb(II) arsenates were high As/Fe, low As/Pb, goethites of small particle size, and especially the presence of chloride, and low sulfate concentrations (at low pH). The opposite conditions favor As(V) adsorption. Surprisingly, precipitation processes are more prevalent than expected and are favored from relatively low As/Fe in the presence of chloride, or with small particle-sized goethites.

1. Introduction

Arsenic contamination of soil and water is one of the worst and most widespread environmental problems facing humanity (Smedley and Kinniburgh, 2002), with a variety of polluting sources including pesticides (Qi and Donahoe, 2009), mobilization of natural deposits in rocks, sediments and soils (Togashi et al., 2000), and wastes arising from mining and metallurgical activities (Stevens and Lubitz, 1998). The latter contribute high concentrations of arsenic concurrently with heavy metals, released to aqueous environments through oxidation of arsenides and (arseno)sulfides. Concentrations of arsenic and metals such as lead, zinc and copper in mine wastes can reach hundreds of milligrams per kilogram, posing great health risks for humans and other biota (Anawar et al., 2002; Eisler, 2004; Fosmire, 1990; Ng, 2005; Papanikolaou et al., 2005; Stevens and Lubitz, 1998; Tangahu et al., 2013; Vaughan, 2006).

Arsenic mobility in oxic environments depends primarily on As(III) and As(V) sorption on metallic (hydr)oxides (Devitre et al., 1991), of which iron (hydr)oxide minerals, such as goethite and ferrihydrite, have been identified as the principal adsorbents in soils and groundwater (Arai et al., 2006; Asta et al., 2009; Craw et al., 2002; Lin and Puls, 2003; Lumsdon et al., 2001; Mamindy-Pajany et al., 2009; Matera et al., 2003; Paktunc et al., 2004; Slowey et al., 2007; Stuben et al., 2001). However, recent evidence for the formation of highly insoluble metal arsenate minerals (mainly of lead and copper) was found as an alternative natural attenuation process for As(V) in soils contaminated with mine residues (Gutierrez-Ruiz et al., 2005; Villalobos et al., 2010), apparently competing against the sorption mechanism described above.

Modeling these contamination scenarios can help us understand the geochemical conditions that promote each of the two mechanisms described above. The challenge from a thermodynamic standpoint lies in the fact that many different equilibria are occurring simultaneously and across different physicochemical phases, such as those at solid mineral-water interfaces, and in the aqueous phase to form dissolved complexes and precipitated minerals.

Modeling interfacial reactions of the binary adsorption of As(V) on goethites has not been trivial because different particle sizes show very different surface reactivities when normalized by surface area (Villalobos and Perez-Gallegos, 2008). Therefore, a thermodynamic

* Corresponding author.
E-mail address: mar.villa@stanfordalumni.org (M. Villalobos).

http://dx.doi.org/10.1016/j.chemgeo.2015.06.007
0009-2541/

description of non-ideal highly surface-reactive goethites, in a manner that is congruent with the behavior of ideal goethite crystals, has required the definition of As(V) surface affinity constants (as well as the essential surface acidity and electrolyte-binding constants) on a per-surface site basis. For this, a variable crystal-face modeling approach was developed and validated previously (Salazar-Camacho and Villalobos, 2010). This model successfully described the adsorption of As(V) on goethite for As(V) concentrations of up to 100 μM, goethites with specific surface areas (SSAs) from 28 to 94 m^2/g, and pH values from 4 to 10 (Salazar-Camacho and Villalobos, 2010).

The work presented here builds upon this binary As(V)/goethite surface complexation modeling to describe a ternary system that contains Pb(II). This new component requires inclusion of additional simultaneous aqueous equilibria, as well as new solid formation reactions to describe the competitive adsorption-precipitation mechanisms of As(V) immobilization.

In a previously published work (Vaca-Escobar et al., 2012) we applied a model that determined under what conditions metal arsenate precipitation prevails over the adsorption mechanism in a simple As(V)/Pb(II)/goethite system, with a "bottom-up approach" attempt to begin understanding the key parameters involved. The model predicted that from very low total As(V)/Fe(III) molar ratios (>0.022 at pH 7) precipitation significantly influences the attenuation of As(V), and rapidly becomes the dominant process over adsorption along the continuing range of As(V)/Fe(III). Modeling was performed using an ideal goethite with a high SSA (94 $m^2\ g^{-1}$) as the iron (hydr-)oxide source (Vaca-Escobar et al., 2012), and was validated with experimental wet chemical data generated for this simple system. The applied model coupled the previous As(V) surface complexation model (Salazar-Camacho and Villalobos, 2010) with lead(II) arsenate minerals solubility [with updated solubility product constants (Gutierrez-Ruiz et al., 2005; Villalobos et al., 2010)], and with all available equilibria in the aqueous phase.

In the present work we expand the previous investigation by evaluating the influence of a higher number of simultaneous variables in the system, in order to gradually approach the geochemical complexity of real contaminated scenarios; namely, different As/Pb ratios, the presence of a more surface-reactive (less ideal) goethite mineral (SSA of 50 $m^2\ g^{-1}$), and the inclusion of two other major anions that may substantially affect Pb(II) speciation (chlorides and sulfates). The added system components may either enhance adsorption or lead arsenate precipitation, and we report here the quantitative degree to which these effects are predicted to occur.

2. Materials and methods

Most of the work performed in this research involved a thermodynamic model developed and validated previously with wet chemical experiments (Vaca-Escobar et al., 2012). These and additional wet-chemical experimental validation confirmed the robustness of the adopted model, and provided us with enough confidence to progressively decrease the number of experimental points for model validation as geochemical conditions were made more complex.

2.1. Thermodynamic modeling

Arsenic behavior in the α-FeOOH/As(V)/Pb(II)/carbonate system was studied by coupling thermodynamic models through the Visual Minteq geochemical equilibrium and speciation interface (Gustafsson, 2010). This program was updated with adsorption and solid formation constants described in Tables 1 and 2, respectively. The adsorption segment of the model has been described in detail previously for the As(V)/goethite system (Salazar-Camacho and Villalobos, 2010). It uses combined tenets of the Triple-Layer and CD-MUSIC surface complexation models and unifies the adsorption behavior of goethite, irrespective of its specific surface area (SSA), by describing the adsorption reactions per type of reactive site on the goethite surface. For this, a variable crystal face composition model for goethite was developed, as a function of its SSA (Salazar-Camacho and Villalobos, 2010).

Activities of surface species in the mass action expression of this model were previously defined with a 1.0 M standard state. The Visual Minteq interface (Gustafsson, 2010) was used in the present work and defines these activities using a standard state of 1.0 mole fraction (dimensionless) of the total reactive surface sites. This difference in standard state definitions does not affect the final values of the affinity constants for monodentate reactions in either standard state approach, because the reference to mol/L in the numerator and denominator of the molar-based expression cancels out and also becomes dimensionless (Wang and Giammar, 2013). However, in the case of bidentate or higher denticity reactions for the molar standard state, if the exponent of the corresponding surface species is equated with its mass balance coefficient (e.g., "2" for a bidentate reaction), the reference molarity does not cancel out and the value of the mass action expression becomes dependent on concentration; whereas no concentration dependence occurs with the dimensionless mole fraction approach (Wang and Giammar, 2013).

One possibility, in order to not incur this concentration-dependent problem when using the molar-based approach, is to maintain an exponent of "1" (instead of "2") for this surface species in the corresponding mass action expression (Wang and Giammar, 2013). Such was the model adopted for the As(V)/goethite binary system investigated previously (Salazar-Camacho and Villalobos, 2010), but the values of the mass action expressions obtained cannot be automatically equated to the molar fraction-based values. Only one of the stoichiometries for As(V) binding occupies two equal sites and thus is affected by the choice of standard state. Therefore, the value for its mass action expression as obtained in the previous model had to be adjusted to fit the molar fraction-based approach (cf. Supplementary Data). However, the resulting mole fraction-based values (20.7–21.0) did not differ greatly from the molar-based value (21.6) (cf. Table 1 and Supplementary Data).

For Pb(II) adsorption on goethite, the corresponding surface complexation constants were taken from (Villalobos et al., 2009). The configuration of the As(V) surface complexes are in agreement with recent spectroscopic and molecular modeling evidence, in which a tilted inner-sphere monodentate complex was bound to a singly-coordinated site (Fig. 1), with a second adjacent site attracting an arsenate oxygen through H-bond type interactions (Loring et al., 2009; Otte et al., 2013).

On the main face of the goethite model ({101}) the adjacent site is another singly-coordinated site; while on the more reactive face ({010}) [present both at the particle tips, and intercalating with the main face ({101}) along the elongated sides of the goethite crystal] the adjacent site is a doubly-coordinated site (Salazar-Camacho and Villalobos, 2010). For this reason, two complexes are defined with different affinity constants (Table 1) but with the same general configuration (Fig. 1). Face {010} is more reactive because it has a considerably larger site density of singly-coordinated sites than face {101}, i.e., it has a significantly higher adsorption capacity; although the As(V) surface affinity constants have lower values on face {010} than on face {101} (Table 1). The model assumes that goethites with larger particle sizes – lower SSAs – show a higher proportion of face {010} than the smaller more ideal goethites, which explains the larger adsorption capacities, albeit lower affinities, of the former.

Other electrostatic and physicochemical parameters required by the adsorption model are listed in Table 3, including two electrical capacitances (C_1 and C_2) and densities of surface sites (n_s), which are dependent on the specific crystal face contributions exposed on each goethite sample (Villalobos et al., 2009; Villalobos and Perez-Gallegos, 2008) (Table 4). We should note that this adsorption model has proven successful in describing As(V) adsorption with equal affinity constants to goethites over a wide range of particle sizes (SSAs from 28 to 94 $m^2\ g^{-1}$), and a large span of As(V) concentrations and pH, applied

Table 1
Surface complexation reactions uploaded in Visual Minteq with formation constants described per type of surface site (Vaca-Escobar et al., 2012; Villalobos and Perez-Gallegos, 2008).

Acid–base[c]	Reactions[a]	Log K[b] SOH =		
		FeOH	Fe_2OH	Fe_3OH
$SOH + H^+ \rightleftharpoons SOH_2^+$	$K = \frac{[SOH_2^+]}{\gamma_1 [SOH][H^+]} e^{\frac{F}{RT}(\psi_0)}$	6.8[d]	nr	7.66
$SOH \rightleftharpoons SO^- + H^+$	$K = \frac{\gamma_1 [SO^-][H^+]}{[SOH]} e^{-\frac{F}{RT}(\psi_0)}$	−10.8	nr	−11.66
Electrolytes complexation (outer-sphere)				
$SOH + H^+ + NO_3^- \rightleftharpoons SO_2^+ \cdots NO_3^-$	$K = \frac{[SOH_2^+ \cdots NO_3^-]}{\gamma_1^2 [SOH][H^+][NO_3^-]} e^{\frac{F}{RT}(\psi_0 - \psi_\beta)}$	8.02	nr	9.025
$SOH + H^+ + Cl^- \rightleftharpoons SO_2^+ \cdots Cl^-$	$K = \frac{[SOH_2^+ \cdots Cl^-]}{\gamma_1^2 [SOH][H^+][Cl^-]} e^{\frac{F}{RT}(\psi_0 - \psi_\beta)}$	8.4	nr	8.9
$SOH + Na^+ \rightleftharpoons SO^- \cdots Na^+ + H^+$	$K = \frac{[SO^- \cdots Na^+][H^+]}{[SOH][Na^+]} e^{\frac{F}{RT}(\psi_\beta - \psi_0)}$	−9.43	nr	−11.095
Inner-sphere complexation				
$SOH + Pb^{2+} \rightleftharpoons SOPb^+ + H^+$	$K = \frac{[SOPb^+][H^+]}{\gamma_1^3 [SOH][Pb^{2+}]} e^{\frac{F}{RT}(\psi_0)}$	0.64	nr	nr
$FeOH + SOH + H^+ + AsO_4^{3-} \rightleftharpoons FeO^{-0.7}AsO_3^{-1.3} \cdots HOS + H_2O$	$K = \frac{[FeO^{-0.7}AsO_3^{-1.3} \cdots HOS]}{\gamma_1^{10} [FeOH]^d [H^+][AsO_4^{3-}]} e^{(-0.7\psi_0 - 1.3\psi_\beta)\frac{F}{RT}}$	21/20.7[e]	18.75[f]	nr
$FeOH + SOH + 2H^+ + AsO_4^{3-} \rightleftharpoons FeO^{-0.7}AsO_3H^{-0.3} \cdots HOS + H_2O$	$K = \frac{[FeO^{-0.7}AsO_3H^{-0.3} \cdots HOS]}{\gamma_1^{11} [FeOH][H^+]^2 [AsO_4^{3-}]} e^{(-0.7\psi_0 - 0.3\psi_\beta)\frac{F}{RT}}$	nr	19.6[f]	nr
$SOH + H^+ + CO_3^{2-} \rightleftharpoons SO^{-0.2}CO_2^{-0.8} + H_2O$	$K = \frac{[SO^{-0.2}CO_2^{-0.8}]}{\gamma_1^5 [SOH][CO_3^{2-}][H^+]} e^{\frac{F}{RT}(-0.2\psi_0 - 0.8\psi_\beta)}$	13.55	13.32	nr
Outer-sphere complexation				
$SOH + Pb^{2+} + H_2O \rightleftharpoons SO^- \cdots PbOH^+ + 2H^+$	$K = \frac{[SO^- \cdots PbOH^+][H^+]^2}{\gamma_1^2 [SOH][Pb^{2+}]} e^{\frac{F}{RT}(\psi_\beta - \psi_0)}$	−10.1	−8.6	nr

[a] SOH can be FeOH, Fe_2OH or Fe_3OH groups. As(V) surface complexation constants were taken or adjusted from (Salazar-Camacho and Villalobos, 2010), and those for Pb(II) from (Villalobos et al., 2009).
[b] nr = non-reactive group.
[c] The log of acidity constants used was established through a ΔpKa of 4 around each pH of PZNPC for each site type, which were 8.8 and 9.66, for FeOH and Fe_3OH groups, respectively.
[d] The exponent is 1 when SOH is Fe_2OH and 2 when it is FeOH.
[e] The log of formation constant used was 21 for GOE94 and GOE106, and 20.7 for GOE50 and GOE43. This differs from the value of 21.6 ± 0.7 from (Salazar-Camacho and Villalobos, 2010) because the standard state for activities of surface species in the latter is 1.0 M, while the one used for modeling in the present work is 1.0 mole fraction (see text).
[f] Fe_2OH groups adjacent to FeOH groups are present only on face (0 1 0), and their density corresponds to half of that of all FeOH groups present in that face. Therefore, the value of the reactive site density used toward binding of As(V) was half of the total FeOH site density on that face.

to both adsorption isotherm data and pH adsorption edge data (Salazar-Camacho and Villalobos, 2010).

Following is the sequence of the modeling procedure:

a) As(V) adsorption isotherms at pH 7 and 4: the adsorption model was applied using different As(V) total concentrations and keeping the goethite solid concentration fixed at 0.2 g L^{-1}, until reaching the adsorption maxima for high and low specific surface area goethites (GOE94 — 94 m^2 g^{-1} and GOE50 — 50 m^2 g^{-1}, respectively).
b) The sums of solid, adsorbed and aqueous As(V) species distribution were calculated using different fixed As/Pb molar ratios of 0, 1, 2, and 3/5 (corresponding to the stoichiometric ratio in hydroxymimetite [$Pb_5(AsO_4)_3OH$], which is the stable lead arsenate mineral under circumneutral pH conditions) (Fig. 2). Pb(II) species distributions were also calculated.
   For each As/Pb molar ratio studied, the molar As/Fe ratio was in turn varied, using a constant goethite solid concentration of 0.2 g L^{-1}. Three different values were chosen to represent: (i) very low As soil concentrations (molar As/Fe = 0.04%), (ii) intermediate soil concentrations (molar As/Fe = 2.22%), and (iii) high soil concentrations (molar As/Fe = 11.55%), equivalent to the average found in actual Mexican soils contaminated by a Pb(II) smelter (Villalobos et al., 2010).
   c) Values for pH were set between 5 and 10, and As(V) species distributions were computed for two goethites: GOE94 and GOE50.
   d) Additional As(V) species distribution was computed by including chloride in the system, at very low concentrations (1×10^{-5} to 1×10^{-2} M), since the Cl-containing mineral mimetite [$Pb_5(AsO_4)_3Cl$] has a solubility 20 orders of magnitude lower than its OH-containing counterpart, hydroxymimetite (Table 2). For this system we used an As/Pb molar ratio of 3/5, both GOE94 and GOE50, and pH 7. Precipitation of mimetite is expected to compete more favorably than hydroxymimetite with adsorption.
e) In an additional set of model calculations, As(V) species distribution was computed in the presence of high sulfate concentrations equal to 3.3×10^{-3} M (Harris et al., 2003), corresponding to actual concentrations in mining-contaminated scenarios, at pH 4. Sulfate is expected to compete with arsenate for precipitation of Pb(II) but only under acidic pH values.
f) Finally, As(V) species distribution was modeled for a set of data including both Cl^- and sulfate simultaneously at pH 4.
   Thermodynamic modeling described in e) and f) was performed only for GOE94, because the general behavior observed is similar to that for GOE50.

2.2. Wet chemical experiments

Solutions and suspensions were prepared using high-purity ion-exchanged water (NANOpure, 18.2 MΩ cm). All reagents used were analytical grade.

2.2.1. Goethite synthesis

Goethite was synthesized following the basic protocol of Atkinson et al. (1967), in which $Fe(NO_3)_3$ solutions are hydrolyzed with NaOH to pH > 12 and aged at 60 °C for 24 h. Experimental details for obtaining preparations of different specific surface areas (SSAs) using this protocol are described elsewhere (Villacís-García et al., in press). In summary, the crucial experimental parameter used to control the final goethite SSA was the speed of base addition to the Fe(III) solution, which is inversely proportional to the resulting SSA. For GOE43 (43 m^2 g^{-1}), the

Table 2
Main solid and aqueous species formation constants from their components, used in the thermodynamic model [taken from the Visual Minteq Database (Gustafsson, 2010)].

Mineral name	Chemical formula	Log K_f
Solid species		
Hydroxymimetite	$Pb_5(AsO_4)_3OH$	62.115 [a]
Mimetite	$Pb_5(AsO_4)_3Cl$	83.571 [a]
Plumbonacrite	$Pb_{10}(OH)_6O(CO_3)_6$	8.760
Schultenite	$PbHAsO_4$	23.969 [a]
Hydrocerussite	$Pb_3(OH)_2(CO_3)_2$	18.77
Cerussite	$PbCO_3$	13.13
Laurionite	$PbCl(OH)$	−0.623
Shannonite	Pb_2OCO_3	0.558
Massicot	PbO	−12.894
Litharge	PbO	−12.694
Natron	$Na_2CO_3 \cdot 10H_2O$	1.311
Thermonatrite	$Na_2CO_3 \cdot H_2O$	−0.637
	$Pb_3O_2CO_3$	−11.02
	PbO	−8.15
	$Pb_2O(OH)_2$	−26.188
	$Pb(OH)_2$	−8.15
	$PbO \cdot 0.3H_2O$	−12.98
	As_2O_5	34.694
Phosgenite	$(PbCl)_2CO_3$	19.810
Cotunnite	$PbCl_2$	4.78
Halite	$NaCl$	−1.603
	$Pb(OH)_3Cl$	−8.793
Anglesite	$PbSO_4$	−7.79
Larnakite	$Pb_2(OH)_2SO_4$	−0.4344
Mirabilite	$Na_2SO_4 \cdot 10H_2O$	−1.114
Thernardite	Na_2SO_4	0.3217
	$Pb_3OSO_{4(s)}$	10.6864
	$Pb_4(OH)_6SO_{4(s)}$	21.1
	$Pb_4O_3SO_{4(s)}$	21.8772
Aqueous species		
	$PbCl_{2(aq)}$	2.200
	$PbCl^+$	1.55
	$PbCl_3^-$	1.800
	$PbCl_4^{2-}$	1.460
	$NaSO_4^-$	0.74
	$PbSO_{4(aq)}$	2.69
	$Pb(SO_4)_2^{2-}$	3.47
	HSO_4^-	1.99
	$HAsO_4^{2-}$	11.6
	$H_2AsO_4^-$	18.35
	H_3AsO_4	20.6
	$PbH_2AsO_4^+$	19.736 [a]
	$PbHAsO_4$	14.038 [a]
	$Pb(OH)_2$	−17.897
	$Pb(NO_3)_2$	1.4
	$PbNO_3^+$	1.17
	$PbOH^+$	−7.597
	$Pb_4(OH)_4^{4+}$	−19.988
	$Pb_2(OH)^{3+}$	−6.397
	$Pb(OH)_3^-$	−28.091
	$Pb(OH)_4^{2-}$	−39.699
	$Pb_3(OH)_4^{2+}$	−23.888
	H_2CO_3	16.681
	HCO_3^-	10.329
	$NaHCO_3$	10.079
	$PbHCO_3^+$	13.200
	$NaCO_3^-$	1.270
	$PbCO_3$	6.478
	$Pb(CO_3)_2^{2-}$	9.938

[a] Log K_f taken from Villalobos et al. (2010) and added to the Visual Minteq Database (Gustafsson, 2010).

complete NaOH solution was added at once in the reactor, and for GOE106 (106 $m^2\ g^{-1}$), the base addition rate was 1 mL min^{-1}. Goethite precipitates were repeatedly washed, shaken, and centrifuged. Dilute HNO_3 was used to drop the pH to 7 for the initial washes. For the sequential washes nanopure water was used until a value of conductivity of 0.1 μS cm^{-1} was reached. Samples were dried at 110 °C and X-ray powder diffraction (Shimadzu — XRD-6000) was used to confirm the identity of both goethites. Specific surface area measurements were performed by the nitrogen adsorption BET method (Quantachrome Autosob-1-C).

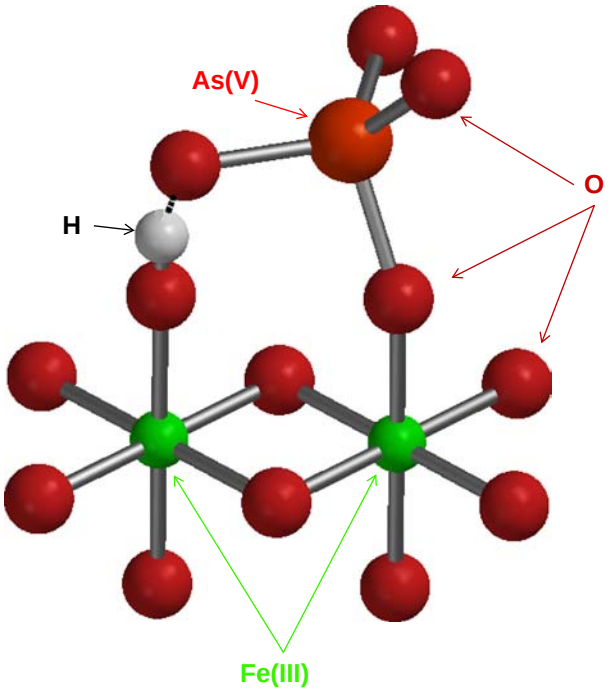

Fig. 1. Structural configuration of the As(V) adsorption complex on two adjacent Fe–O octahedra of the goethite crystal faces, forming an inner-sphere bond to one singly-coordinated oxygen, and a hydrogen bond to the adjacent oxygen, which can either be singly-coordinated on face (101) (in the structure shown), or doubly-coordinated on face (010).

2.2.2. As(V) adsorption isotherms at pH 7

First, adsorption isotherms were measured on GOE43 and GOE106, using initial As(V) concentrations of 650, 600, 480, 360, 240, 160, 120, 80, 40, 20 and 0 μmol L^{-1}, placed in polypropylene reactors. The systems were kept open to atmospheric CO_2, with an ionic strength of 0.01 M $NaNO_3$, pH 7 and goethite concentration of 0.2 g L^{-1}. The total volume was 100 mL.

The suspensions in the reactor were continuously stirred (900 rpm), and aliquots (10 mL) of the goethite suspensions were sampled after 24 h. The aliquots were filtered through nitrocellulose membranes of 0.05 μm pore size. The filtered solutions were analyzed for As using Hydride Generation– AA Spectroscopy (Varian SPECTRAA110) (detection limit of 1 μg L^{-1} or 0.013 μM). The experimental results for GOE106 and GOE43 were modeled with the parameters obtained previously for GOE94 and for GOE50, respectively.

Table 3
Additional parameters used in the surface complexation model (Salazar-Camacho and Villalobos, 2010).

Parameter	Value	Units
C_1 (GOE94)	0.729	F m^{-2}
C_1 (GOE50)	1.17	F m^{-2}
C_2	0.200	F m^{-2}
Specific surface area (GOE94)	94	$m^2\ g^{-1}$
Specific surface area (GOE50)	50	$m^2\ g^{-1}$
Solids concentration	0.2	g L^{-1}
Ionic strength	0.01	mol L^{-1}
Log PCO_2	−3.5	Log (atm)

Table 4
Site-density analysis of the two goethites used (Villalobos and Perez-Gallegos, 2008).

Goethite	Face contributions (%)			Reactive surface site densities (sites nm^{-2})		
	101	001	010	≡FeOH	≡Fe_2OH	≡Fe_3OH
GOE94	70	30	0	3.12	0.00	3.12
GOE50[a]	37	0	63	6.85	2.87	1.12

[a] For GOE50 the site densities were distributed as follows: For face 010 FeOH site densities were 2.87 for sites adjacent to Fe_2OH [i.e., those reactive to As(V)], 2.87 for sites not adjacent to the latter [i.e., for sites not reactive to As(V)], and 2.87 for Fe_2OH. For face (101) FeOH site density was 1.11, and Fe_3OH site density was 1.12.

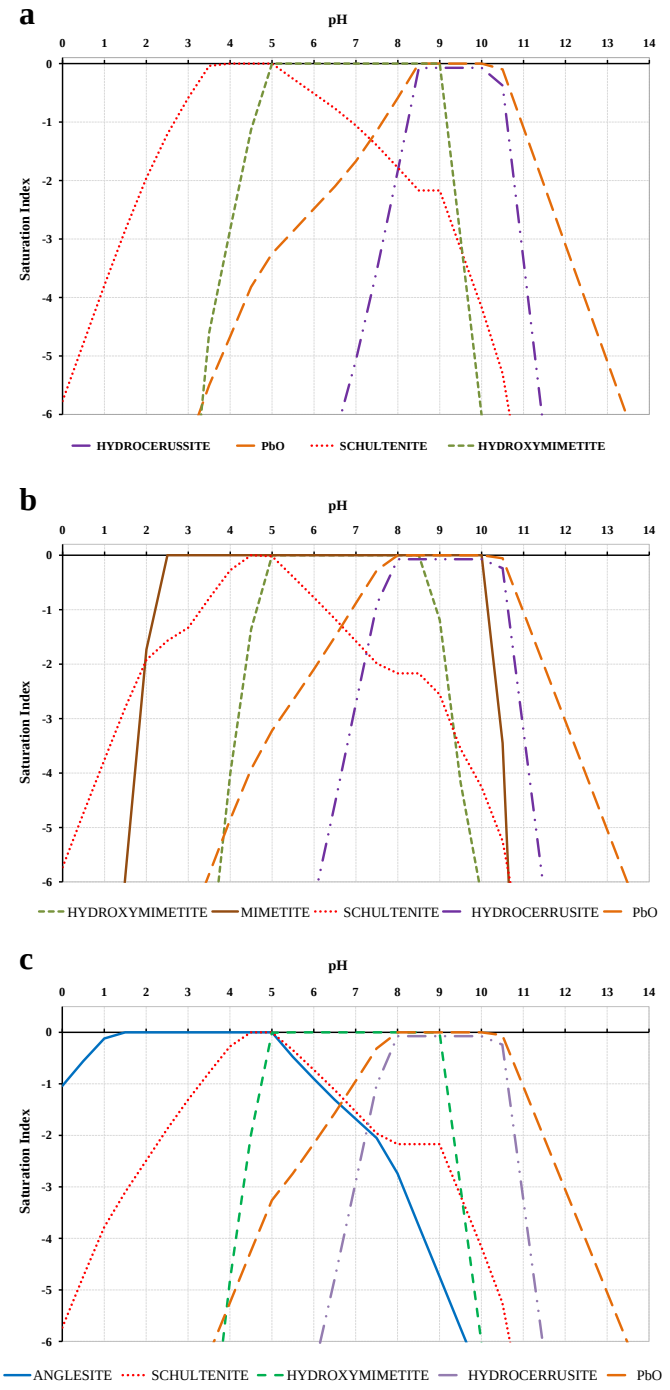

Fig. 2. Saturation indices of As–Pb solids in the absence of goethite, for a system composed of $[AsO_4^{3-}] = 5 \times 10^{-5}$ M, $[Pb^{2+}] = 8.33 \times 10^{-5}$ M (As/Pb = 3/5) and I = 0.01 M $NaNO_3$, a) no additional ions, b) $[Cl^{-1}] = 1 \times 10^{-5}$ M, and c) $[SO_4^{-2}] = 3.3 \times 10^{-3}$ M. Chemical formulas of minerals shown are listed in Table 2.

2.2.3. Spot checks of As(V)/Pb(II)/goethite systems

Limited experimental spot checks were performed to compare with the modeling results, at pH 7 for both goethites (pH 4 for systems with sulfate). The experimental details were described previously (Vaca-Escobar et al., 2012) and basically consist of the following. A cellulose dialysis tube membrane (MWCO = 8000 Da) closed on both ends was placed inside the goethite suspension, itself inside a 250 mL polycarbonate bottle (Fig. 3). Each tube was filled prior to closing the other end with volumes ranging from 0.025 mL to 6.5 mL, depending on the experiment, of a suspension of either hydroxymimetite [$Pb_5AsO_4(OH)_3$] or hydrocerussite [$Pb_3(OH)_2(CO_3)_2$]. For the latter, As(V) was added to the system in the form of NaH_2AsO_4.

The dialysis membrane only lets ions and water molecules pass through its walls in the aqueous suspension, such that precipitation and adsorption processes may be easily separated physically because the goethite is found only in the external suspension, and thus adsorption reactions take place only outside the tubing. The solid Pb(II) source is always placed inside the dialysis tube, such that precipitation always takes place inside this membrane. This allows separate quantification of both processes.

From the previous work, the minimum time to reach invariant aqueous concentrations was 9 days for the fastest equilibrating systems. Therefore, to ensure arrival at equilibrium conditions for all experiments, a period of 14 days stirring was set prior to sampling for analyses. The concentrations used for the different As/Fe and As/Pb experimental conditions are shown in Table 5. The suspension in the reactor with the floating dialysis tube was continuously stirred (900 rpm), and aliquots (10 mL) of the goethite (outside) suspension were sampled separately for total aqueous and total adsorbed As(V) and Pb(II) analysis. The aliquots were filtered through 0.05 μm-pore nitrocellulose membranes. The solid retained on the filter membrane was slightly washed with nanopure water and was dissolved with concentrated HCl (36%) and made up to 25 mL with water to yield a final pH of 1 (no $PbCl_2$ precipitates were formed). Both the filtered and the digested solutions were analyzed for As(V) and for Pb(II) (for dissolved and adsorbed fractions, respectively). The precipitated fractions were calculated indirectly from the following mass balance equation:

$$[\text{Total species}] = [\text{Adsorbed species}] + [\text{Dissolved species}] + [\text{Precipitated species}]$$

Precipitated species were considered to reside only inside the dialysis tube because in control experiments without goethite no precipitates

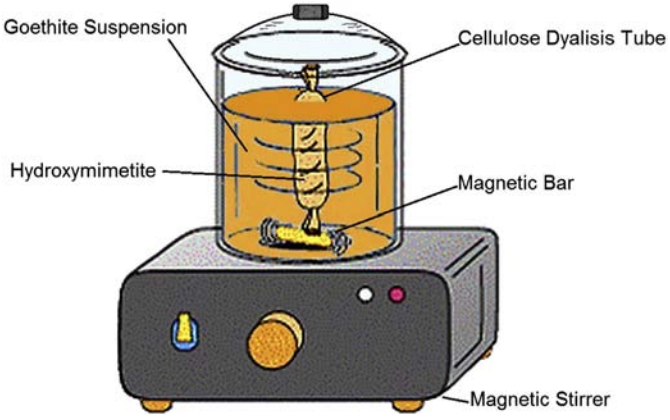

Fig. 3. Schematics of the reactor used for quantifying equilibrium concentrations in a system composed of As(V) in the presence of goethite, and other aqueous components. Pb(II)-bearing precipitates were maintained separately from the goethite adsorbent by placing the Pb(II) source inside the dialysis tube at the beginning of the experiments.

Table 5
Experimental conditions used in the spot checks of As(V)/Pb(II)/goethite systems, in 0.2 g/L goethite, and 0.01 M $NaNO_3$.

Molar ratio As/Fe (mol/mol)	Concentration (M)		As and Pb sources
	As(V)	Pb(II)	
0.0004	1.0×10^{-6}	1.67×10^{-6}	$Pb_5(AsO_4)_3OH$
0.1155	2.6×10^{-4}	4.33×10^{-4}	$Pb_5(AsO_4)_3OH$
0.0222	5.0×10^{-5}	8.33×10^{-5}	$Pb_5(AsO_4)_3OH$
0.1155	2.6×10^{-4}	4.33×10^{-4}	$Pb_3(OH)_2(CO_3)_2 + NaH_2AsO_4$

were found outside the dialysis tube in any of the As/Fe conditions investigated.

2.3. X-ray diffraction

Solid products (goethites, Pb(II) arsenates, and Pb(II) hydroxycarbonates) were all highly crystalline and thus were readily identified by X-ray diffraction. Dry solids were ground with an agate pestle and mortar to <75 μm and mounted in aluminum holders. A Shimadzu XRD-6000 X-ray diffractometer equipped with a Cu tube and graphite monochromator was used. Phase identification was made with a PDF-2 and PDF-4 minerals database using Shimadzu software.

Rietveld refinement of the data was done with TOPAS Academic v.4.1 software (http://www.topas-academic.net/). This software implements the fundamental parameter approach [FPA (Cheary and Coelho, 1992)], and full axial divergence model (Cheary and Coelho, 1998a, 1998b). The specimen-dependent parameters which were refined were the zero error, displacement error, Chebyshev polynomial fitting for the background with six coefficients, cell parameters, crystallite size, and atomic coordinates.

3. Results and discussion

3.1. Goethites synthesized

The identity and purity of the synthesized goethites were confirmed by XRD (not shown). The BET SSA were 43 (±2) $m^2\ g^{-1}$ and 106 (±3) $m^2\ g^{-1}$. The former was considered close enough to the GOE50 previously thoroughly characterized for crystal face distribution (Salazar-Camacho and Villalobos, 2010; Villalobos et al., 2009; Villalobos and Perez-Gallegos, 2008), and therefore, it was possible to compare the ensuing modeling results for GOE50 with the experimental spot checks on GOE43. The value of 106 $m^2\ g^{-1}$ is within the SSA range of ideal goethite crystals and thus GOE106 shows the same adsorption behavior as GOE94 when normalized by SSA (Fig. 4a).

3.2. Thermodynamic modeling

3.2.1. As(V) adsorption isotherms

As(V) adsorption maxima at pH 7 in the absence of Pb(II) were calculated using the previously developed thermodynamic model, and determined experimentally (through adsorption isotherms — Fig. 4). When normalized by surface area (Fig. 4a), model lines coincide closely with the experimental data, which confirms that the experimental reactivities of GOE106 and of GOE43 are equivalent to those of GOE94 and of GOE50, respectively, on a per-surface area basis. This is important because the complete set of model parameters has been previously obtained only for GOE94 and GOE50 (Salazar-Camacho and Villalobos, 2010). The good fit to the experimental data in Fig. 4a demonstrates that the model can be safely applied to GOE106 and GOE43, respectively. The four goethites were used for model validation throughout the work. The adsorption maxima were close to 2.0 μmol m^{-2} for GOE106/94, and close to 2.50 μmol m^{-2} for GOE43/50. Finally, the isotherms show that GOE43/50 has a higher adsorption capacity than GOE106/94 when normalized by SSA (Fig. 4a), as expected (Salazar-Camacho and Villalobos, 2010). However, when the adsorption data are normalized by goethite mass the reverse is observed (Fig. 4b), and the adsorption maxima increased in the order of their respective goethite SSAs, despite the fact that GOE50/43 have a considerably larger site density than GOE94/106 (cf. Table 4). Mass normalized data then show somewhat higher As(V) adsorption for GOE50 than for GOE43, and for GOE106 as compared to GOE94. This is important to consider in the ensuing investigation, when comparing certain experimental data performed on one goethite (e.g., GOE43 or GOE106) with the corresponding model predictions (e.g., GOE50 or GOE94, respectively), since goethite masses were kept constant.

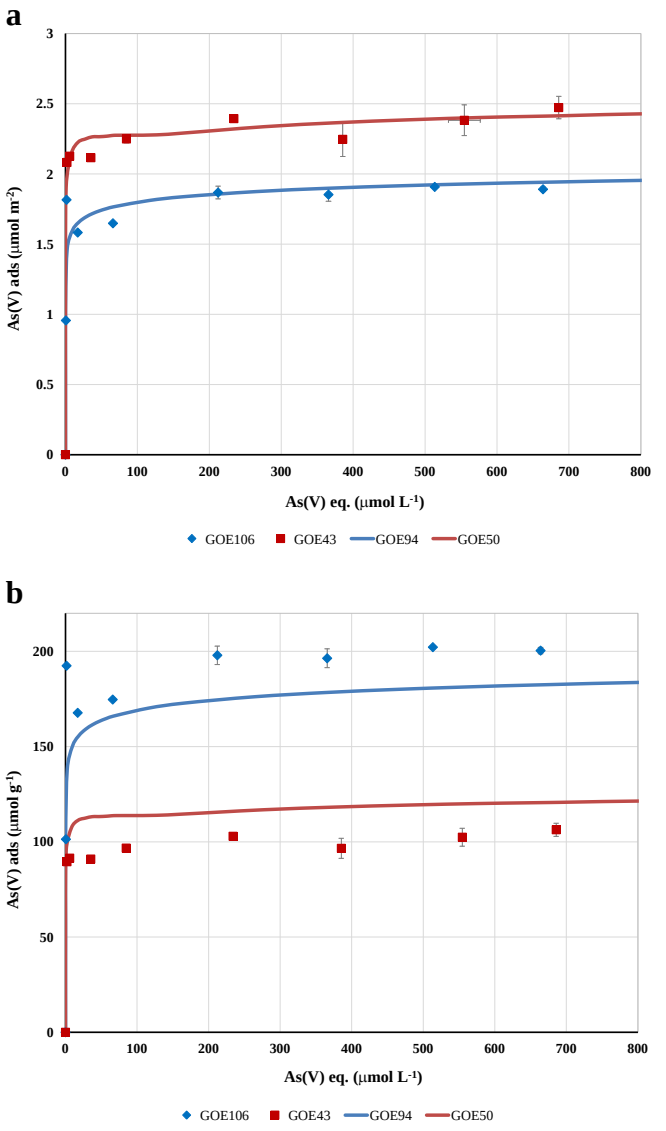

Fig. 4. Arsenate adsorption isotherms for goethites GOE106 and GOE43 (experimental — symbols), and for GOE94 and GOE50 (model — lines) at pH 7 in systems at 0.01 M $NaNO_3$, normalized by surface area (a), and by goethite mass (b). Solid concentration used was 0.2 g L^{-1}.

3.2.2. Influence of goethite particle size (at As/Pb = 3/5)

In the absence of goethite (i.e., of adsorption) the speciation model predicts formation of hydroxymimetite [$Pb_5(AsO_4)_3OH$] in a pH range of 5–9 (Fig. 2a), at a total As(V) concentration corresponding to an As/Fe molar ratio = 0.019 with 0.2 g L^{-1} goethite. Formation of this solid was experimentally confirmed by XRD (cf. next section).

Fig. 5 shows the distribution of total adsorbed, precipitated, and dissolved species, when goethite and Pb(II) are present, as a function of the

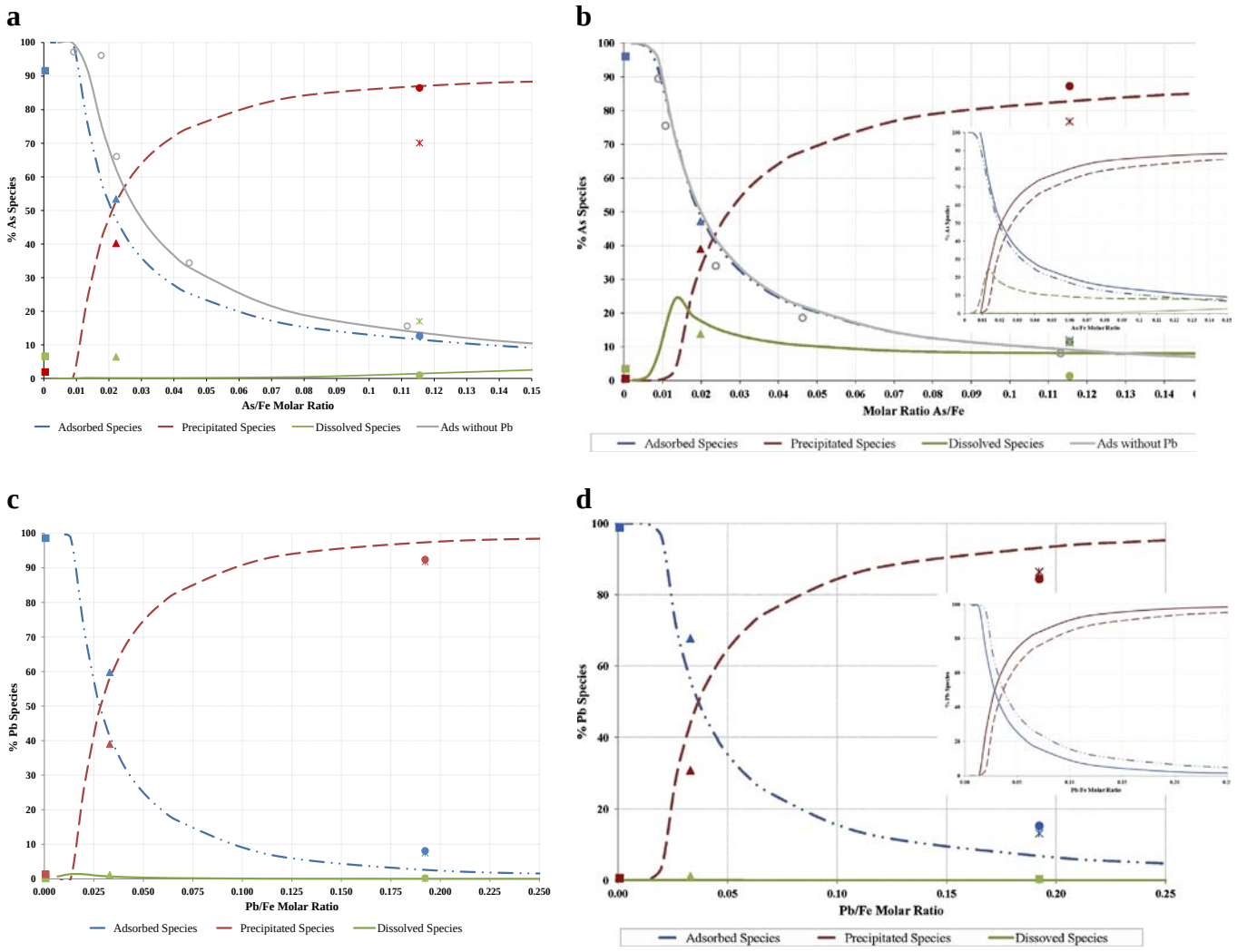

Fig. 5. As(V) species distribution in the presence of Pb(II) and goethite at pH 7 and a As/Pb of 3/5 a) for GOE94, and b) for GOE50, with predicted As(V) adsorption in the absence of Pb(II) shown by the gray line, gray circles show the corresponding experimental As(V) adsorbed concentrations for GOE106 and for GOE43, respectively (lines: model predictions; symbols: experimental data — squares correspond to As/Fe = 0.0004, triangles to As/Fe = 0.0222, circles to As/Fe = 0.1155 initially adding hydroxymimetite inside the dialysis tube, and asterisks to As/Fe = 0.1155 initially adding hydrocerrusite [$Pb_3(OH)_2(CO_3)_2$ — inside the dialysis tube] and a soluble Na arsenate salt [outside the tube]) (total As/Pb is always 3/5). Pb(II) species distribution in the systems described above for c) GOE94, and d) GOE50. The figure insets in (b) and (d) compare the model behavior between both goethites — continuous lines are for GOE94 and broken lines for GOE50.

relative proportion of As versus the goethite concentration, measured as total Fe. The adsorption curves for both goethites show a similar high prevalence at low As/Fe ratios, and they begin decreasing after a similar As/Fe ratio at the expense of the Pb(II) arsenate precipitating out for GOE94 (Fig. 5a), or initially at the expense of the appearance of dissolved As(V), for GOE50 (Fig. 5b), and later also due to precipitation of Pb(II) arsenate.

In addition to the important difference in the behavior of dissolved As(V) between both goethites, an interesting difference in the behavior of the other two species can also be observed (Fig. 5b-inset). Despite the fact that GOE94/106 adsorb a considerably higher concentration of As(V) in the absence of Pb(II) (Fig. 4b and gray lines and symbols in Fig. 5a and b), unexpectedly, only these goethites show a decrease in As(V) adsorption when Pb(II) is present (Fig. 5a); closely approaching As(V) adsorption for GOE50 with or without Pb(II) (Fig. 5b-inset). For GOE94, Pb(II) arsenate appears at the expense of the decrease in As(V) adsorption, and dissolved As(V) is negligible (Fig. 5a). In contrast, GOE50 shows considerable concentrations of dissolved As(V) (up to 25%, Fig. 4b), and always shows lower precipitated concentrations than GOE94 (Fig. 5b-inset). An important implication of the difference in adsorption behavior between goethites is that in the presence of Pb(II), the As/Fe ratios required to saturate the surface sites of GOE94 are much larger than in its absence (see Section 3.2.10).

3.2.3. Deviations of experimental results in hydrocerussite system or between goethites

The experimental data closely match the model predictions, except in the case where Pb(II) is added initially as the Pb(II) hydroxy-carbonate, hydrocerussite [$Pb_3(CO_3)_2(OH)_2$] (asterisk-shaped symbols in Fig. 5). This is most likely because the hydroxymimetite precipitate forms starting from the surface of hydrocerussite and inwards through its interaction with aqueous As(V), and the thickness of the Pb(II)-arsenate layer formed eventually prevents further reactivity of the internal Pb(II) in hydrocerussite with more aqueous As(V). This mechanism is supported by the XRD pattern (Fig. 6) of the final solid inside the dialysis tubing at equilibrium in the GOE94 system (Fig. 5a), which shows a mixture of both Pb(II) minerals. A Rietveld refinement analysis showed that 70–80% of the solid formed was hydroxymimetite. The experimentally

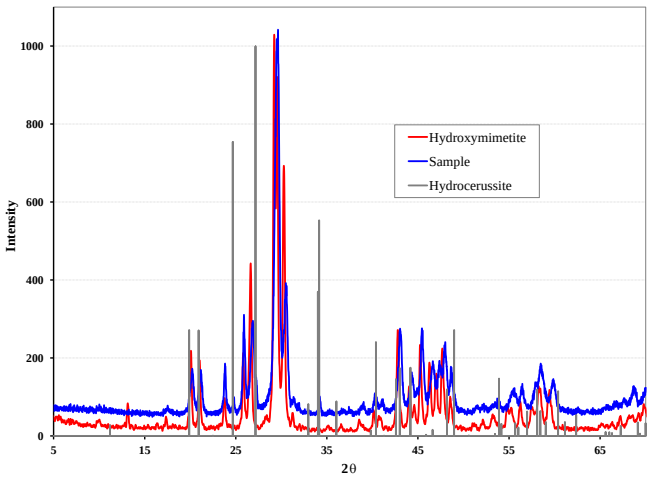

Fig. 6. X-ray diffraction pattern of solid inside dialysis tube at the end of experiment where Pb(II) was added initially as hydrocerussite, and comparison with hydroxymimetite pattern and hydrocerussite peaks from the crystallographic database PDF-4 minerals 2013 RDB.

precipitated As(V) was 15% lower than the predicted value (as hydroxymimetite), at the expense of a similar increase (17%) in aqueous As(V) detected experimentally (Fig. 5a).

The experimental adsorption data for the systems in the absence of Pb(II) (gray circles Fig. 5a and b) deviated slightly from the model lines (gray lines). This is because the data are implicitly normalized by the mass of goethite, and thus the actual SSA of the goethite is important and the differences between GOE106 and GOE94, and between GOE43 and GOE50 are significant (cf. Fig. 4b), as explained in Section 3.2.1 above. As expected, for the first pair, the experimental data (for GOE106) yielded higher concentrations of As(V) adsorbed than the model (for GOE94) (Fig. 5a); and for the second pair, the opposite occurred (Fig. 5b).

3.2.4. Behavior of Pb(II) species

The corresponding Pb(II) species behavior is shown in Fig. 5c for GOE94 and in 5d for GOE50. Dissolved species were always negligible for both goethites, thus only adsorbed and precipitated species play a role. These two curves are similar between goethites except that they are shifted toward higher As/Fe for GOE50 with respect to GOE94 (Fig. 5d-inset). This means that GOE50 adsorbs more Pb(II) than GOE94, but promotes less precipitation of Pb(II); and herein lies the explanation of the differences observed in the behavior of adsorbed As(V) between the presence and absence of Pb(II), and of precipitated As(V) between goethites (Fig. 5a and b): The higher surface reactivity of GOE50 for Pb(II) leaves less available Pb(II) for arsenate precipitation, and thus no effect is observed on As(V) adsorption when Pb(II) is added (Fig. 5b), despite the fact that GOE50 adsorbs less total As(V) in the absence of Pb(II), and leaves more available As(V). This latter appears as aqueous As(V), and less precipitated arsenate as compared to the system with GOE94.

3.2.5. Influence of increasing As/Pb molar ratios (>3/5 = 0.6)

Increasing As(V) relative to Pb(II) is predicted by the model to decrease the driving force to precipitate the Pb(II) arsenate (Fig. 7a), and thus promotes large concentrations of As(V) to come into solution (Fig. 7b), but causes only small changes in the prevalence of adsorption over a larger range of As/Fe ratios (Fig. 7c). Evidently, changes in adsorption are only relevant for the case of GOE94. This behavior makes sense since there is progressively less Pb(II) available to form hydroxymimetite, which contains an As/Pb of 3/5. The onset of precipitation appears at increasing As/Fe with increasing As/Pb, but

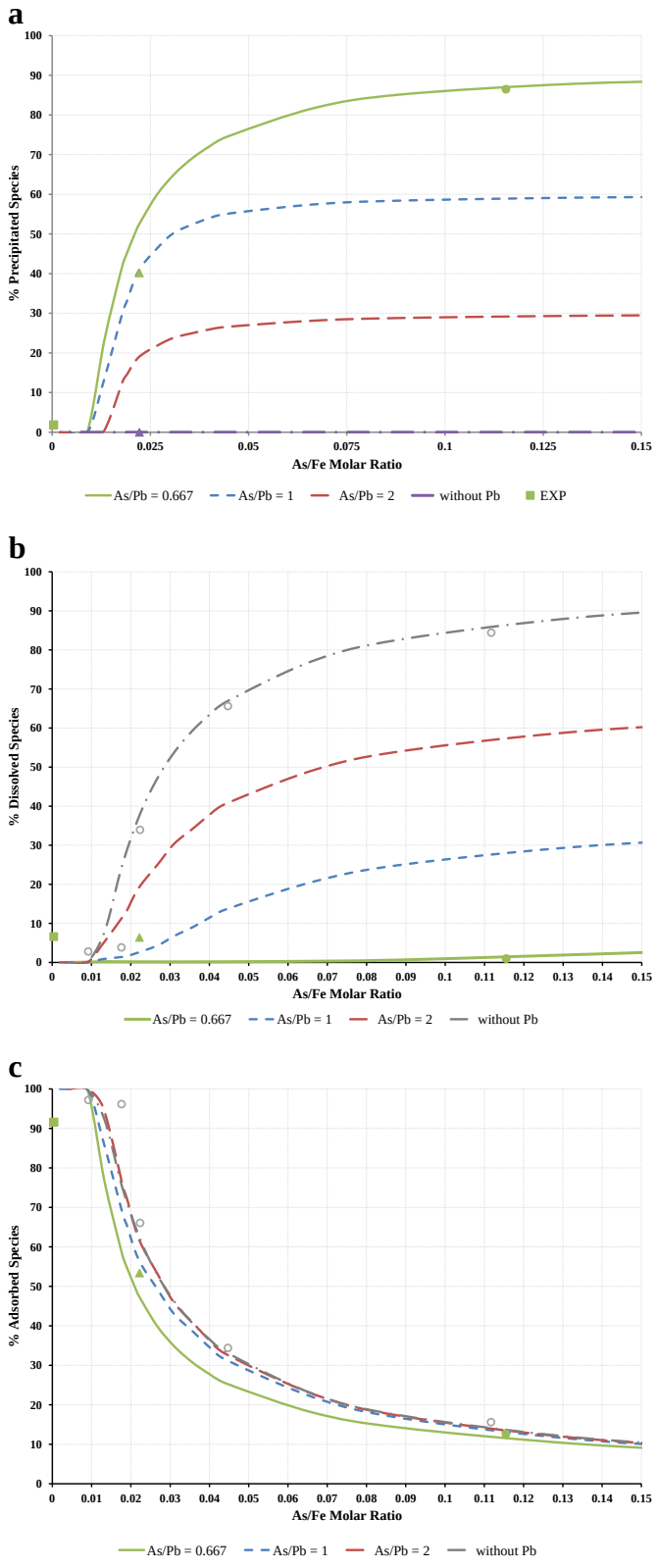

Fig. 7. As(V) species distribution at pH 7 for GOE94, at different As/Pb molar ratios: a) precipitated species, b) dissolved species, and c) adsorbed species.

more importantly, the maxima attained decreases considerably (Fig. 7a): at As/Pb = 1 it reached 60% of the total As species, and at As/Pb = 2, only 30%, whereas the appearance of dissolved As(V) followed the opposite trend and increased considerably as As/Pb increased (Fig. 7b), but was zero at an As/Pb of 3/5.

3.2.6. Effect of pH

In the pH range of 4 to 9 a similar behavior as shown in the previous figures (Fig. 5a and b) at pH 7 is observed for As/Pb of 3/5. However, the crossing point between adsorbed and precipitated species tends to move to higher As/Fe ratios upon moving away from pH 7.5 for GOE94, and pH 6 for GOE50 (Fig. 8), on both sides of the pH scale. This means that adsorption is favored when pH is far from 6 to 7.5, and this effect is larger for GOE94 than for GOE50 but only below pH 7.5. At higher pH values the rate of increase with pH for both goethites is similar. As/Fe values of the crossing point for equal contribution of both immobilization processes range from 0.02 to 0.039. At the low pH range this increase in adsorption contribution is explained by the formation of a different Pb(II) arsenate solid, schultenite ($PbHAsO_4$) (Fig. 2), which has a higher solubility than hydroxymimetite (Table 2), allowing a larger contribution of As(V) species to adsorb. At higher pH values, hydroxymimetite will start dissolving, allowing adsorption to again increase in relation to precipitation. However, at sufficiently high pH adsorption will also begin decreasing because of competition with OH^-, causing a net increase in the model-predicted dissolved species (not shown).

3.2.7. Influence of Cl^-

Small concentrations of Cl^- in the system without goethite have a dramatic effect on the species distribution curves because the Pb(II) arsenate that forms, mimetite [$Pb_5(AsO_4)_3Cl$] has a solubility product more than twenty orders of magnitude lower than hydroxymimetite [$Pb_5(AsO_4)_3OH$] (10^{-84} vs. 10^{-62} — Table 2). This causes mimetite to appear at pH values as low as 2.5 and to stay precipitated up to pH 10 (Fig. 2b), coexisting with hydroxymimetite in its typical stability pH range of 5 to 8.5 (Fig. 2b). The presence of mimetite has been inferred in mine waste-contaminated soils (Villalobos et al., 2010).

Chloride concentrations as low as 10^{-5} M increased considerably the region of predominance of As(V) precipitated species at the expense of adsorbed species (cf. arrows in Fig. 9). For example, at As/Fe of almost 0.01, adsorbed As(V) species decrease almost 50%, while precipitated species increase an equal amount for GOE94/106 (Fig. 9a); this value is *ca.* 40% for GOE50/43 (Fig. 9b). The main difference between both total Cl^- concentrations investigated was that at 10^{-5} M Cl^- ions are eventually consumed as As/Fe increases and the speciation curves thereafter adjoin the corresponding curves in the absence of Cl^-. At 10^{-4} M Cl^- complete consumption of this anion does not occur and precipitation is always higher than when no Cl^- is present.

The effect of a wider Cl^- concentration span is reported in Table 6, in the form of the As/Fe ratio at which the same contribution of adsorbed and precipitated As(V) species occurs, i.e., the crossing point between both speciation curves. It is evident that this crossing point moves progressively to lower As/Fe ratios for both goethites as Cl^- is increased, indicating a progressive predominance of the precipitation region, at the expense of a decrease in the adsorption predominance region. Limited experimental spot checks were performed at the lowest Cl^- concentration investigated of 10^{-5} M for both goethites (Fig. 9). These data closely matched the model predictions. Experimentally determined dissolved species (not shown) were always below 5%.

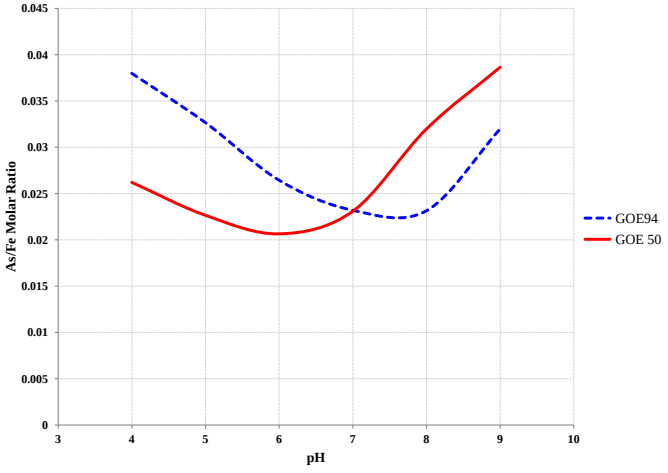

Fig. 8. As/Fe molar ratios at which an equal contribution of adsorbed and precipitated As(V) species are predicted to occur, as a function of pH for both goethites (As/Pb = 3/5).

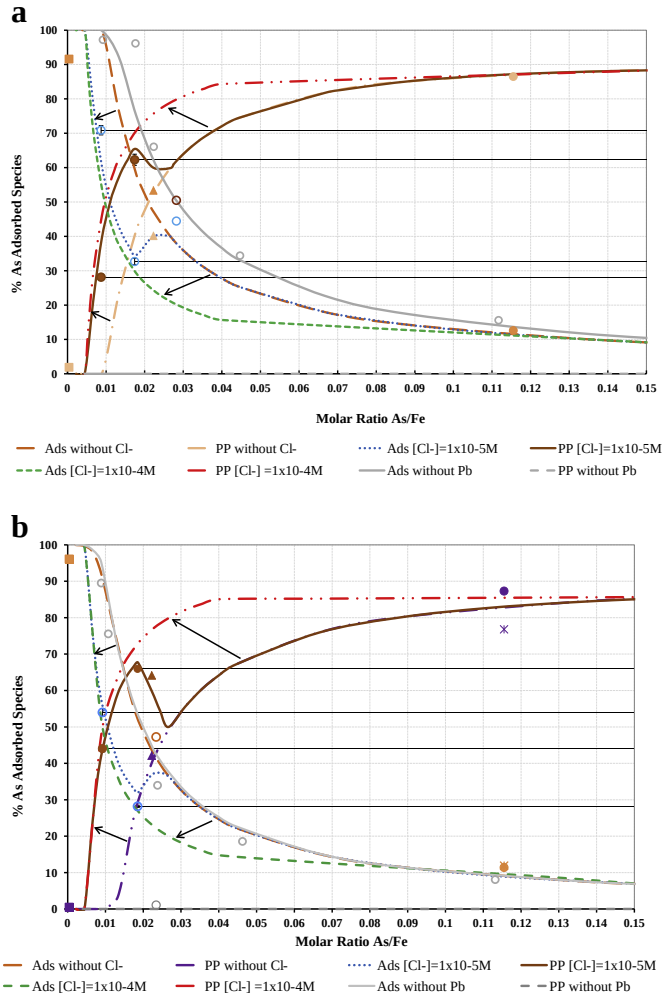

Fig. 9. As(V) species distribution at pH 7 and an As/Pb molar ratio = 3/5, with the addition of chloride: a) GOE94, and b) GOE50. "Ads" corresponds to adsorbed species, and "PP" to precipitated species. The black arrows show the trend observed for adsorbed and for precipitated species upon adding Cl^-. Experimental data correspond to GOE106 and GOE43, respectively.

3.2.8. Influence of SO_4^{2-}

Solid speciation in the absence of adsorption shows that the presence of high sulfate concentrations (3.3×10^{-3} M), simulating

Table 6
As/Fe molar ratio where the same percentage of adsorbed and precipitated species are predicted, under different chloride concentrations in the system at pH 7.

Chloride concentration	GOE94	GOE50
Without chloride	0.026	0.0305
1×10^{-5} M	0.016	0.020
1×10^{-4} M	0.0135	0.018
1×10^{-3} M	0.012	0.0165
1×10^{-2} M	0.0106	0.0104

those found in mining environments arising from sulfide oxidation, have an effect on the system only at pH values between 1.5 and 5. This happens through the appearance of the $PbSO_4$ mineral, anglesite (Fig. 2c), which apparently shortens the stability region of schultenite but does not affect the formation of hydroxymimetite at higher pH values. Therefore, sulfate ions have no effect on the previous speciation diagrams at pH 7 (not shown). At pH 4, however, the model predicts a considerable effect on As(V) precipitates and dissolved species, but minor effects on the adsorbed species behavior (Fig. 10). The onset of precipitation is moved toward larger values of As/Fe, whereas that of dissolved species does not move because it occurs initially at the expense of desorption (which does not change in the presence of sulfate either). Because of the delay in the onset of Pb(II)-arsenate precipitation, the extent to which dissolved species appear is considerably increased from a maximum of 13% without sulfate, to 45% in its presence.

The observed net effect may be explained as a competitive mechanism between sulfate and arsenate for binding Pb(II), which results in the release of aqueous As(V). Very similar effects were observed for GOE50 (not shown). The limited experimental spot checks at pH 4 matched closely the model predictions.

3.2.9. Simultaneous influence of Cl^- and SO_4^{2-}

The simultaneous presence of Cl^- at 10^{-5} M and sulfate at pH 4 shows a drastic counterbalancing effect to that observed in the sole presence of sulfate, because precipitation of mimetite $[Pb_5(AsO_4)_3Cl]$ occurs from very low pH values (Fig. 2b). Although the adsorption curve is not largely affected, the onset of precipitation is moved to considerably lower As/Fe values (Fig. 10b); while the onset of dissolution is moved significantly in the opposite direction, and its extent is decreased to a maximum of *ca.* 30% dissolved.

Chloride is therefore confirmed to be a potentially very valuable remediation species for As(V) and Pb(II) in a wide pH range in the form of precipitated species, although insufficient when sulfate is present at low pH because aqueous As(V) concentrations remain considerable. Fortunately, in these scenarios, formation of other secondary ferric hydroxysulfate minerals, such as jarosites, may play an important role in both As(V) and Pb(II) sequestration.

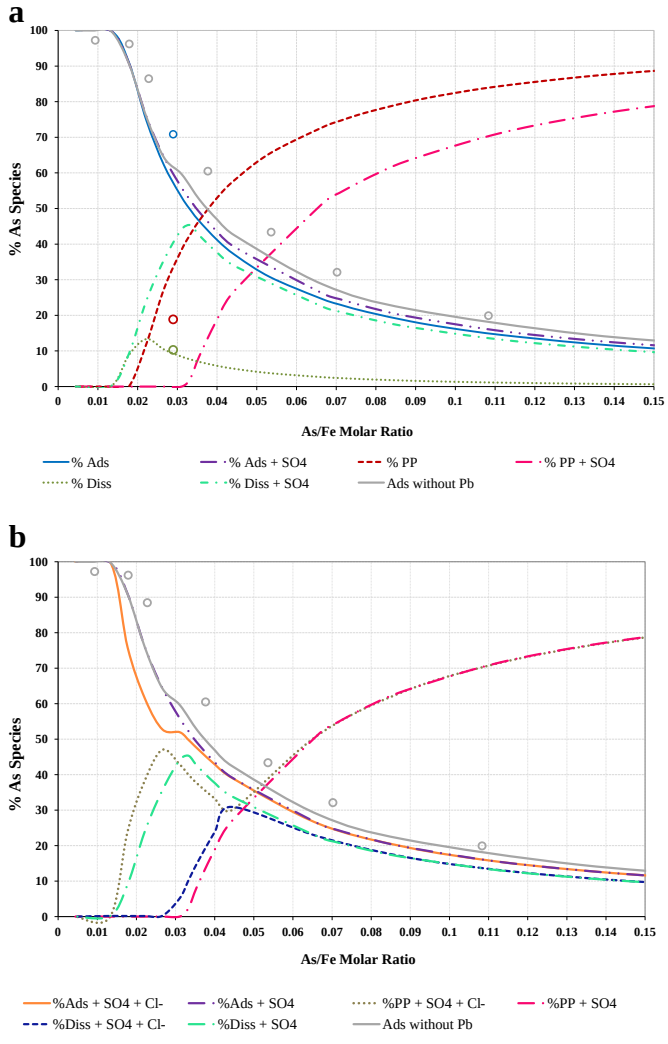

Fig. 10. As(V) species distribution at pH 4, and an As/Pb molar ratio = 3/5 in the presence of GOE94 with the addition of a) $[SO_4^{2-}] = 3.3 \times 10^{-3}$ M, b) $[SO_4^{2-}] = 3.3 \times 10^{-3}$ M and $[Cl^-] = 1 \times 10^{-5}$ M. Experimental data correspond to GOE106.

3.2.10. Implications for goethite surface saturation with As(V)

The influence of Pb(II) may also be analyzed with respect to the goethite surface and its conditions for achieving saturation with As(V). A calculation was performed to define the "beginning" of the flat segment of the As(V) adsorption isotherm curves as the absolute maximum peak value of their second derivative curves (i.e., the inflection point of the first derivative curves). These values correspond to 1.68 μmol m^{-2} for GOE106/94, and to 2.26 μmol m^{-2} for GOE43/50.

Table 7 shows a summary of the As/Fe values required for As(V) to reach surface saturation as defined above at the different conditions investigated. For GOE94 at pH 7, when As/Pb is 0.60 (= 3/5), and in the presence or absence of 10^{-5} M Cl^-, As/Fe must increase considerably from 0.018 to 0.089 to achieve surface saturation; when Cl^- is increased to 10^{-4} M, this As/Fe value must be increased even further to 0.138. For GOE50, Pb(II) by itself does not affect the surface saturation with As(V), but the presence of Cl^- requires an As/Fe increase to achieve saturation, which occurs at values considerably lower than for GOE94 (0.024 and 0.075 — Table 7).

For both goethites at pH 4, the only condition that requires As/Fe values to increase when Pb(II) is present to reach surface saturation is the presence of Cl^-. This means that at this lower pH, As(V) adsorption is a much more efficient process because of the more favorable surface electrostatic conditions, and only the extremely insoluble mimetite precipitate (cf. Table 2) is able to compete toward binding As(V) with the goethite surface.

4. Conclusions

An accurate model description of As(V) mobility and speciation was attained in a system composed of goethite/As(V)/Pb(II) as a function of a series of critical geochemical variables. The description was possible through coupling a robust surface complexation model developed for

Table 7
Model As/Fe molar ratios at which surface site saturation[a] was reached under the different experimental conditions investigated.

	Conditions	As/Fe GOE94	As/Fe GOE50
pH 7	Without Pb	0.018	0.013
	As/Pb = 0.6	0.089	0.013
	As/Pb = 1	0.022	0.013
	As/Pb = 2	0.018	0.013
	As/Pb = 0.6 + $[Cl^-] = 10^{-5}$ M	0.089	0.024
	As/Pb = 0.6 + $[Cl^-] = 10^{-4}$ M	0.138	0.075
pH 4	Without Pb	0.022	0.016
	As/Pb = 0.6	0.022	0.016
	As/Pb = 0.6 + $[SO_4^{2-}] = 3.3 \times 10^{-5}$ M	0.022	0.016
	As/Pb = 0.6 + $[SO_4^{2-}] = 3.3 \times 10^{-5}$ M + $[Cl^-] = 10^{-5}$ M	0.036	0.027

[a] Surface site saturation values considered were those occurring at 95% of those calculated at the beginning of the flattening segment of the corresponding adsorption isotherms (calculated as a peak maximum in the second derivative of the curves). These 95% values were for GOE94: 1.60 μmol m^{-2} at pH 7, and 2.015 μmol m^{-2} at pH 4; and for GOE50: 2.15 μmol m^{-2} at pH 7, and 2.48 μmol m^{-2} at pH 4.

the binary As(V)/goethite adsorption system, to an aqueous-solid thermodynamic speciation model. The geochemical behavior modeled simulated contaminated environments where As(V) and Pb(II) are simultaneously present at high concentrations, using controlled systems that approximate the complexity of scenarios such as mine-impacted environments.

At near-neutral pH, the presence of Pb(II) impacts the adsorption of As(V) on goethite through precipitation of a highly insoluble Pb(II) arsenate, but only for the high SSA goethite (94 $m^2 g^{-1}$), and indirectly because of its lower surface reactivity toward Pb(II). Model and experimental results showed that adsorption is predominant only at very low As/Fe molar ratios, while Pb(II) arsenate precipitation quickly begins competing as this ratio increases, preventing goethite surface site saturation with As(V) until reaching As/Fe values five times higher than in the absence of Pb(II). Under a limited range of As/Fe ratios both processes contributed in similar proportions. At higher As/Fe ratios, corresponding to the real contaminated soil scenarios investigated previously, Pb arsenate precipitation is the dominant process controlling As(V) speciation.

No effect of Pb(II) was observed on As(V) adsorption for a highly surface reactive goethite with a lower SSA (50 $m^2 g^{-1}$), despite the fact that it adsorbs considerably less As(V) per goethite mass in the absence of Pb(II) than the 94 $m^2 g^{-1}$ goethite. The lower SSA goethite tended to stabilize a considerable fraction of aqueous phase As(V) in the presence of Pb(II) after As(V) surface saturation because of its higher adsorption of Pb(II).

In the presence of very small concentrations of chloride, a Pb(II) arsenate-chloride, mimetite, with a solubility product 20 orders of magnitude lower than its hydroxy counterpart, imposed a large competition for As(V) binding versus its adsorption on both goethites. The presence of high sulfate concentrations affected the above equilibria only at low pH values by forming insoluble anglesite ($PbSO_4$), and thereby releasing As(V) for both higher adsorption and higher aqueous concentrations. However, if chloride were present simultaneously with sulfate, the effect was reversed and Pb(II) arsenate precipitation tended to control As(V) mobility under most conditions of total As/Fe. All previous results are valid for a total As/Pb ratio of 3/5. At higher ratios, precipitation became progressively less prevalent, and aqueous As(V) appeared in considerable concentrations after goethite surface saturation occurred.

The above results have important geochemical implications for the behavior of As(V) in real contaminated environments. As(V) is successfully immobilized through adsorption and/or precipitation in the presence of Pb(II) and Fe (hydr)oxide. The specific reactivity of this Fe (hydr)oxide source will determine how prevalent adsorption will be versus solid formation. Chloride ions, from very small concentrations, will promote precipitation as the prevailing mechanism, and sulfate (in the absence of chloride) will promote adsorption but also higher As(V) aqueous concentrations, and only at low pH values. In this manner, chloride ions appear to be excellent remediating agents to ensure highly unavailable As(V) [and Pb(II)] in contaminated environments.

Precipitation, especially in the presence of chloride, seems to offer an advantageous mechanism for arsenate and Pb(II) simultaneous attenuation in contaminated environments where both elements occur in similar total concentrations, showing a high stability based on the pH range of occurrence of the three Pb-arsenate minerals: mimetite, hydroxymimetite and schultenite.

Acknowledgments

This research was funded by the CONACyT through Project # CB-2010-01-153723. We thank the students and technicians from LABQA at the Chemistry School, UNAM for their help with handling the analytical equipment and techniques, in particular ICP-AES and Atomic Absorption Spectroscopy. K. V.-E. is grateful to CONACyT for the Ph.D. student fellowship received. Finally, we are thankful for the excellent comments provided by three anonymous reviewers and Editor, Carla Koretsky, which helped improve considerably the clarity of the manuscript.

Appendix A. Supplementary data

Supplementary data to this article can be found online at http://dx.doi.org/10.1016/j.chemgeo.2015.06.007.

References

Anawar, H.M., Akai, J., Mostofa, K.M.G., Safiullah, S., Tareq, S.M., 2002. Arsenic poisoning in groundwater — health risk and geochemical sources in Bangladesh. Environ. Int. 27 (7), 597–604.
Arai, Y., et al., 2006. Spatial and temporal variability of arsenic solid-state speciation in historically lead arsenate contaminated soils. Environ. Sci. Technol. 40 (3), 673–679.
Asta, M.P., Cama, J., Martinez, M., Gimenez, J., 2009. Arsenic removal by goethite and jarosite in acidic conditions and its environmental implications. J. Hazard. Mater. 171 (1–3), 965–972.
Atkinson, R.J., Posner, A.M., Quirk, J.P., 1967. Adsorption of potential-determining ions at the ferric oxide-aqueous electrolyte interface. J. Phys. Chem. 71 (5), 9.
Cheary, R.W., Coelho, A., 1992. A fundamental parameters approach to X-ray line-profile fitting. J. Appl. Crystallogr. 25 (2), 109–121.
Cheary, R.W., Coelho, A.A., 1998a. Axial divergence in a conventional X-ray powder diffractometer. I. Theoretical foundations. J. Appl. Crystallogr. 31 (6), 851–861.
Cheary, R.W., Coelho, A.A., 1998b. Axial divergence in a conventional X-ray powder diffractometer. II. Realization and evaluation in a fundamental-parameter profile fitting procedure. J. Appl. Crystallogr. 31 (6), 862–868.
Craw, D., Koons, P.O., Chappell, D.A., 2002. Arsenic distribution during formation and capping of an oxidised sulphidic minesoil, Macraes mine, New Zealand. J. Geochem. Explor. 76 (1), 13–29.
Devitre, R., Belzile, N., Tessier, A., 1991. Speciation and adsorption of arsenic on diagenetic iron oxyhydroxides. Limnol. Oceanogr. 36 (7), 1480–1485.
Eisler, R., 2004. Arsenic hazards to humans, plants, and animals from gold mining, reviews of environmental contamination and toxicology. Reviews of Environmental Contamination and Toxicology. Springer, New York, pp. 133–165.
Fosmire, G.J., 1990. Zinc toxicity. Am. J. Clin. Nutr. 51 (2), 225–227.
Gustafsson, J.P., 2010. Visual MINTEQ. Ver. 3.0. A free equilibrium speciation model software. VISUAL MINTEQ VER 3.
Gutierrez-Ruiz, M., Villalobos, M., Romero, F., Fernandez-Lomelin, P., 2005. Natural attenuation of arsenic in semiarid soils contaminated by oxidized arsenic wastes. In: Oday, P.A., Vlassopoulos, D., Meng, Z., Benning, L.G. (Eds.), Advances in Arsenic Research: Integration of Experimental and Observational Studies and Implications for Mitigation. ACS Symposium Series, pp. 235–252.
Harris, P., et al., 2003. Measuring sulfate in subgrade soil — difficulties and triumphs. Geomaterials 2003: Soils, Geology, and Foundations. Transportation Research Record. Transportation Research Board Natl Research Council, Washington, pp. 3–11.
Lin, Z., Puls, R.W., 2003. Potential indicators for the assessment of arsenic natural attenuation in the subsurface. Adv. Environ. Res. 7 (4), 825–834.
Loring, J.S., Sandstrom, M.H., Noren, K., Persson, P., 2009. Rethinking arsenate coordination at the surface of goethite. Chem. Eur. J. 15 (20), 5063–5072.
Lumsdon, D.G., Meeussen, J.C.L., Paterson, E., Garden, L.M., Anderson, P., 2001. Use of solid phase characterisation and chemical modelling for assessing the behaviour of arsenic in contaminated soils. Appl. Geochem. 16 (6), 571–581.
Mamindy-Pajany, Y., Hurel, C., Marmier, N., Roméo, M., 2009. Arsenic adsorption onto hematite and goethite. C. R. Chim. 12 (8), 876–881.
Matera, V., et al., 2003. A methodological approach for the identification of arsenic bearing phases in polluted soils. Environ. Pollut. 126 (1), 51–64.
Ng, J.C., 2005. Environmental contamination of arsenic and its toxicological impact on humans. Environ. Chem. 2 (3), 146–160.
Otte, K., Schmahl, W.W., Pentcheva, R., 2013. DFT + U study of arsenate adsorption on FeOOH surfaces: evidence for competing binding mechanisms. J. Phys. Chem. C 117 (30), 15571–15582.
Paktunc, D., Foster, A., Heald, S., Laflamme, G., 2004. Speciation and characterization of arsenic in gold ores and cyanidation tailings using X-ray absorption spectroscopy. Geochim. Cosmochim. Acta 68 (5), 969–983.
Papanikolaou, N.C., Hatzidaki, E.G., Belivanis, S., Tzanakakis, G.N., Tsatsakis, A.M., 2005. Lead toxicity update. A brief review. Med. Sci. Monit. 11 (10), RA329–RA336.
Qi, Y., Donahoe, R.J., 2009. Modeling arsenic desorption from herbicide-contaminated soils. Environ. Toxicol. Chem. 28 (6), 1338–1345.
Salazar-Camacho, C., Villalobos, M., 2010. Goethite surface reactivity: iii. Unifying arsenate adsorption behavior through a variable crystal face — site density model. Geochim. Cosmochim. Acta 74 (8), 2257–2280.
Slowey, A.J., Johnson, S.B., Newville, M., Brown, G.E., 2007. Speciation and colloid transport of arsenic from mine tailings. Appl. Geochem. 22 (9), 1884–1898.
Smedley, P.L., Kinniburgh, D.G., 2002. A review of the source, behaviour and distribution of arsenic in natural waters. Appl. Geochem. 17 (5), 517–568.
Stevens, J., Lubitz, L., 1998. Symptomatic zinc deficiency in breast-fed term and premature infants. J. Paediatr. Child Health 34 (1), 97–100.
Stuben, D., Berner, Z., Kappes, B., Puchelt, H., 2001. Environmental monitoring of heavy metals and arsenic from Ag–Pb–Zn mining. A case study over two millennia. Environ. Monit. Assess. 70 (1–2), 181–200.
Tangahu, B.V., et al., 2013. Phytotoxicity of wastewater containing lead (Pb) effects *Scirpus grossus*. Int. J. Phytoremediation 15 (8), 814–826.

Togashi, S., et al., 2000. Young upper crustal chemical composition of the orogenic Japan Arc. Geochem. Geophys. Geosyst. 1.
Vaca-Escobar, K., Villalobos, M., Ceniceros-Gomez, A.E., 2012. Natural arsenic attenuation via metal arsenate precipitation in soils contaminated with metallurgical wastes: iii. Adsorption versus precipitation in clean As(V)/goethite/Pb(II)/carbonate systems. Appl. Geochem. 27 (11), 2251–2259.
Vaughan, D.J., 2006. Arsenic. Elements 2 (2), 71–75.
Villacís-García, M., Ugalde-Arzate, M., Vaca-Escobar, K., Villalobos, M., Zanella, R., Martínez-Villegas, N., 2015. Laboratory synthesis of goethite and ferrihydrite of controlled particle sizes. Bol. Soc. Geol. Mex. (in press).
Villalobos, M., Perez-Gallegos, A., 2008. Goethite surface reactivity: a macroscopic investigation unifying proton, chromate, carbonate, and lead(II) adsorption. J. Colloid Interface Sci. 326 (2), 307–323.
Villalobos, M., Cheney, M.A., Alcaraz-Cienfuegos, J., 2009. Goethite surface reactivity: II. A microscopic site-density model that describes its surface area-normalized variability. J. Colloid Interface Sci. 336 (2), 412–422.
Villalobos, M., Garcia-Payne, D.G., Lopez-Zepeda, J.L., Ceniceros-Gomez, A.E., Gutierrez-Ruiz, M.E., 2010. Natural arsenic attenuation via metal arsenate precipitation in soils contaminated with metallurgical wastes: i. Wet chemical and thermodynamic evidences. Aquat. Geochem. 16 (2), 225–250.
Wang, Z., Giammar, D.E., 2013. Mass action expressions for bidentate adsorption in surface complexation modeling: theory and practice. Environ. Sci. Technol. 47, 3982–3996.

México, D.F., 18 de Marzo, 2015

A QUIEN PUEDA INTERESAR

En mi calidad de editor en jefe del *Boletín de la Sociedad Geológica Mexicana*, me complace hacer constar que el manuscrito intitulado "*Modeling the additive effects of Pb(II) and Cu(II) on the competitive attenuation of As(V) through solid precipitation versus adsorption to goethite*", sometido por K. Vaca-Escobar y M. Villalobos ha sido aceptado para su publicación en el número de nuestra revista, "From micro to molecular scale investigations in geochemistry", tras su revisión por dos árbitros expertos independientes y un editor a cargo.

Saludos cordiales,

Dr. Antoni Camprubí
Editor en Jefe, Boletín de la Sociedad Geológica Mexicana

Modeling the additive effects of Pb(II) and Cu(II) on the competitive attenuation of As(V) through solid precipitation versus adsorption to goethite

Katherine Vaca-Escobar,† and Mario Villalobos*††

† Earth Sciences Graduate Program, ††Environmental Bio-Geochemistry Group, Geology Institute, Universidad Nacional Autónoma de México (UNAM), Coyoacán, Ciudad Universitaria, México 04510, D.F.

* Address correspondence: Tel: (52-55)5622-4336; FAX: (52-55)5622-4352. E-mail address: mar.villa@stanfordalumni.org (M. Villalobos)

ABSTRACT

Mine-related activities cause widespread contamination of aqueous environments with high concentrations of arsenic in conjunction with heavy metals. The natural attenuation of As(V) in soils and groundwater under oxic conditions occurs mainly through sorption processes to iron and aluminum (hydr)oxides; as well as through the formation of highly insoluble heavy metal(II) arsenates.

In the present investigation we used thermodynamic modeling to predict the environmental geochemical behavior of As(V) in the presence of Pb(II), Cu(II) and goethite, in an effort to approach the complexity of multi-component real contaminated scenarios. The key to this modeling was the coupling of a highly robust Surface Complexation Model of As(V) adsorption to goethite, which uses combined tenets of the Triple-Layer and CD-MUSIC models, together with appropriate metal(II) arsenate solid formation constants as well as those of all chemical equilibria taking place in the aqueous phase. Mixed-metal arsenates were predicted to form and increase the predominance region of the precipitation reactions for a highly surface reactive goethite, at the expense of the adsorption mechanism, but the model yielded no aqueous As(V) released at any condition investigated.

KEYWORDS: Adsorption, precipitation, arsenate, goethite, lead, copper, Surface Complexation Model, Triple-Layer Model, CD-MUSIC Model.

RESUMEN

Las actividades relacionadas con la minería provocan contaminación extendida de ambientes acuosos conjuntamente de arsénico y metales pesados. La atenuación natural de As(V) en suelos y acuíferos en condiciones óxicas ocurre principalmente a través de procesos de adsorción a (hidr)óxidos de hierro y aluminio; así como a través de la formación de arseniatos de metales(II) pesados altamente insolubles.

En esta investigación utilizamos modelación termodinámica para predecir el comportamiento geoquímico ambiental del As(V) en presencia de Pb(II), Cu(II) y goetita, tratando de aproximarnos a la complejidad de escenarios multicomponentes de contaminación real. La clave de esta modelación fue el acoplamiento de un modelo de complejación superficial altamente robusto de adsorción de As(V) en goetita, el cual utiliza postulados combinados de los modelos de Triple Capa y CD-MUSIC, junto con constantes apropiadas de formación de arseniatos de metales divalentes sólidos y de todos los equilibrios químicos que ocurren en la fase acuosa. Se predice la formación de arseniatos metálicos mixtos que aumentan la región de predominio de las reacciones de precipitación, a expensas del mecanismo de adsorción en goetitas de alta reactividad superficial, pero el modelo predice que no se libera As(V) acuoso en ninguna de las condiciones investigadas.

PALABRAS CLAVE: Adsorción, precipitación, arseniato, goetita, plomo, cobre, Modelo de Complejación Superficial, Modelo de Triple Capa, Modelo CD-MUSIC.

1. Introduction

63 Arsenic is a metalloid that is a constituent of more than 245 minerals, and is associated most
64 frequently to other metals such as copper, gold, lead, and zinc in sulfidic ores (Cullen and
65 Reimer, 1989; Oremland and Stolz, 2003; Shen *et al.*, 2013). Many sources of arsenic
66 contamination result from human activities such as the disposal of industrial chemical wastes,
67 including mine wastes, the smelting of arsenic-bearing minerals, the burning of fossil fuels and
68 the application of arsenic compounds in many products, especially in the past few hundred years
69 (Garelick *et al.*, 2008; Chang *et al.*, 2009; Mirza *et al.*, 2014). For example, arsenic
70 concentrations measured in soils near a lead smelter were in average 2 g/kg, near a copper
71 smelter 0.55 g/kg, and near a gold smelter from 0.5 to 9.3 g/kg (Bissen and Frimmel, 2003).

72 The reduction of arsenic levels in contaminated drinking water and soils is one of the priority
73 environmental challenges worldwide (Thirunavkukkarasu *et al.*, 2002). In Mexico, arsenic
74 contamination problems in water and soils have been reported in the following regions: Villa La
75 Paz, San Luis Potosí, (Gamiño-Gutiérrez *et al.*, 2013); Matehuala, San Luis Potosí (Martínez-
76 Villegas *et al.*, 2013); Comarca Lagunera in the NW of Mexico (Ordáz *et al.*, 2013); Zimapán,
77 Hidalgo (Romero *et al.*, 2008); Guanajuato (Arroyo *et al.*, 2013); and Zacatecas and Guadalupe,
78 Zacatecas (Mireles *et al.*, 2012). To reduce arsenic contamination, it is of utmost importance to
79 understand all aspects of arsenic environmental geochemistry, which in turn will provide useful
80 information to optimize treatment and remediation schemes for contaminated environments.

81 The reactivity of Arsenate [As(V)] with individual soil minerals determines the general mobility
82 of arsenic in soils. As(V) is the predominant inorganic species of arsenic under oxidizing soil
83 conditions (Goldberg, 2011; Camacho *et al.*, 2011), and is retained in soils by adsorption
84 processes (Smith and Naidu, 2009; Goldberg and Glaubig, 1988). Important minerals that control
85 the As(V) adsorption capacity of soils include Fe and Al oxides, such as goethite, ferrihydrite,

86 gibbsite, etc (Violante *et al.*, 2010; Smedley and Kinniburgh, 2013). However, there is evidence
87 that in situations where the metal contents that accompany As(V) are high (as in smelting, mining
88 and metallurgical wastes), formation of (highly insoluble) heavy metal arsenates occurs, such as
89 duftite, mimetite, hydroxymimetite and bayldonite; making precipitation the predominant
90 immobilization mechanism, over the adsorption process (Gutierrez-Ruiz *et al.*, 2005; Villalobos
91 *et al.*, 2010; Drahota and Filippi, 2009; Vaca-Escobar *et al.*, 2012). For example, Villalobos *et al.*
92 (2010) reported various As-contaminated soils with pH values between 4.5 and 10.2, As/Fe molar
93 ratios of 0.03–2.5, As/Pb molar ratios of 0.53–300, and As/Cu molar ratios of 0.44 – 32, in which
94 the presence of mixed heavy metal arsenates was identified.

95 In the present research, we use thermodynamic modeling to investigate the environmental
96 geochemical conditions of arsenate mobility in aqueous environments, focusing on the
97 competition between formation of Pb and Cu arsenates and adsorption mechanisms to an Fe
98 oxide. We chose goethite because it is thermodynamically one of the most stable iron oxides in
99 the environment (Schwertmann and Cornell, 2007), and therefore it is well characterized and the
100 subject of many studies on surface complexation modeling (Hayes et al., 1991; Mathur and
101 Dzombak, 2006). We build from our previous research with Pb(II)-only arsenate/goethite
102 systems, in a "bottom-up" approach to progressively describe more complex systems in a
103 quantitative manner, particularly those with various heavy metals present simultaneously (Vaca-
104 Escobar *et al.*, 2012). In this previous work we found that As(V) adsorption is favored at low
105 As/Fe molar ratios (less than 0.021) or high As/Pb molar ratios (above 0.667), but also, with
106 highly reactive goethites of large particle sizes. In opposite conditions, Pb(II) precipitation
107 becomes the more competitive immobilizing mechanism (Vaca-Escobar *et al.*, 2012).

The main question asked here is whether the simultaneous presence of Cu(II) with Pb(II) promotes a higher predominance region of precipitated metal arsenates versus As(V) adsorption to goethite, and to what extent does this occur. Also, in conditions that favor precipitation, how prevalent are the mixed Pb(II)-Cu(II) arsenates in comparison with the single Pb(II) or Cu(II) arsenates.

2. Materials and methods

2.1. Thermodynamic modeling

The arsenic species distribution was calculated by thermodynamic modeling using the Visual Minteq geochemical equilibrium and speciation interface, version 3.0 (Gustafsson, 2010). This program was updated with surface complexation constants for goethite reported by Salazar-Camacho and Villalobos (2010), who used combined tenets of the Triple-Layer and CD-MUSIC surface complexation models (SCMs) to describe in a unified manner the adsorption behavior of goethite, irrespective of its specific surface area (SSA), by defining the adsorption reactions per type of reactive site on the goethite surface. The two goethites for which the unified model has been calibrated are a 50 $m^2 g^{-1}$ (GOE50) and a 94 $m^2 g^{-1}$ (GOE94) goethites) (Salazar-Camacho and Villalobos, 2010). The latter corresponds to small ideal goethite crystals, and the former to larger particles that show higher reactivity per unit area.

Table 1 lists all surface complexation constants used, including their expressions and the corresponding formation reactions. Binary adsorption data for the unified goethite model were available for As(V) and Pb(II) (Salazar-Camacho and Villalobos, 2010), but not for Cu(II). Pb(II) shows a higher binding affinity for goethite (and other minerals) than Cu(II) (Christophi

130 and Axe, 2000). Therefore, we hypothesized that As(V) (Kingston et al., 1972) and Pb(II)
131 (Kooner, 1993) adsorption are sufficiently stronger than Cu(II) adsorption to goethite, that the
132 exclusion of the latter would not affect the modeling results. To test this hypothesis, we modeled
133 the Pb(II)/As(V)/goethite system in the presence and absence of the binary Pb(II) adsorption
134 reactions. We found no difference in the As(V) speciation results, but only when modeling the
135 more surface reactive GOE50. Therefore, we decided to perform the modeling for the complete
136 system including Cu(II) only with this GOE50, and for the moment to exclude GOE94 since we
137 could not ensure that the absence of Cu(II) surface binding constants would affect the results for
138 the latter.

139 To complete the SCM, other input parameters are required in addition to the surface
140 complexation constants, including the specific surface area ($50 m^2 g^{-1}$); the surface site density,
141 which is dependent on the specific crystal faces contributions exposed for the goethite sample
142 used (calculated from chromate adsorption maxima at pH 4 - 6.86 sites nm^{-2} for ≡FeOH, 2.87
143 sites nm^{-2} for $\equiv Fe_2OH$ and 1.12 sites nm^{-2} for $\equiv Fe_3OH$ groups, with a face distribution of 37% for
144 {101} and 63% for {010}) (Salazar-Camacho and Villalobos, 2010); two electrical capacitances
145 (C_1 = 1.17 F m^{-2} and C_2 = 0.20 F m^{-2}); a fixed GOE50 solids concentration (0.2 g L^{-1}); ionic
146 strength (I = 0.01 mol L^{-1} $NaNO_3$); $LogPCO_2$ = -3.5. Computations were performed by varying
147 the concentration of total As(V), essentially increasing the total As/Fe ratio.

148 The SCM was coupled to an aqueous and solid thermodynamic speciation model, for which the
149 corresponding available formation constants of all species are listed in Table 2. The complete
150 thermodynamic model applied was validated previously by wet chemical experimental results
151 which matched closely the model results for the As(V)/Pb(II)/goethite system (Vaca-Escobar *et*
152 *al.*, 2012). Therefore, we are confident that the model employed represents well the behavior of

153 the system when one additional component, i.e., Cu(II), is added, so no additional experimental
154 verification of the model results was performed..

155 For the As(V)/Pb(II)/Cu(II) system, two different ratios of total concentrations added were
156 chosen (1/1/1 and 2/1/3), to represent those of the two main mixed-metal arsenates that form:
157 duftite [$PbCu(AsO_4)(OH)$] and bayldonite [$PbCu_3(AsO_4)_2(OH)_2$].

158

159 **3. Results**

160 The first step was to determine the solid speciation expected as a function of pH in the absence of
161 adsorption processes, in order to gain knowledge of the metal(II) solids expected to compete for
162 As(V) binding with the goethite surface (Fig. 1). Table 3 summarizes the results by reporting the
163 expected solids and their stability pH range at the different As(V)-Cu(II)-Pb(II) molar ratios
164 studied.
165 After this, the complete model that includes adsorption onto goethite (GOE50) was applied, and
166 the sum of three main types of As(V) species predicted were plotted as percentage of the total
167 As(V) applied: adsorbed, precipitated, and dissolved species. This was done as a function of the
168 molar As/Fe ratio, to determine the species contributions as As(V) increased relative to goethite
169 (Figs. 2 and 3).

170

171 3.1 Simple As(V)-Pb(II) systems.

172 The As(V)/Pb(II) system was investigated previously and the mineral hydroxymimetite
173 [$Pb_5(AsO_4)_3OH$] was identified as the main solid forming in a pH range of 5 to 9 (Vaca-Escobar
174 *et al.*, 2012) (figure not shown).

175 When adsorption processes to GOE50 were included in the model, this retention mechanism
176 controlled As(V) speciation, and precipitation of hydroxymimetite did not occur until all surface
177 sites were saturated, in the As/Fe scale. This was in stark contrast to the behavior shown by
178 GOE94, in which precipitation of hydroximimetite occurred considerably before surface site
179 saturation with As(V) was attained, and quickly became the predominant mechanism as As/Fe
180 was further increased (Vaca-Escobar *et al.*, 2012).
181
182 3.2 Simple As(V)-Cu(II) systems.
183 The Cu(II) arsenate is predicted to precipitate in a very narrow pH range around 6, which is the
184 pH of minimal As(V) solubility, for As/Cu molar ratios of 1 (Fig. 1a) and 2/3 (Fig. 1b).
185 Therefore, pH 6 was one of the values chosen for further investigations in the complete system.
186 In the presence of goethite, adsorption of As(V) was not disrupted by the presence of Cu(II) (Fig.
187 2), and even after surface site saturation in the As/Fe scale, before the onset of the Cu(II) arsenate
188 precipitation, dissolved As(V) reached values above 40% at the maxima for both As/Cu ratios
189 investigated at pH 6. At an As(V)/Cu(II) molar ratio of 1 (Fig. 2a) the dissolved species
190 contribution stabilized at around 30%, while at the lower As(V)/Cu(II) molar ratio (2/3) the
191 dissolved species decreased to less than 10% at high As(V)/Fe(III) molar ratios (Fig. 2b), and
192 thus precipitation of the arsenate became highly predominant in this latter system. Therefore, in
193 comparison with the As(V)-Pb(II) systems, the As(V)-Cu(II) systems are predicted to be much
194 less efficient in removing aqueous As(V).
195
196 3.3 As(V)-Pb(II)-Cu(II) systems.
197 In the As(V) system where both metals are present a more complex precipitation behavior was
198 observed (Figs. 1c and d), in which several solids may coexist over wide pH intervals (Table 3).

199 For both As(V)/Pb(II)/Cu(II) molar ratios used in this research (1/1/1 and 2/1/3), pH 7 was
200 chosen for investigating the system in the presence of goethite because at this value they showed
201 the lowest As(V) solubility. At a 1/1/1 ratio the only solid predicted to form at pH 7 was duftite
202 [$PbCu(AsO_4)(OH)$] (Fig. 1c), while at the 2/1/3 ratio three simultaneous solids were predicted,
203 two of them being mixed-metal arsenates: duftite [$PbCu(AsO_4)(OH)$], and bayldonite
204 [$PbCu_3(AsO_4)_2(OH)_2$]. However, a much lower As(V) solubility was predicted in the former
205 case ($10^{-7.6}$ M – not shown in the scale of Fig. 1c), in comparison to the latter (10^{-6} M – Fig. 1d);
206 as well as a wider pH range of insolubility.

207 In the systems that include adsorption to GOE50, the first important difference observed from
208 those in the absence of Cu(II) is that the As/Fe region of predominance of the adsorption
209 mechanism was diminished, on account of an increase in the corresponding region of arsenate
210 precipitation. The As(V) insolubility behavior described above is well reflected here by showing
211 a larger decrease in the adsorbed species distribution for the system with an As/Pb/Cu molar ratio
212 of 1/1/1 (Fig. 3a), and the corresponding increase in the precipitation of duftite, as compared to
213 the system with a 2/1/3 ratio (Fig. 3b). It is interesting to note that the onset of precipitation
214 occurred at a very similar As/Fe ratio for both systems, but the former showed a considerably
215 steeper precipitation curve, such that the crossing point where adsorption and precipitated species
216 were equal appeared at a considerably lower As/Fe value (Fig. 3a) than for the 2/1/3 system (Fig.
217 3b) (0.019 for the 1/1/1 ratio and 0.027 for the 2/1/3 ratio).

218 In the 1/1/1 system at the As/Fe ratio of 0.01, at which site saturation occurs in the absence of
219 metals, adsorption decreased to approximately 70%; whereas in the 2/1/3 system the adsorption
220 decrease was small (*ca*. to 90%) at this As/Fe ratio, and the adsorption curve in general was close

221 to the one in the absence of metals. *et al.*Dissolved species did not appear in this system, because
222 As(V) species were distributed exclusively between adsorbed and precipitated.

223

224 **4. Discussion and conclusions**

225 Thermodynamic modeling is a powerful tool for predicting the behavior of complex multi-
226 component systems, in which adsorption and solid mineral precipitation occur as potential
227 attenuation processes. This is the case for As(V) in the presence of heavy metals (II) and goethite,
228 for which accurate geochemical modeling is possible when a robust adsorption model is
229 available.This research can be of great interest because we have not found other investigations
230 that combine adsorption and precipitation processes in compounded thermodynamic modeling to
231 predict As(V) behavior in soils, and to propose remediation methods.

232 Previously it was found that in the presence of Pb(II), As(V) may form very insoluble minerals
233 before it saturates the goethite surface, but only for an ideal goethite of small particle sizes. For
234 larger more surface-reactive goethites, the adsorption mechanism prevails, and precipitation does
235 not occur until all surface sites are occupied [except in the presence of chloride because of
236 mimetite formation, which is considerably more insoluble than other lead arsenates (Vaca-
237 Escobar et al., 2015)].

238 In the present work we investigated the behavior of As(V) when a second metal component
239 [Cu(II)] was added to the system, in an effort to approach the complexity of mine waste-
240 contaminated environments. A considerable decrease in the adsorption of As(V) to a large
241 goethite was found when the three components were added at a ratio of 1/1/1, in a similar fashion
242 to the decrease observed in the presence of Cl^- and in the absence of Cu(II), due to formation of

243 the extremely insoluble mimetite mineral (Vaca-Escobar et al., 2015). The adsorption decrease
244 in the presence of Cu(II) was caused by the precipitation of a mixed-metal arsenate called duftite:
245 $PbCu(AsO_4)(OH)$.

246 At an added ratio of 2/1/3 for As/Pb/Cu, corresponding to another mixed-metal arsenate,
247 bayldonite [$PbCu_3(AsO_4)_2(OH)_2$], a much lower effect on the adsorption of As(V) to goethite was
248 observed, despite the fact that both mixed Pb(II)-Cu(II) minerals are predicted to precipitate
249 simultaneously.

250 In the mixed-metal systems none of the existing single-metal arsenates were predicted to form, at
251 the two ratios investigated, and no aqueous As(V) appeared under any of the conditions
252 investigated. In this manner, the interplay between adsorption and precipitation, whether one
253 mechanism or the other prevails allows for an efficient attenuation of As(V) in aqueous systems
254 contaminated with As(V) and heavy metals Pb(II) and Cu(II).

255 Conversely, in the As(V)/Cu(II) system [i.e., without Pb(II) added], the Cu(II) arsenate solubility
256 was not low enough to affect the adsorption process, and in fact a considerable fraction of
257 aqueous As(V) appeared beginning from an As/Fe ratio of *ca*. 0.02. Therefore, it seems
258 advantageous from an environmental perspective that more than one metal(II) be present
259 simultaneously with As(V) in a contamination scenario to ensure their immobilization, in which
260 the formation of insoluble mixed-metal arsenates seems to be a predominant attenuation
261 mechanism. Given that mixed metal arsenates have been detected in contaminated soils, and that
262 in previous laboratory experiments less than 14 days were required to reach equilibrium for
263 Pb(II) arsenate solid formation, we believe no major kinetic impediments exist for the formation
264 of mixed metal arsenates in contaminated environments.

265 The results of this work are highly relevant for understanding the environmental geochemistry of
266 As(V) in aqueous environments, such as soils, with high contents of heavy metals, and for the
267 conceptual design of efficient remediation schemes of As-contaminated environments by
268 controlled addition of other heavy metal wastes in systems with a high As/Fe molar ratio.

269

270 **5. Acknowledgements**

271 This research was funded by the CONACyT through Project # CB-2010-01-153723. K. V.-E. is
272 grateful to CONACyT for the Ph.D. student fellowship received.

273

274 **6. References**

275

276 Arroyo, Y.R.R., Muñoz, A.H.S., Barrientos, E.Y., Huerta, I.R., Wrobel, K., Wrobel, K., 2013.
277 Natural Decrease of Dissolved Arsenic in a Small Stream Receiving Drainages of Abandoned
278 Silver Mines in Guanajuato, Mexico. Bulletin of environmental contamination and toxicology 91,
279 539-544.

280 Bissen, M., Frimmel, F.H., 2003. Arsenic — a Review. Part I: Occurrence, Toxicity, Speciation,
281 Mobility. Acta hydrochimica et hydrobiologica 31, 9-18.

282 Camacho, L.M., Gutiérrez, M., Alarcón-Herrera, M.T., Villalba, M.d.L., Deng, S., 2011.
283 Occurrence and treatment of arsenic in groundwater and soil in northern Mexico and
284 southwestern USA. Chemosphere 83, 211-225.

285 Cullen, W.R., Reimer, K.J., 1989. Arsenic speciation in the environment. Chemical Reviews 89,
286 713-764.

287 Chang, J.-S., Yoon, I.-H., Kim, K.-W., 2009. Heavy metal and arsenic accumulating fern species
288 as potential ecological indicators in As-contaminated abandoned mines. Ecological Indicators 9,
289 1275-1279.

290 Drahota, P., Filippi, M., 2009. Secondary arsenic minerals in the environment: a review.
291 Environment international 35, 1243-1255.

292 Gamiño-Gutiérrez, S., González-Pérez, C.I., Gonsebatt, M., Monroy-Fernández, M., 2013.
293 Arsenic and lead contamination in urban soils of Villa de la Paz (Mexico) affected by historical
294 mine wastes and its effect on children's health studied by micronucleated exfoliated cells assay.
295 Environmental Geochemistry and Health 35, 37-51.

296 Garelick, H., Jones, H., Dybowska, A., Valsami-Jones, E., 2008. Arsenic Pollution Sources,
297 Reviews of Environmental Contamination Volume 197. Springer New York, pp. 17-60.

298 Goldberg, S., 2011. Chemical Equilibrium and Reaction Modeling of Arsenic and Selenium in
299 Soils. Dynamics and Bioavailability of Heavy Metals in the Rootzone, 65.

300 Goldberg, S., Glaubig, R., 1988. Anion sorption on a calcareous, montmorillonitic soil—arsenic.
301 Soil Science Society of America Journal 52, 1297-1300.

302 Gustafsson, J.P., 2010. Visual MINTEQ. Ver. 3.0. A free equilibrium speciation model software.
303 VISUAL MINTEQ VER 3.

304 Gutierrez-Ruiz, M., Villalobos, M., Romero, F., Fernandez-Lomelin, P., 2005. Natural
305 attenuation of arsenic in semiarid soils contaminated by oxidized arsenic wastes, in: Oday, P.A.,

306 Vlassopoulos, D., Meng, Z., Benning, L.G. (Eds.), Advances in Arsenic Research: Integration of
307 Experimental and Observational Studies and Implications for Mitigation, pp. 235-252.

308 Hayes, K.F., Redden, G., Ela, W., Leckie, J.O., 1991. Surface complexation models: an
309 evaluation of model parameter estimation using FITEQL and oxide mineral titration data. Journal
310 of colloid and interface science 142, 448-469.

311 Kingston, F., Posner, A., Quirk, J.T., 1972. Anion adsorption by goethite and gibbsite. Journal of
312 Soil Science 23, 177-192.

313 Kooner, Z.S., 1993. Comparative study of adsorption behavior of copper, lead, and zinc onto
314 goethite in aqueous systems. Environmental Geology 21, 242-250.

315 Martínez-Villegas, N., Briones-Gallardo, R., Ramos-Leal, J.A., Avalos-Borja, M., Castañón-
316 Sandoval, A.D., Razo-Flores, E., Villalobos, M., 2013. Arsenic mobility controlled by solid
317 calcium arsenates: A case study in Mexico showcasing a potentially widespread environmental
318 problem. Environmental Pollution 176, 114-122.

319 Mathur, S., Dzombak, D., 2006. Surface complexation modeling: goethite. Interface Science and
320 Technology 11, 443-468.

321 Mireles, F., Davila, J.I., Pinedo, J.L., Reyes, E., Speakman, R.J., Glascock, M.D., 2012.
322 Assessing urban soil pollution in the cities of Zacatecas and Guadalupe, Mexico by instrumental
323 neutron activation analysis. Microchemical Journal 103, 158-164.

324 Mirza, N., Mahmood, Q., Maroof Shah, M., Pervez, A., Sultan, S., 2014. Plants as Useful
325 Vectors to Reduce Environmental Toxic Arsenic Content. The Scientific World Journal 2014, 11.

326 Ordáz, G.H., Castruita, M.A.S., Pico, L.C.Á.G., Nuncio, R.A.A., Hernández, M.F., Cervantes,
327 G.G., 2013. Comportamiento del arsénico en suelos de la región lagunera de Coahuila, México.
328 Terra Latinoamericana 31, 295-303.

329 Oremland, R.S., Stolz, J.F., 2003. The Ecology of Arsenic. Science 300, 939-944.

330 Romero, F.M., Villalobos, M., Aguirre, R., Gutierrez, M.E., 2008. Solid-phase control on lead
331 bioaccessibility in smelter-impacted soils. Archives of Environmental Contamination and
332 Toxicology 55, 566-575.

333 Salazar-Camacho, C., Villalobos, M., 2010. Goethite surface reactivity: III. Unifying arsenate
334 adsorption behavior through a variable crystal face - Site density model. Geochimica Et
335 Cosmochimica Acta 74, 2257-2280.

336 Schwertmann, U., Cornell, R.M., 2007. The Iron Oxides, Iron Oxides in the Laboratory. Wiley-
337 VCH Verlag GmbH, pp. 5-18.

338 Shen, S., Li, X.-F., Cullen, W.R., Weinfeld, M., Le, X.C., 2013. Arsenic Binding to Proteins.
339 Chemical Reviews 113, 7769-7792.

340 Smedley, P.L., Kinniburgh, D., 2013. Arsenic in Groundwater and the Environment, in: Selinus,
341 O. (Ed.), Essentials of Medical Geology. Springer Netherlands, pp. 279-310.

342 Smith, E., Naidu, R., 2009. Chemistry of inorganic arsenic in soils: kinetics of arsenic
343 adsorption–desorption. Environmental geochemistry and health 31, 49-59.

344 Thirunavkukkarasu, O.S., Viraraghavan, T., Subramanian, K.S., Tanjore, S., 2002. Organic
345 arsenic removal from drinking water. Urban Water 4, 7.

346 Vaca-Escobar, K., Villalobos, M., Ceniceros-Gomez, A.E., 2012. Natural arsenic attenuation via
347 metal arsenate precipitation in soils contaminated with metallurgical wastes: III. Adsorption
348 versus precipitation in clean As(V)/goethite/Pb(II)/carbonate systems. Applied Geochemistry 27,
349 2251-2259.

350 Vaca-Escobar, K., Villalobos, M., Pi-i-Puig, T., Zanella, R. (2015) Approaching the geochemical
351 complexity of As(V)-contaminated scenarios through thermodynamic modeling. Accepted for
352 publication in Chemical Geology.

353 Villalobos, M., Cheney, M.A., Alcaraz-Cienfuegos, J., 2009. Goethite surface reactivity: II. A
354 microscopic site-density model that describes its surface area-normalized variability. Journal of
355 Colloid and Interface Science 336, 412-422.

356 Villalobos, M., Garcia-Payne, D.G., Lopez-Zepeda, J.L., Ceniceros-Gomez, A.E., Gutierrez-
357 Ruiz, M.E., 2010. Natural Arsenic Attenuation via Metal Arsenate Precipitation in Soils
358 Contaminated with Metallurgical Wastes: I. Wet Chemical and Thermodynamic Evidences.
359 Aquatic Geochemistry 16, 225-250.

360 Violante, A., Cozzolino, V., Perelomov, L., Caporale, A.G., Pigna, M., 2010. Mobility and
361 bioavailability of heavy metals and metalloids in soil environments. Journal of soil science and
362 plant nutrition 10, 268-292.

363
364
365
366
367

368 **Figure Captions**

369

370 **Fig. 1.** Saturation indices of As-Cu-Pb solids in the absence of goethite, for a system composed
371 of **a)** $[AsO_4^{3-}] = 1x10^{-4}$ M, $[Cu^{2+}] = 1x10^{-4}$ M (As/Cu=1/1); **b)** $[AsO_4^{3-}] = 2x10^{-4}$ M, $[Cu^{2+}] =$
372 $3x10^{-4}$ M (As/Cu=2/3); **c)** $[AsO_4^{3-}] = 1x10^{-4}$ M, $[Cu^{2+}] = 1x10^{-4}$ M, $[Pb^{2+}] = 1x10^{-4}$ M
373 (As/Pb/Cu=1/1/1); and **d)** $[AsO_4^{3-}] = 2x10^{-4}$ M, $[Cu^{2+}] = 3x10^{-4}$ M, $[Pb^{2+}] = 1x10^{-4}$ M
374 (As/Pb/Cu=2/1/3). All systems have I = 0.01 M $NaNO_3$. Chemical formulas of solid minerals
375 shown are listed in table 2.

376

377 **Fig. 2** As(V) species distribution in the presence of Cu(II) and goethite (GOE50) at pH 6 and I =
378 0.01M $NaNO_3$ **a)** As/Cu molar ratio = 1, and **b)** As/Cu molar ratio = 2/3.

379

380 **Fig. 3** As(V) species distribution in the presence of Pb(II), Cu(II), and goethite (GOE50) at pH 7
381 and I = 0.01M $NaNO_3$ **a)** As/Pb/Cu molar ratio = 1/1/1, and **b)** As/Pb/Cu molar ratio = 2/1/3.

382

a)

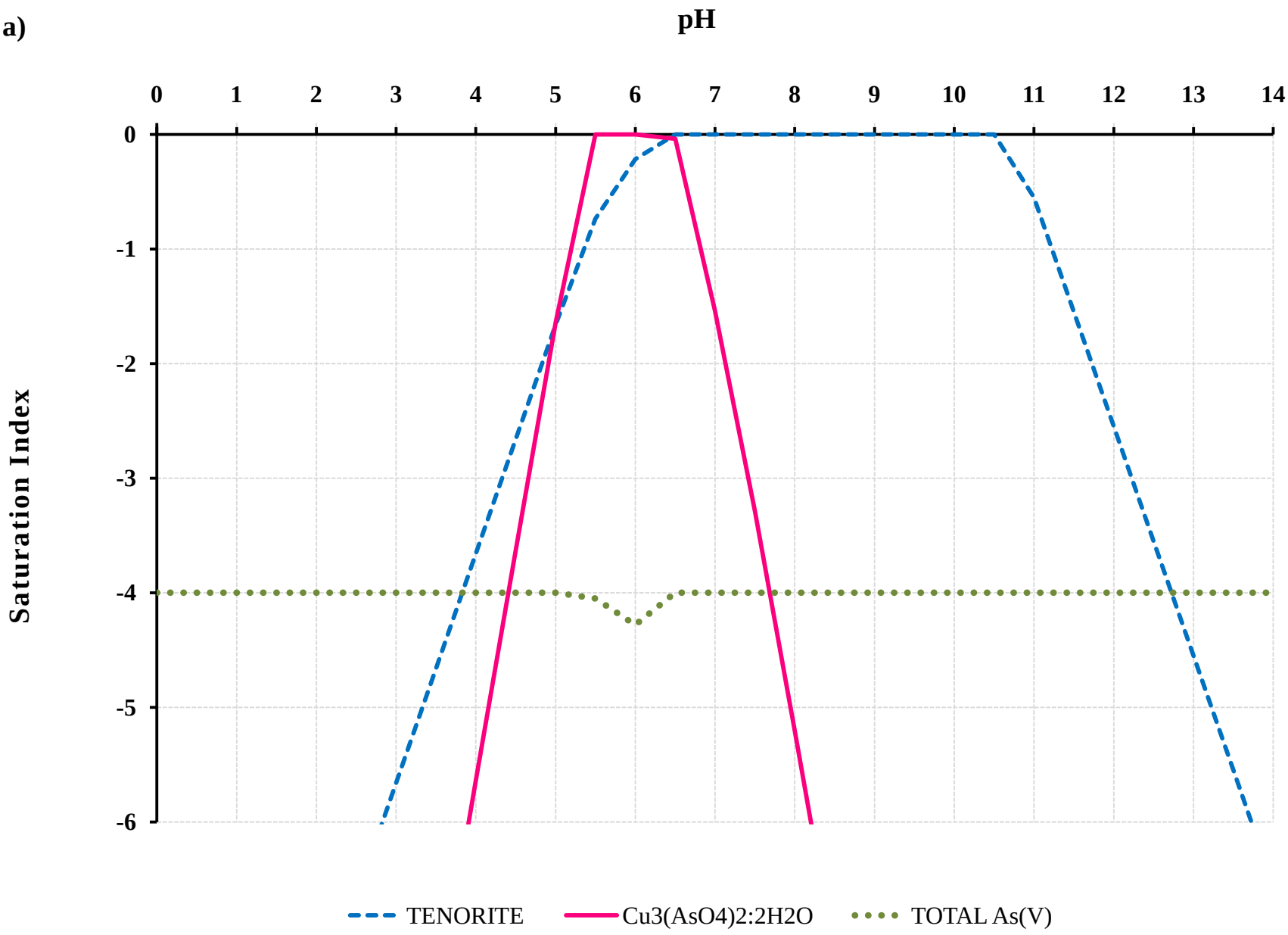
pH
0
1
2
3
4
5
6
7
8
9
10
11
12
13
14
Saturation Index
0
-1
-2
-3
-4
-5
-6
TENORITE
Cu3(AsO4)2:2H2O
TOTAL As(V)

b)

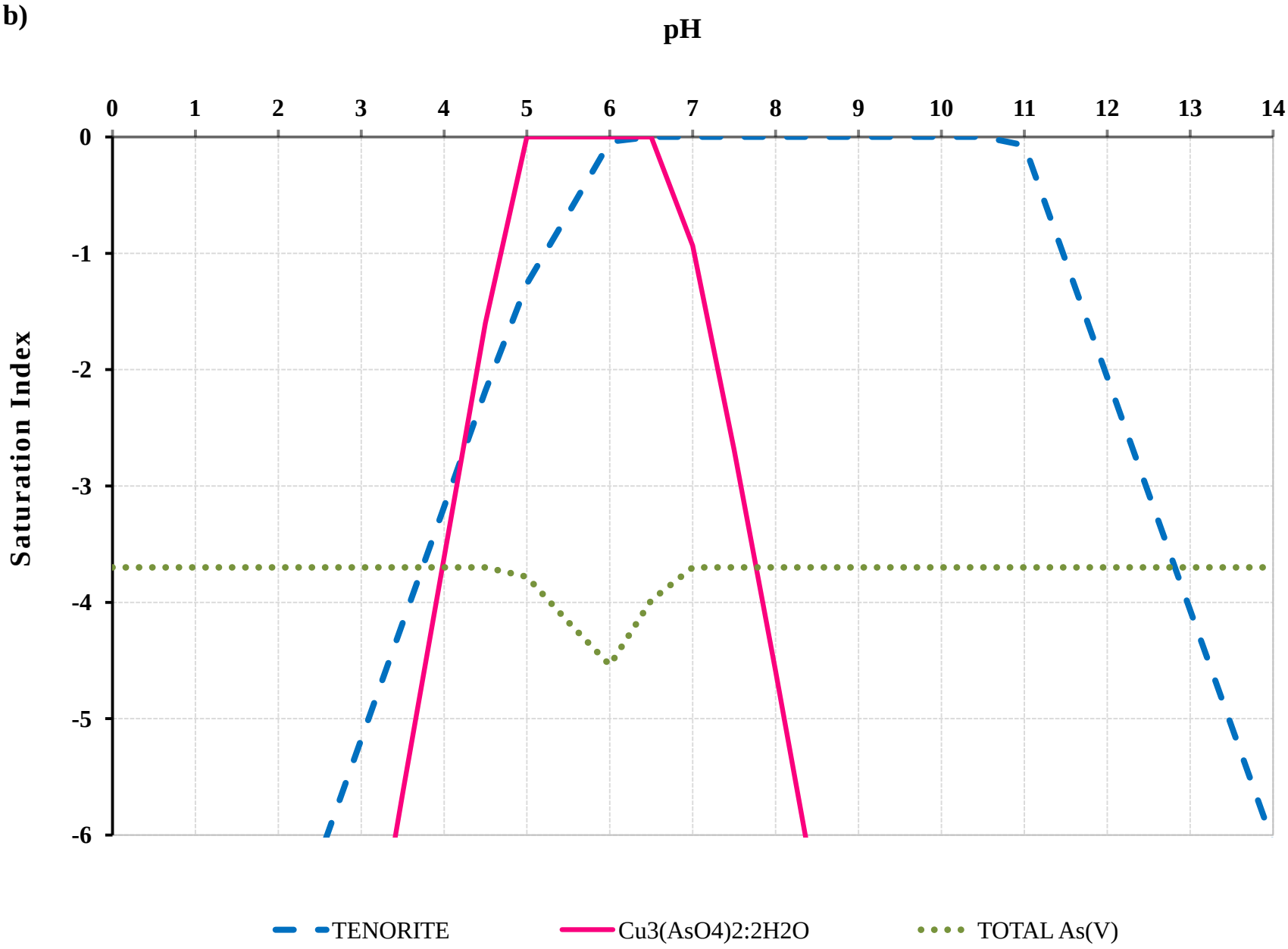
pH
0
1
2
3
4
5
6
7
8
9
10
11
12
13
14
Saturation Index
0
-1
-2
-3
-4
-5
-6
TENORITE
Cu3(AsO4)2:2H2O
TOTAL As(V)

c)

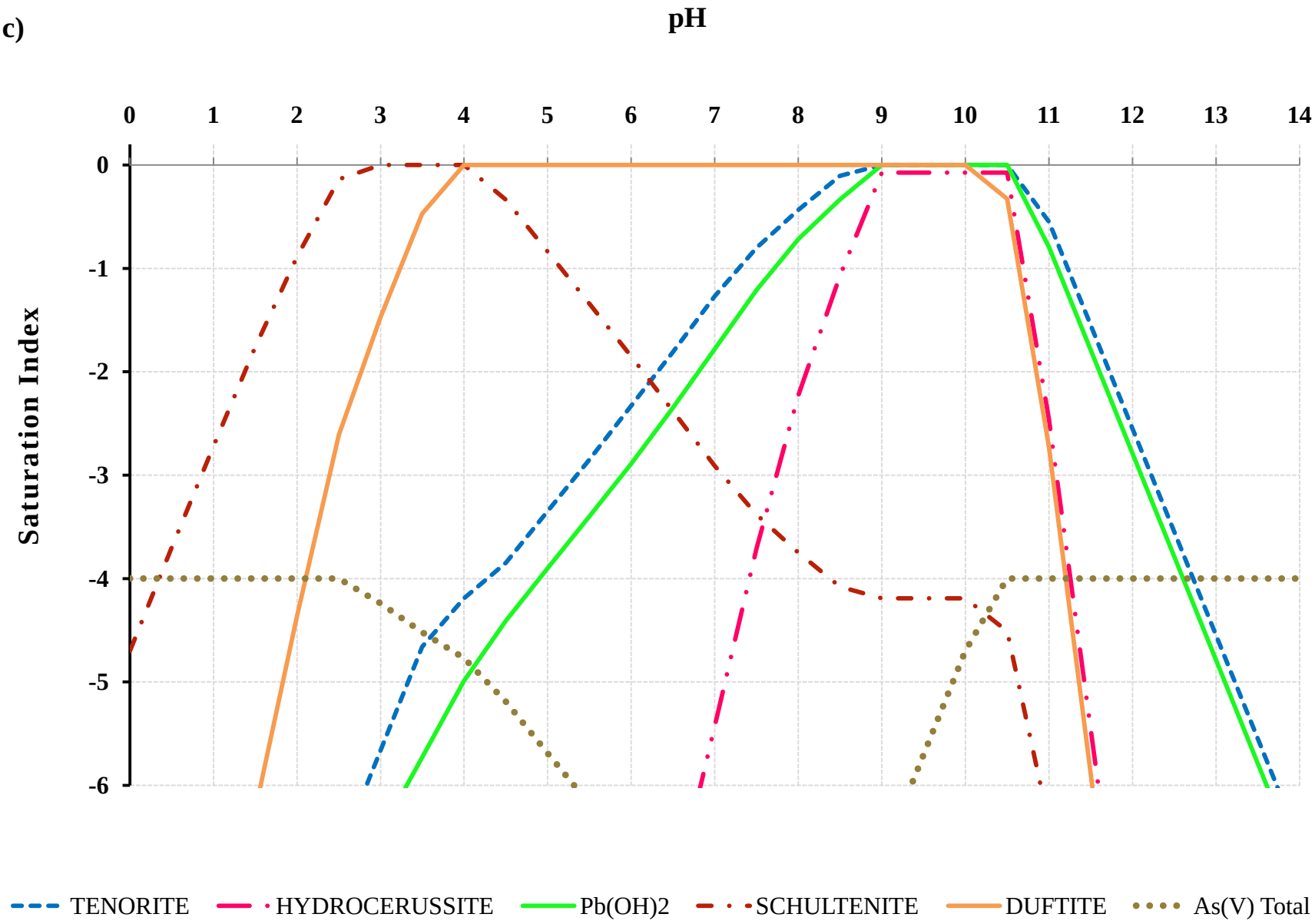
pH
0
1
2
3
4
5
6
7
8
9
10
11
12
13
14
Saturation Index
0
-1
-2
-3
-4
-5
-6
TENORITE
HYDROCERUSSITE
Pb(OH)2
SCHULTENITE
DUFTITE
As(V) Total

d)

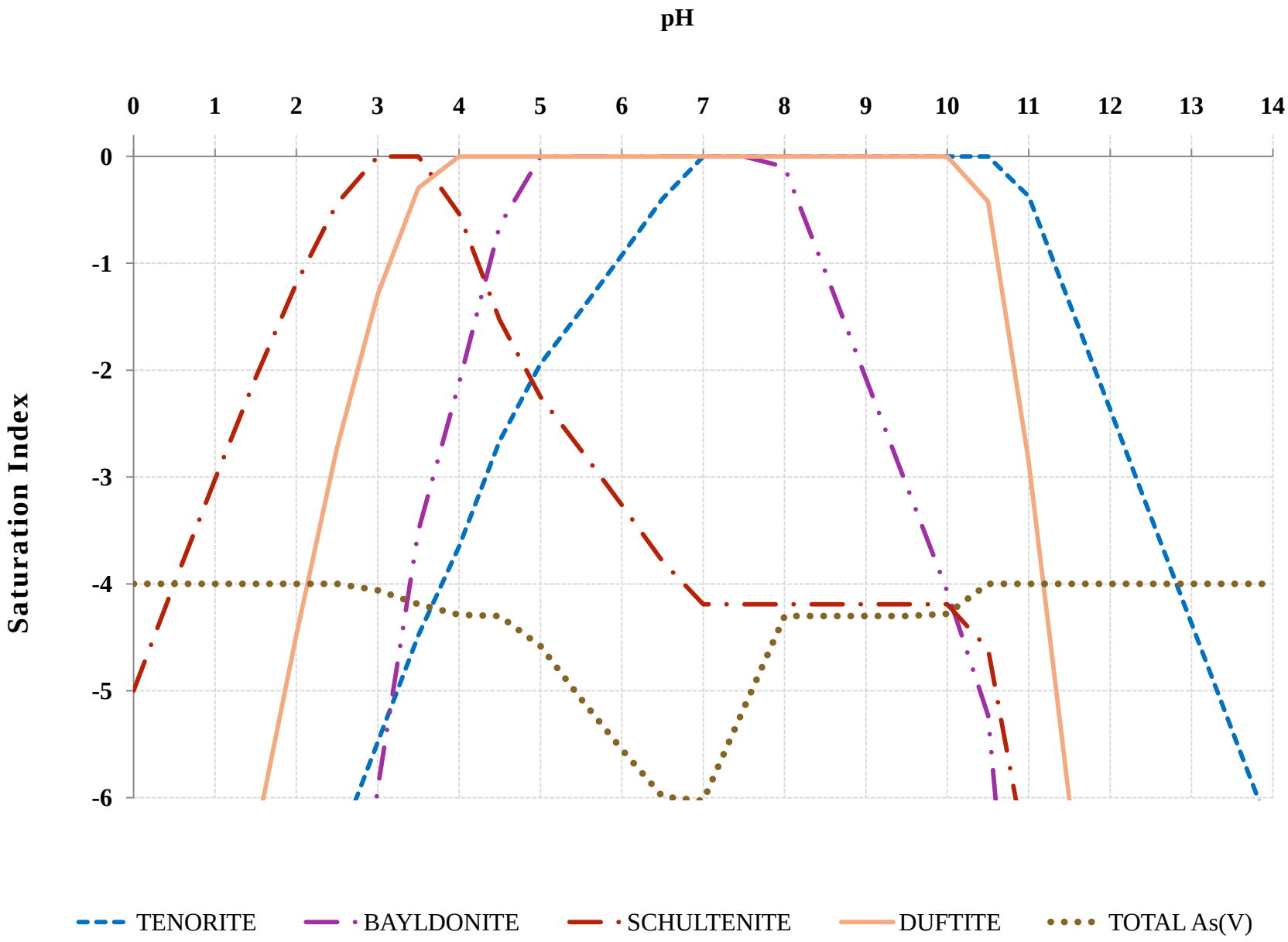
pH
0 1 2 3 4 5 6 7 8 9 10 11 12 13 14
Saturation Index
0 -1 -2 -3 -4 -5 -6
TENORITE
BAYLDONITE
SCHULTENITE
DUFTITE
TOTAL As(V)

a)

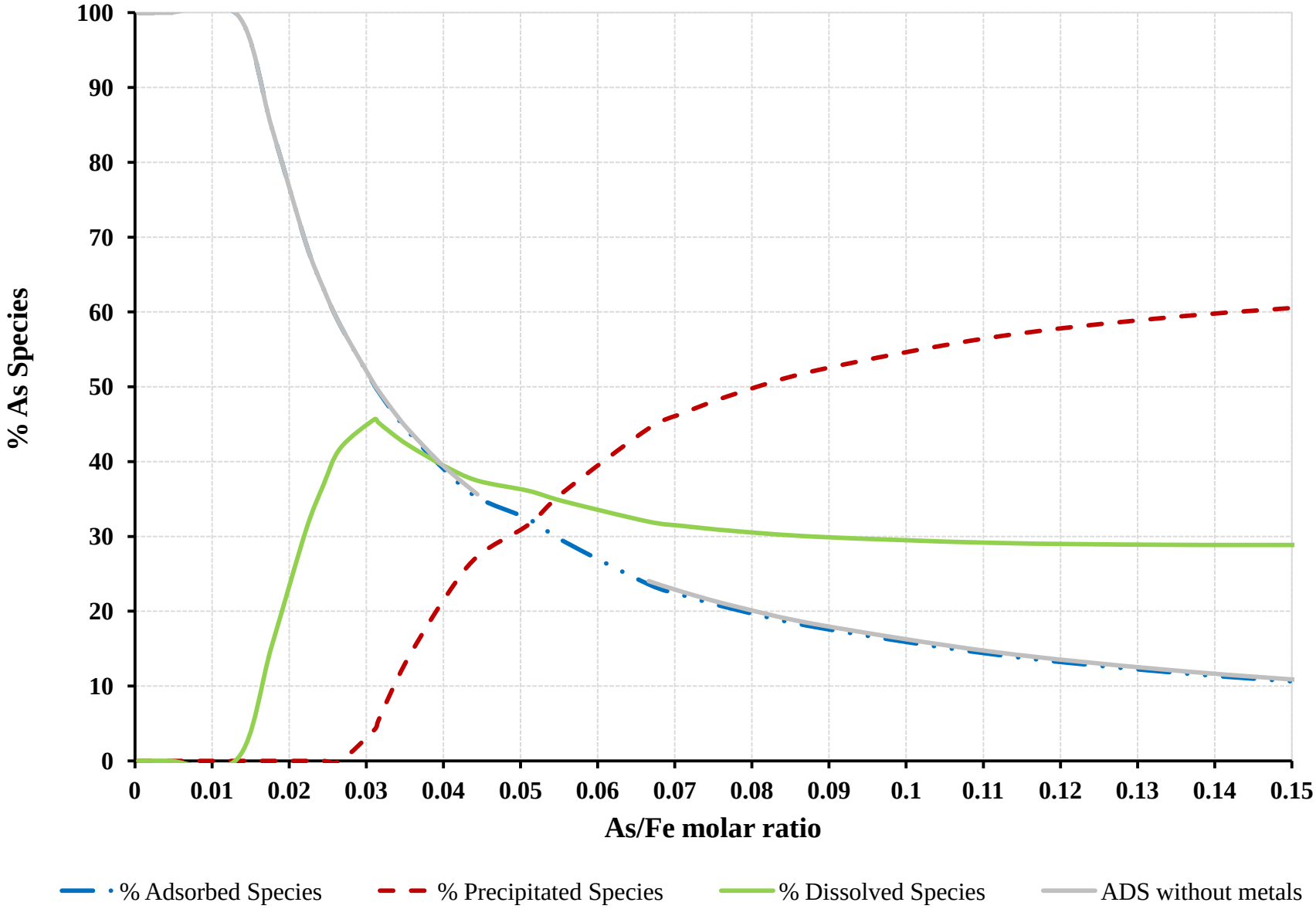
100
90
80
70
60
50
40
30
20
10
0
% As Species
0
0.01
0.02
0.03
0.04
0.05
0.06
0.07
0.08
0.09
0.1
0.11
0.12
0.13
0.14
0.15
As/Fe molar ratio
% Adsorbed Species
% Precipitated Species
% Dissolved Species
ADS without metals

b)

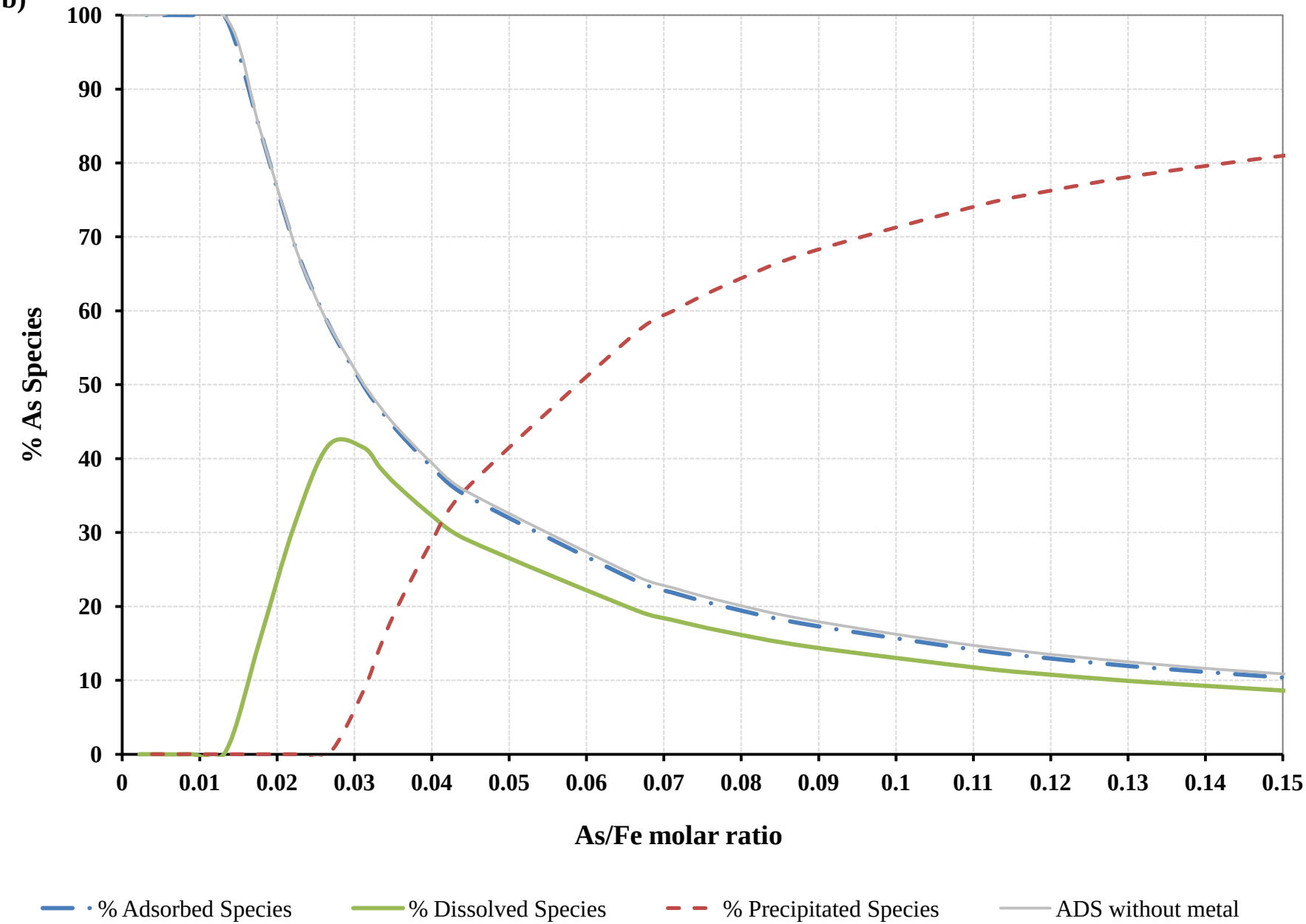
100
90
80
70
60
50
40
30
20
10
0
% As Species
0
0.01
0.02
0.03
0.04
0.05
0.06
0.07
0.08
0.09
0.1
0.11
0.12
0.13
0.14
0.15
As/Fe molar ratio
% Adsorbed Species
% Dissolved Species
% Precipitated Species
ADS without metal

a)

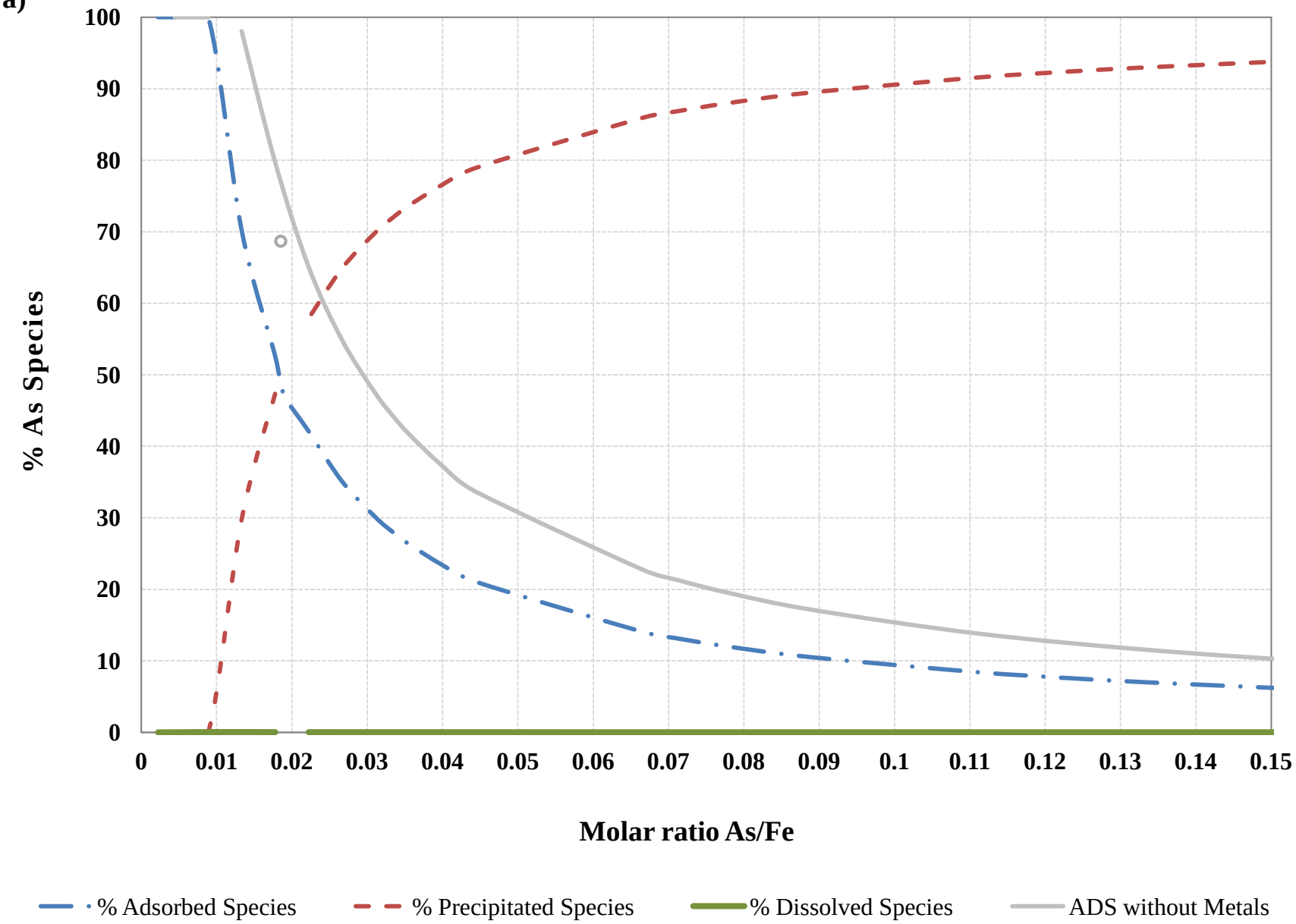
100
90
80
70
60
50
40
30
20
10
0
% As Species
0
0.01
0.02
0.03
0.04
0.05
0.06
0.07
0.08
0.09
0.1
0.11
0.12
0.13
0.14
0.15
Molar ratio As/Fe
% Adsorbed Species
% Precipitated Species
% Dissolved Species
ADS without Metals

b)

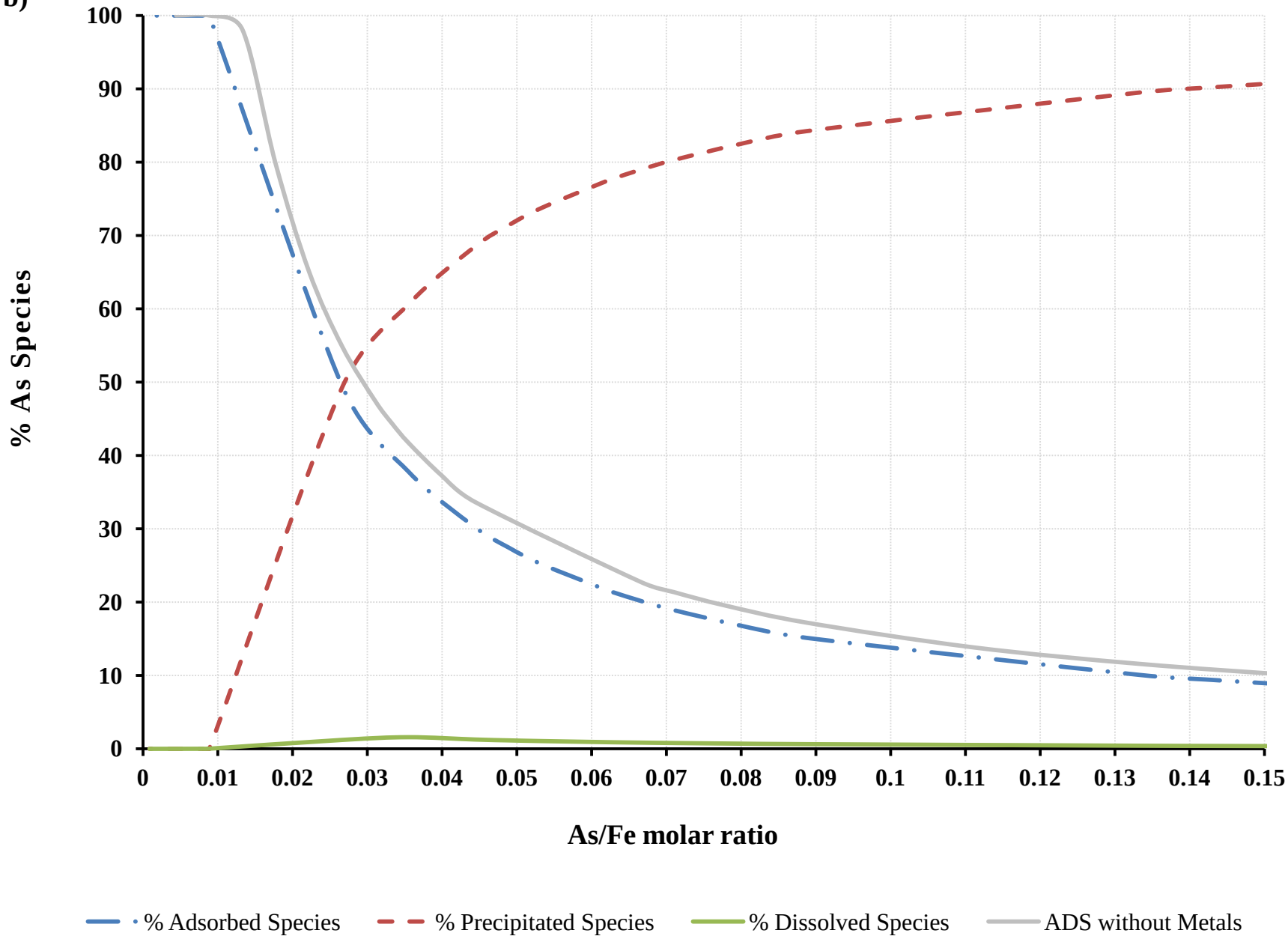
100
90
80
70
60
50
40
30
20
10
0
% As Species
0
0.01
0.02
0.03
0.04
0.05
0.06
0.07
0.08
0.09
0.1
0.11
0.12
0.13
0.14
0.15
As/Fe molar ratio
% Adsorbed Species
% Precipitated Species
% Dissolved Species
ADS without Metals

Tables

Table 1. Surface complexation reactions uploaded in Visual Minteq with formation constants described per type of surface site (Vaca-Escobar et al., 2012; Villalobos et al., 2009).

REACTIONS [a]	***Log K*** [b]		
Acid-base [c]***:***	***FeOH***	***Fe_2OH***	***Fe_3OH***
$SOH + H^+ \rightleftharpoons SOH_2^+$	6.8	nr	7.66
$SOH \rightleftharpoons SO^- + H^+$	-10.8	nr	-11.66
Electrolytes complexation (outer-sphere):			
$SOH + H^+ + NO_3^- \rightleftharpoons SO_2^{+\cdots}NO_3^-$	8.02	nr	9.025
$SOH + Na^+ \rightleftharpoons SO^{-\cdots}Na^+ + H^+$	-9.43	nr	-11.095
Inner-sphere complexation:			
$SOH + Pb^{2+} \rightleftharpoons SOPb^+ + H^+$	0.64	nr	nr
$FeOH + SOH + H^+ + AsO_4^{3-} \rightleftharpoons FeO^{-0.7}AsO_3^{-1.3\cdots}HSO + H_2O$	21.6	18.75	nr
$FeOH + SOH + 2H^+ + AsO_4^{3-} \rightleftharpoons FeO^{-0.7}AsO_3H^{-0.3\cdots}HOS + H_2O$	nr	19.6	nr
$SOH + H^+ + CO_3^{2-} \rightleftharpoons SO^{-0.2}CO_2^{-0.8} + H_2O$	13.55	13.32	nr
Outer-sphere complexation:			
$SOH + Pb^{2+} + H_2O \rightleftharpoons SO^{-\cdots}PbOH^+ + 2H^+$	-10.1	-8.6	nr

[a] SOH can be FeOH, Fe_2OH or Fe_3OH groups. As(V) surface complexation constants were taken from (Salazar-Camacho and Villalobos, 2010), and those for Pb(II) from (Villalobos et al., 2009).
[b] nr = non-reactive group.
[c] The log of acidity constants used was established through a ΔpKa of 4 around each pH of PZNPC for each site type, which were 8.8 and 9.66, for FeOH and Fe_3OH groups, respectively.

Table 2. Solid and aqueous species formation constants from their components, used in the thermodynamic model (Taken from Visual Minteq Database).

Mineral Name	Chemical Formula	Log K_f
SOLID SPECIES		
Hydroxymimetite	$Pb_5(AsO_4)_3OH$	62.115 [a]
Plumbonacrite	$Pb_{10}(OH)_6O(CO_3)_6$	8.760
Schultenite	$PbHAsO_4$	23.969 [a]
Hydrocerrusite	$Pb_3(OH)_2(CO_3)_2$	18.77
Cerrusite	$PbCO_3$	13.13
Shannonite	Pb_2OCO_3	0.558
Massicot	PbO	-12.894
Litharge	PbO	-12.694
Natron	$Na_2CO_3.10H_2O$	1.311
Thermonatrite	$Na_2CO_3.H_2O$	-0.637
Azurite	$Cu_3(CO_3)_2(OH)_2$	16.906
Malachite	$Cu_2(CO_3)(OH)_2$	5.306
Tenorite (c)	CuO	-7.644
Tenorite (am)	CuO	-8.49
Bayldonite	$PbCu_3(AsO_4)_2(OH)_2$	37.050
Duftite	$PbCu(AsO_4)(OH)$	20.512
	$CuCO_3$	11.50
	$Cu_3(AsO_4)_2.H_2O$	35.119
	$Cu(OH)_2$	-8.674
	$Pb_3O_2CO_3$	-11.02
	PbO	-8.15
	$Pb_2O(OH)_2$	-26.188
	$Pb(OH)_2$	-8.15
	$PbO.0.3H_2O$	-12.98
	As_2O_5	34.694

Continued on next page

AQUEOUS SPECIES

$Cu_2(OH)_2^{2+}$	-10.494
$Cu(CO_3)_2^{2-}$	10.20
$Cu(NO_3)_2$	-0.40
$Cu(OH)_2$	-16.23
$Cu(OH)_3^-$	-26.64
$Cu(OH)_4^{2-}$	-39.73
Cu_2OH^{3+}	-6.71
$Cu_3(OH)_4^{2+}$	-20.788
$CuCO_3$	6.77
$CuHCO_3^+$	12.129
$CuNO_3^+$	0.50
$CuOH^+$	-7.497
$NaNO_3$	-0.55
NaOH	-13.897
OH^-	-13.997
$HAsO_4^{2-}$	11.6
$H_2AsO_4^-$	18.35
H_3AsO_4	20.6
$PbH_2AsO_4^+$	19.736 [a]
$PbHAsO_4$	14.038 [a]
$Pb(OH)_2$	-17.897
$Pb(NO_3)_2$	1.4
$PbNO_3^+$	1.17
$PbOH^+$	-7.597
$Pb_4(OH)_4^{4+}$	-19.988
$Pb_2(OH)^{3+}$	-6.397
$Pb(OH)_3^-$	-28.091
$Pb(OH)_4^{2-}$	-39.699
$Pb_3(OH)_4^{2+}$	-23.888

Continued on next page

H_2CO_3	16.681
HCO_3^-	10.329
$NaHCO_3$	10.079
$PbHCO_3^+$	13.200
$NaCO_3^-$	1.270
$PbCO_3$	6.478
$Pb(CO_3)_2^{2-}$	9.938

[a] Log Kf taken from Villalobos et al., 2010) and included in Visual Minteq Database.

Table 3. pH range in which there are solid formations with respect to composition.

As/Pb/Cu molar ratio	Solid formed[a]	pH range
3/5/0[b]	Schultenite	3.5 – 5.0
	Hydroxymimetite	5.0 – 9.0
	PbO	8.0 – 10.5
1/1/0[a]	Schultenite	2.0 - 6.0
	Hydroxymimetite	5.0 – 9.5
	PbO	9.5 – 10.5
1/0/1	$Cu_3(AsO_4)_{2.2}H_2O$	5.5 – 6.5
	Tenorite	6.5 – 10.5
2/0/3	$Cu_3(AsO_4)_{2.2}H_2O$	5.0 – 6.5
	Tenorite	6.0 – 11.0
1/1/1	Schultenite	3.0 – 4.0
	Duftite	4.0 – 10.0
	Tenorite	8.5 – 10.5
	Hydrocerussite	9.0 – 10.5
	PbO	9.0 – 10.5
2/1/3	Schultenite	3.0 – 3.5
	Duftite	4.0 – 10.0
	Bayldonite	5.0 – 8.0
	Tenorite	7.0-10.5

[a] The corresponding chemical formulas are listed in Table 2
[b] Molar ratios taken from (Vaca-Escobar et al., 2012)

CAPÍTULO 4

4. CONCLUSIONES

Se determinaron las condiciones geoquímicas que favorecen la formación de arseniatos metálicos, y aquellas que favorecen procesos de adsorción del As(V) a goetita en sistemas compuestos principalmente por goetita/As(V)/Pb(II), y luego con Cu(II), considerando los varios componentes reactivos en el sistema, de modo que gradualmente se aproximen a la complejidad geoquímica de los medios naturales. Además, se logró una descripción adecuada de la movilidad y especiación del As(V) a través de un modelo termodinámico desarrollado mediante el acoplamiento de un modelo de complejación superficial altamente robusto desarrollado para goetita y su interacción de adsorción con As(V), junto con un modelo de especiación sólida-acuosa. Los sistemas investigados se modelaron para condiciones en que el As(V) y Pb(II) se encuentran presentes simultáneamente en altas concentraciones, como se ha reportado en ambientes contaminados, incrementando progresivamente la complejidad de los sistemas de modo que se aproximen a escenarios reales.

Comparado con el comportamiento de adsorción de As(V) sobre goetita, la presencia de Pb(II) tiene un impacto importante sobre este comportamiento, pero sólo para la goetita de alta ASE (94 m^2 g^{-1}), pues promueve la formación de arseniatos de Pb(II) altamente insolubles (precipitación), y así disminuye la adsorción de As(V). Los resultados, tanto de modelación como experimentales, muestran que el proceso de adsorción predomina solamente a relaciones molares As/Fe muy bajas, mientras la precipitación de arseniato de Pb(II) comienza a ser un proceso competitivo cuando esta relación incrementa, evitando la saturación de sitios superficiales con As(V) solo para la goetita de mayor ASE. Los procesos de adsorción y de precipitación contribuyen en proporciones similares en un intervalo limitado de relaciones As/Fe. En una relación molar As/Fe alta (mayores a 0.02, correspondiente a escenarios reales de suelos contaminados), la precipitación de arseniatos de plomo es el proceso dominante y no existe saturación de sitios superficiales con As(V) hasta tener una relación molar As/Fe

cinco veces mayor (0.089) a la mostrada para la adsorción de As(V) en ausencia de Pb(II) (0.018).

En contraste, para una goetita altamente reactiva con una baja ASE (50 m^2 g^{-1}) pero considerablemente mayor densidad de sitios superficiales, no se observó efecto de la presencia de Pb(II) que sí se observó para la goetita de alta ASE. A pesar de que para esta goetita se adsorbe menor cantidad de As(V) por masa de goetita que para la de alta ASE, el mecanismo ocurre a través de mayor reactividad de la goetita de baja ASE para adsorber Pb(II), y por tanto dejar menos Pb(II) disponible para precipitar como arseniato. Es decir, la disminución de adsorción de la goetita de mayor ASE ocurre a través de un mecanismo indirecto.

De manera inversa, la presencia de cloruro en el sistema, incluso en concentraciones muy bajas ($1x10^{-5}$M), permiten la precipitación de un arseniato-cloruro de Pb(II) con un producto de solubilidad de 20 órdenes de magnitud más baja que su contraparte de hidroxilo, imponiendo una competencia para enlazar al As(V) versus su adsorción en ambas goetitas.

La especiación descrita anteriormente se ve afectada por la presencia de sulfato en altas concentraciones pero sólo a valores de pH bajos (< 5), ya que bajo estas condiciones se promueve la formación de anglesita insoluble ($PbSO_4$), y de este modo liberan As(V) provocando alta adsorción y altas concentraciones acuosas. Sin embargo, en presencia de iones cloruro simultáneamente con los sulfato, el efecto es revertido y la precipitación del arseniato-cloruro de Pb(II) tiende a controlar la movilidad del As(V) bajo la mayoría de las condiciones de As/Fe. Todos los resultados previos fueron validados para una relación de As/Pb igual a 3/5.

Si se incrementa la proporción de As(V) en el sistema, es decir a relaciones molares As/Pb altas, el mecanismo de precipitación llega a ser progresivamente menos dominante, para dar lugar al de adsorción, y de presencia de As(V) acuoso después de saturar la superficie de la goetita.

La presencia de Cu(II) en el sistema goetita/As(V), en lugar de Pb(II), es menos eficiente en la remoción de As(V) acuoso debido a que la constante de formación del arseniato de cobre es menor (27 órdenes de magnitud). Si el sistema presenta ambos metales [Pb(II) y Cu(II)], en una relación molar con As(V) de 1/1/1, la adsorción de

As(V) decrece considerablemente en la goetita de mayor tamaño, de manera similar al decremento en la presencia de Cl^- y en la ausencia de Cu(II). La disminución de especies adsorbidas en presencia de Cu(II) se debe a la precipitación del arseniato metálico mixto llamado duftita: $PbCu(AsO_4)(OH)$; el porcentaje de especies adsorbidas disminuye aún más si la relación molar As(V)/Pb(II)/Cu(II) cambia a 2/1/3, que corresponde a otro arseniato metálico mixto llamado bayldonita $[PbCu_3(AsO_4)_2(OH)_2]$. Lo anterior fue determinado mediante modelación termodinámica. Esta disminución en el porcentaje de especies adsorbidas es debido a que ambos minerales de Pb(II) y Cu(II) precipitan simultáneamente. En el sistema bajo las condiciones mencionadas, no se encuentran especies As(V) acuosas, ni arseniatos simples de Pb(II) o Cu(II). La interacción entre los procesos de adsorción y precipitación ocurre de tal manera que un mecanismo o el otro prevalece, permitiendo una eficiente atenuación del As(V) en sistemas acuosos contaminados con As(V) y los metales pesados Pb(II) y Cu(II).

El proceso de precipitación, especialmente en la presencia de cloruros, parece ofrecer un mecanismo ventajoso para la atenuación de As(V) y Pb(II) en ambientes contaminados donde ambos elementos están presentes en contenidos totales similares, mostrando una alta estabilidad basada en el intervalo de pH en el que los minerales mimetita, hidroximimetita y schultenita son estables.

REFERENCIAS

Asta, M.P., Cama, J., Martinez, M., Gimenez, J., 2009. Arsenic removal by goethite and jarosite in acidic conditions and its environmental implications. J Hazard Mater 171, 965-972.

Atkinson, R.J., Posner, A.M., Quirk, J.P., 1967. Adsorption of Potential-Determining Ions at the Ferric Oxide-Aqueous Electrolyte Interface. The Journal of Physical Chemistry 71, 9.

Bissen, M., Frimmel, F.H., 2003. Arsenic — a Review. Part I: Occurrence, Toxicity, Speciation, Mobility. Acta hydrochimica et hydrobiologica 31, 9-18.

Bowell, R.J., Alpers, C.N., Jamieson, H.E., Nordstrom, D.K., Majzlan, J., 2014a. The Environmental Geochemistry of Arsenic — An Overview —. Reviews in Mineralogy and Geochemistry 79, 1-16.

Cornell, R.M., Posner, A.M., Quirk, J.P., 1974. Crystal morphology and the dissolution of goethite. Journal of Inorganic and Nuclear Chemistry 36, 1937-1946.

Cornell, R.M., Schwertmann, U., 2004a. Surface Area and Porosity, The Iron Oxides. Wiley-VCH Verlag GmbH & Co. KGaA, pp. 95-110.

Cullen, W.R., Reimer, K.J., 1989. Arsenic speciation in the environment. Chemical Reviews 89, 713-764.

Chang, J.-S., Yoon, I.-H., Kim, K.-W., 2009. Heavy metal and arsenic accumulating fern species as potential ecological indicators in As-contaminated abandoned mines. Ecological Indicators 9, 1275-1279.

Duruibe, J., Ogwuegbu, M., Egwurugwu, J., 2007. Heavy metal pollution and human biotoxic effects. International Journal of Physical Sciences 2, 112-118.

Flemming, C.A., Trevors, J.T., 1989. Copper toxicity and chemistry in the environment: a review. Water Air Soil Pollut 44, 143-158.

Garelick, H., Jones, H., Dybowska, A., Valsami-Jones, E., 2008. Arsenic Pollution Sources, Reviews of Environmental Contamination Volume 197. Springer New York, pp. 17-60.

Gustafsson, J.P., 2010. Visual MINTEQ. Ver. 3.0. A free equilibrium speciation model software. VISUAL MINTEQ VER 3.

Gutierrez-Ruiz, M., Villalobos, M., Romero, F., Fernandez-Lomelin, P., 2005. Natural attenuation of arsenic in semiarid soils contaminated by oxidized arsenic wastes, in: Oday, P.A., Vlassopoulos, D., Meng, Z., Benning, L.G. (Eds.), Advances in Arsenic Research: Integration of Experimental and Observational Studies and Implications for Mitigation, pp. 235-252.

Hartley, W., Lepp, N.W., 2008. Remediation of arsenic contaminated soils by iron-oxide application, evaluated in terms of plant productivity, arsenic and phytotoxic metal uptake. The Science of the total environment 390, 35-44.

Järup, L., 2003. Hazards of heavy metal contamination. British medical bulletin 68, 167-182.

Lenoble, V., Omanović, D., Garnier, C., Mounier, S., Đonlagić, N., Le Poupon, C., Pižeta, I., 2013. Distribution and chemical speciation of arsenic and heavy metals in highly contaminated waters used for health care purposes (Srebrenica, Bosnia and Herzegovina). Science of The Total Environment 443, 420-428.

Lin, Z.X., Puls, R.W., 2001. Studies of interfacial reactions between arsenic and minerals and its significance to site characterization. Environmental Geology 40, 1433-1439.

Maderova, L., Watson, M., Paton, G., 2011. Bioavailability and toxicity of copper in soils: Integrating chemical approaches with responses of microbial biosensors. Soil Biology and Biochemistry 43, 1162-1168.

Mamindy-Pajany, Y., Hurel, C., Marmier, N., Roméo, M., 2009. Arsenic adsorption onto hematite and goethite. Comptes Rendus Chimie 12, 876-881.

Matera, V., Le Hecho, I., Laboudigue, A., Thomas, P., Tellier, S., Astruc, M., 2003. A methodological approach for the identification of arsenic bearing phases in polluted soils. Environmental Pollution 126, 51-64.

Mirza, N., Mahmood, Q., Maroof Shah, M., Pervez, A., Sultan, S., 2014. Plants as Useful Vectors to Reduce Environmental Toxic Arsenic Content. The Scientific World Journal 2014, 11.

Morin, G., Calas, G., 2006. Arsenic in soils, mine tailings, and former industrial sites. Elements 2, 97-101.

Oremland, R.S., Stolz, J.F., 2003. The Ecology of Arsenic. Science 300, 939-944.

Ostergren, J.D., Trainor, T.P., Bargar, J.R., Brown Jr, G.E., Parks, G.A., 2000. Inorganic Ligand Effects on Pb(II) Sorption to Goethite (α-FeOOH): I. Carbonate. Journal of Colloid and Interface Science 225, 466-482.

Paktunc, D., Foster, A., Heald, S., Laflamme, G., 2004. Speciation and characterization of arsenic in gold ores and cyanidation tailings using X-ray absorption spectroscopy. Geochimica Et Cosmochimica Acta 68, 969-983.

Papanikolaou, N.C., Hatzidaki, E.G., Belivanis, S., Tzanakakis, G.N., Tsatsakis, A.M., 2005. Lead toxicity update. A brief review. Medical Science Monitor 11, RA329-RA336.

Salazar-Camacho, C., Villalobos, M., 2010. Goethite surface reactivity: III. Unifying arsenate adsorption behavior through a variable crystal face - Site density model. Geochimica Et Cosmochimica Acta 74, 2257-2280.

Schecher, W.D., McAvoy, D.C., 1992. MINEQL+ - A software environment for chemical-equilibrium modeling. Computers Environment and Urban Systems 16, 65-76.

Sevilla, J.L., Mateus, X.A., 2008. Intoxicación por arsénico. Revista Ecuatoriana de Pediatría 9, 5.

Shen, S., Li, X.-F., Cullen, W.R., Weinfeld, M., Le, X.C., 2013. Arsenic Binding to Proteins. Chemical Reviews 113, 7769-7792.

Slowey, A.J., Johnson, S.B., Newville, M., Brown, G.E., 2007. Speciation and colloid transport of arsenic from mine tailings. Applied Geochemistry 22, 1884-1898.

Smedley, P.L., Kinniburgh, D.G., 2002. A review of the source, behaviour and distribution of arsenic in natural waters. Applied Geochemistry 17, 517-568.

Stuben, D., Berner, Z., Kappes, B., Puchelt, H., 2001. Environmental monitoring of heavy metals and arsenic from Ag-Pb-Zn mining. A case study over two millennia. Environmental Monitoring and Assessment 70, 181-200.

Vaca-Escobar, K., Villalobos, M., Ceniceros-Gomez, A.E., 2012. Natural arsenic attenuation via metal arsenate precipitation in soils contaminated with metallurgical wastes: III. Adsorption versus precipitation in clean As(V)/goethite/Pb(II)/carbonate systems. Applied Geochemistry 27, 2251-2259.

van Geen, A., Robertson, A.P., Leckie, J.O., 1994. Complexation of carbonate species at the goethite surface: Implications for adsorption of metal ions in natural waters. Geochimica et Cosmochimica Acta 58, 2073-2086.

Vaughan, D.J., 2006. Arsenic. Elements 2, 71-75.

Vázquez, S., Hevia, A., Moreno, E., Esteban, E., Peñalosa, J.M., Carpena, R.O., 2011. Natural attenuation of residual heavy metal contamination in soils affected by the Aznalcóllar mine spill, SW Spain. Journal of Environmental Management 92, 2069-2075.

Villalobos, M., Cheney, M.A., Alcaraz-Cienfuegos, J., 2009. Goethite surface reactivity: II. A microscopic site-density model that describes its surface area-normalized variability. Journal of Colloid and Interface Science 336, 412-422.

Villalobos, M., Garcia-Payne, D.G., Lopez-Zepeda, J.L., Ceniceros-Gomez, A.E., Gutierrez-Ruiz, M.E., 2010. Natural Arsenic Attenuation via Metal Arsenate Precipitation in Soils Contaminated with Metallurgical Wastes: I. Wet Chemical and Thermodynamic Evidences. Aquatic Geochemistry 16, 225-250.

Villalobos, M., Perez-Gallegos, A., 2008. Goethite surface reactivity: A macroscopic investigation unifying proton, chromate, carbonate, and lead(II) adsorption. Journal of Colloid and Interface Science 326, 307-323.

Villalobos, M., Trotz, M.A., Leckie, J.O., 2001. Surface complexation modeling of carbonate effects on the adsorption of Cr(VI), Pb(II), and U(VI) on goethite. Environmental Science & Technology 35, 3849-3856.

Westall, J.C., Zachary, J.L., Morel, F., 1976. MINEQL, A computer program for the calculation of chemical equilibrium composition of aqueous systems. Technical Note 18, Dept. Civil Eng., MIT, Cambridge, MA.

ANEXO A

Guía rápida para el uso de los programas de especiación química

Visual MINTEQ

La metodología general del programa es descrita por (Gustafsson, 2010), cuyo breve resumen se muestra a continuación:

1. Definir el problema

Para definir el problema bajo estudio es necesario añadir los datos del problema, para ello en el menú principal se debe corroborar lo siguiente:

- El valor de pH y la fuerza iónica usados, además de la temperatura (25°C).
- Elegir las unidades de concentración para los datos de entrada.
- Añadir los componentes del problema, así como sus concentraciones.
- Ya que existe la posibilidad de que se formen fases sólidas, se debe especificar esta condición.

Además, es necesario tomar en cuenta el proceso de adsorción, para ello se debe indicar el modelo que se empleará, así como las características propias de la superficie y definir las reacciones de adsorción que se pueden dar el en problema, en este aspecto cabe recalcar que Visual MINTEQ usa el estado estándar de las especies superficiales en fracción molar.

2. Ejecutar Visual MINTEQ

Una vez definido el problema, es recomendable guardarlo para que se encuentre disponible para futuras modelaciones. Luego de ello se ejecuta el problema presionando *Run*, con lo cual iniciará el cálculo y lo terminará con la pantalla de resultados.

3. Interpretación de resultados

La primera ventana que aparece es la principal de salida, en la cual se muestra el pH al equilibrio, la fuerza iónica, el número de iteraciones realizadas por el programa para alcanzar la resolución del problema y el cálculo del balance de carga en la parte superior. El resto de la ventana está dedicado a la lista de resultados que se presenta en tres columnas: concentración, actividad y logaritmo de la actividad de todas las especies presentes en el sistema bajo estudio (iones, complejos, etc.).

Además, desde esta pantalla se tiene acceso a visualizar: la distribución de especies (mediante el botón *View Species Distribution*), los índices de saturación (a través del botón *Display Saturation Indices*) y la concentración total de cada componente en las fases disuelta, adsorbida y precipitada (en *Equilibrated Mass Distribution*).

Matemáticamente, consideraciones simultáneas de todas las restricciones del balance de masas resultan en un sistema de ecuaciones algebraicas no lineales, las cuales son resueltas con el método de aproximación de Newton- Raphson, el cual es una técnica iterativa para encontrar el valor de x de tal manera que $y(x) = 0$. Para cada iteración se origina el Jacobiano del sistema y las ecuaciones lineales obtenidas son resueltas usando el método de eliminación-sustitución Gaussiana (Allison et al., 1991).

Programa MINEQL+ 4.5

El programa MINEQL+ es muy útil, se pueden usar cuatro modelos de adsorción, para los cuales el programa incluye una herramienta en la que se ingresan las expresiones de acción de masas. Los tres modelos adicionales que presenta la opción de "*modelado de adsorción*" son de complejación superficial y para ello presenta la opción de ingresar al sistema las correcciones electrostáticas de carga superficial. Adicionalmente, se deben introducir correctamente las expresiones de acción de masas y se tendrá que seleccionar el modelo que será empleado.

Para esta investigación el modelo empleado fue el de *triple capa,* razón por la cuál a continuación se mostrarán los pasos necesarios para calcular el modelo de triple capa en MINEQL+:

1. Al iniciar el programa, se muestra una lista de todos los componentes presentes en el sistema a modelar, los que conforman todas las especies presentes: disueltas (incluyendo las que son parte de la imposición de la fuerza iónica y las que se tiene por disociación del agua), sólidas y gaseosas; presionar *Scan THERMO.*
2. La siguiente pantalla que aparece es la que permite verificar que el programa tiene en su base de datos todas las reacciones correspondientes a las especies acuosas (*Type II – Aqueous Species*) presentes en el sistema que se modelará, además, de ser necesario se pueden modificar valores de constantes, agregar o quitar especies. Presionar *Close.*
3. A continuación aparece la pantalla *Tableau Switch,* la cual permite ver los datos para otros tipos de especies, como: entidades fijas (*Fixed Entities)*, sólidos disueltos (*Dissolved Solids)* y especies no consideradas (*Species Not Considered).* Para este caso, presionar *No.*
4. Aparece la pantalla *Run Time Manager,* aquí establecer las condiciones de fuerza iónica, y de ser necesario la corrección por temperatura. Presiona *Wizard.*
5. Usando *Calculation Wizard*, ingresar las concentraciones totales de los componentes del sistema, y las condiciones de trabajo, es decir: pH (es fijo, o si el cálculo se realizará en un intervalo determinado) y carbonato (si es abierto a la atmósfera o si el sistema no tiene carbonatos). Presionar *Cancel.*
6. Luego presionar el botón *MultiRun*, establecer el tipo de cálculo que se realizará, en este caso titulación *(Tritation)* y seleccionar que los datos se presenten como *Log K of pH,* además establecer el intervalo de pH en el que se va a trabajar y el número de puntos. Y para finalizar se presiona el botón *Run*.
7. En la tabla *Output Manager* se selecciona el modo en el que se desea se presenten los valores de salida, por ejemplo si se desea que los datos se presenten de manera gráfica, se selecciona esta opción, las especies de interés (solo se pueden ver hasta diez especies) y la forma cómo se muestren los datos, es decir si se los requiere como concentración (molar) o en escala logarítmica de la concentración.
8. Se pueden guardar los datos como *Bloc de Notas*, y se los extrae de acuerdo a las necesidades del usuario.

ANEXO B

Constantes de formación de especies acuosas y sólidas

A continuación se muestran todas las constantes de formación de especies acuosas y de especies sólidas necesarias para la modelación termodinámica de los sistemas bajo estudio, éstas se muestran a continuación:

Tabla B1. Constantes de formación de especies acuosas y sólidas usadas en los programas de modelación termodinámica (Base de datos de la USEPA).

Nombre Mineral	**Fórmula Química**	**Log K_f**
ESPECIES SÓLIDAS		
Hidroximimetita	$Pb_5(AsO_4)_3OH$	62.115 [a]
Mimetita	$Pb_5(AsO_4)_3Cl$	83.571 [a]
Plumbonacrita	$Pb_{10}(OH)_6O(CO_3)_6$	8.760
Schultenita	$PbHAsO_4$	23.969 [a]
Hidrocerusita	$Pb_3(OH)_2(CO_3)_2$	18.77
Cerusita	$PbCO_3$	13.13
Laurionita	$PbCl(OH)$	-0.623
Shannonita	Pb_2OCO_3	0.558
Masicote	PbO	-12.894
Litargirio	PbO	-12.694
Natrón	$Na_2CO_3.10H_2O$	1.311
Termonatrita	$Na_2CO_3.H_2O$	-0.637
Azurita	$Cu_3(CO_3)_2(OH)_2$	16.906
Malaquita	$Cu_2(CO_3)_2(OH)_2$	5.306
Tenorita (c)	CuO	-7.644
Tenorita (am)	CuO	-8.49

Continúa en la siguiente página

Bayldonita	$PbCu_3(AsO_4)_2(OH)_2$	37.050
Duftita	$PbCu(AsO_4)(OH)$	20.512
Fosgenita	$(PbCl)_2CO_3$	19.810
Cotunnita	$PbCl_2$	4.78
Halita	$NaCl$	-1.603
Anglesita	$PbSO_4$	-7.79
Lanarkita	$Pb_2(OH)_2SO_4$	-0.4344
Mirabilita	$Na_2SO_4.10H_2O$	-1.114
Thernardita	Na_2SO_4	0.3217
	$Pb_3O_2CO_3$	-11.02
	$Pb_2O(OH)_2$	-26.188
	$Pb(OH)_2$	-8.15
	$PbO.0.3H_2O$	-12.98
	As_2O_5	34.694
	$CuCO_3$	11.50
	$Cu_3(AsO_4)_2.H_2O$	35.119
	$Cu(OH)_2$	-8.674
	$Pb(OH)_3Cl$	-8.793
	$Pb_3OSO_{4\ (s)}$	10.6864
	$Pb_4(OH)_6SO_{4\ (s)}$	21.1
	$Pb_4O_3SO_{4\ (s)}$	21.8772
ESPECIES ACUOSAS		
	$Cu_2(OH)_2^{2+}$	-10.494
	$Cu(CO_3)_2^{2-}$	10.20
	$Cu(NO_3)_2$	-0.40
	$Cu(OH)_2$	-16.23
	$Cu(OH)_3^-$	-26.64
	$Cu(OH)_4^{2-}$	-39.73
	Cu_2OH^{3+}	-6.71
	$Cu_3(OH)_4^{2+}$	-20.788

Continúa en la siguiente página

$CuCO_3$	6.77
$CuHCO_3^+$	12.129
$CuNO_3^+$	0.50
$CuOH^+$	-7.497
$NaNO_3$	-0.55
$NaOH$	-13.897
$PbCl_{2\ (aq)}$	2.200
$PbCl^+$	1.55
$PbCl_3^-$	1.800
$PbCl_4^{2-}$	1.460
$NaSO_4^-$	0.74
$PbSO_{4\ (aq)}$	2.69
$Pb(SO_4)_2^{2-}$	3.47
HSO_4^-	1.99
OH^-	-13.997
$HAsO_4^{2-}$	11.6
$H_2AsO_4^-$	18.35
H_3AsO_4	20.6
$PbH_2AsO_4^+$	19.736 [a]
$PbHAsO_4$	14.038 [a]
$Pb(OH)_2$	-17.897
$Pb(NO_3)_2$	1.4
$PbNO_3^+$	1.17
$PbOH^+$	-7.597
$Pb_4(OH)_4^{4+}$	-19.988
$Pb_2(OH)^{3+}$	-6.397
$Pb(OH)_3^-$	-28.091
$Pb(OH)_4^{2-}$	-39.699
$Pb_3(OH)_4^{2+}$	-23.888
H_2CO_3	16.681

Continúa en la siguiente página

HCO_3^-	10.329
$NaHCO_3$	10.079
$PbHCO_3^+$	13.200
$NaCO_3^-$	1.270
$PbCO_3$	6.478
$Pb(CO_3)_2^{2-}$	9.938

[a] Log K_f tomada de Villalobos et al. (2010) e incluidas en la base de datos de Visual Minteq (Gustafsson, 2010).